NASA Contractor Report 177369
LIMITED DISTRIBUTION

Propulsion and Airframe Aerodynamic Interactions of Supersonic V/STOL Configurations

Phase I: Final Report

M.R. Mraz
P.E. Hiley

CONTRACT NAS2-10791
SEPTEMPER 1985

Date for general release: August 1987.

NASA

NASA Contractor Report 177370

Propulsion and Airframe Aerodynamic Interactions of Supersonic V/STOL Configurations

Phase I: Final Report

M.R. Mraz
P.E. Hiley
McDonnell Aircraft Company
St. Louis, Missouri

until August 1987.

Prepared for
Ames Research Center
under Contract NAS2-10791
September 1985

National Aeronautics and
Space Administration

AMES RESEARCH CENTER
Moffett Field, California 94035

TABLE OF CONTENTS

TABLE OF CONTENTS (Concluded)

LIST OF FIGURES

LIST OF FIGURES (Continued)

LIST OF FIGURES (Concluded)

LIST OF ABBREVIATIONS, ACRONYMS AND SYMBOLS

Abbreviations

A	Area
A_C	Inlet Capture Area
ADEN	Augmented Deflector Exhaust Nozzle
A_8	Nozzle Throat Area
AEDC	Arnold Engineering Development Center
AE57	CMAPS Mixer Area
AFAPL	Air Force Aeropropulsion Laboratory
AFWAL	Air Force Wright Aeronautical Laboratories
ALBEN	Aerodynamic Load Balance Exhaust Nozzle
ANC	Advanced Nozzle Concepts
Avg	Average
A/B	Afterburning
A/C	Aircraft
AR	Aspect Ratio, b^2/Sw
A_V	Bleed Venturi Area
b	Wingspan
B.L.	Butt Line
$\bar{c}$	Mean Aerodynamic Chord
C_D	Drag Coefficient, D/(q Sw)
C_L	Lift Coefficient, L/(q Sw)
C_M	Pitching Moment Coefficient, $PM/(q\bar{c}\ S_w)$
CMAPS	Compact Multimission Aircraft Propulsion Simulator
C_P	Pressure Coefficient, $(P - P_\infty)/q$
CR	Inlet Contraction Ratio
C_R	Wing Chord at Root
C_T	Wing Chord at Tip or Aerodynamic Thrust Coefficient, $F_G/(q\ Sw)$
D	Drag
DLE	Direct Lift Engine
DLI	Deck Launched Intercept
DRAG COUNT	D/(q Sw) = 0.0001
EPR	Engine Pressure Ratio

LIST OF ABBREVIATIONS, ACRONYMS AND SYMBOLS

Abbreviations

E.S.	Engine Station
F	Thrust in Drag Direction, $F_G \cos(\alpha + \delta_v)$
FS	Fuselage Station
F-T	Flow Through
G.E.	General Electric
IRAD	Independent Research and Development
J-E	Jet Effects
L	Lift
L/C	Lift/Cruise
L/D	Lift Over Drag Ratio
M	Mach Number
Max	Maximum
MCAIR	McDonnell Aircraft Company
Min	Minimum
MFR	Inlet Mass Flow Ratio
MRM	Medium Range Missile
M_t	Inlet Throat Mach Number
n	Number of Data Measurements
NASA	National Aeronautics and Space Administration
NPR	Nozzle Pressure Ratio
P	Pressure
PCNLR	Percent Corrected Compressor Rotor Speed
P&WA	Pratt & Whitney Aircraft Company
PM	Pitching Moment
P_T	Total Pressure
P_{T_0}	Freestream Total Pressure
P_{T_2}	Compressor Entrance Total Pressure
Q,q	Dynamic Pressure
R_e	Reynolds Number
SRM	Short Range Missile
S_{TOT}	Theoretical Total Wing Planform Area
S_W,S	Wing Planform Area

Abbreviations

T	Temperature
TS	Tunnel Station
TV	Thrust Vectoring
2-D	Two-Dimensional
UPWT	Unitary Plan Wind Tunnel
V/STOL	Vertical/Short Take-Off and Landing
WA2R, $(\frac{W\sqrt{\theta}}{\delta S})_{t_2}$	Compressor Corrected Airflow
WL	Waterline
$\bar{Y}$	Distance in Lateral Plane From Aircraft Centerline to $\bar{c}$

Greek Symbols

α	Angle of Attack
β	Sideslip Angle
Δ	Incremental Value
δ_c	Canard Deflection Angle
δ_{STATIC}	Static Thrust Vector Angle
δ_v	Nozzle Deflection Angle
Λ_{LE}	Leading Edge Sweep Angle
λ	Taper Ratio, C_R/C_T
σ	Standard Deviation

Subscripts

AMB	Ambient Static
j	Jet
SLSI	Sea Level Static Installed
T,t	Total
∞,o	Freestream

SUMMARY

A wind tunnel model of a supersonic V/STOL fighter configuration has been conceptually designed to measure the aerodynamic interaction effects which can result from geometrically close-coupled propulsion system/airframe components. The approach is to configure the model for tests representing two different test techniques. One is the conventional test technique, where absolute configuration aerodynamics (including inlet/airframe interactions) are measured in a flow-through mode, and incremental nozzle/airframe interactions are measured in a jet-effects mode. The other is a propulsion simulator technique, where a sub-scale, externally powered engine is mounted in the model, thus allowing measurement of inlet/airframe and nozzle/airframe interactions simultaneously.

Comparison of the aerodynamic characteristics between the two test techniques is a direct indication of the extent to which inlet and nozzle flowfields are coupled together. If significant coupling does exist, then the simulator test technique may be required in the future to properly measure the aerodynamic characteristics of compact fighter configurations.

Measurement of these propulsion/airframe interaction effects is being carried out in a three phase program, sponsored by the NASA Ames Research Center, involving preliminary model design, detailed model design and fabrication, and high speed (up to Mach 1.4) testing. In Phase 1, the preliminary design of the wind tunnel model has been completed.

The aerodynamic configuration is a canard/wing concept designed for high transonic maneuverability, employing non-axisymmetric, vectorable exhaust nozzles located near the wing trailing edge. The external airframe components are existing hardware from an Air Force sponsored nozzle research program now in progress.

The model has been extensively re-designed internally to meet NASA objectives, and a new strut support system has been designed. The model is designed for testing in the flow-through, jet-effects, and simulator modes under the philosphy to maximize hardware commonality. The metric arrangement in all modes is identical, wherein a single internal balance is used to measure all external aerodynamic forces except on the nozzle boattail. External pressures are used to measure the boattail aerodynamics. The commonality feature extends to all three metric break locations and seal bridging mechanisms. The purpose of commonality is to eliminate bias error sources between modes, so that comparison of aerodynamic data will represent inlet/nozzle coupling effects, not differences due to test technique. The metric arrangement is considered a relatively low risk approach, since only configuration external aerodynamics are measured by the balance (i.e., thrust is not measured), and the metric break seal arrangements are based on extensive recent experience at MCAIR.

Considerable effort was also expended to design the model inlet systems for compatibility with the simulator up to 25° angle of attack at high speed, and 90° angle of attack at low speed. An active thermal control system was also designed for the internal balance, so that errors would not be introduced by the wide range of flow temperatures used to power the simulator.

The model preliminary design is a product of extensive design and analysis by MCAIR propulsion and model design engineers. It was designed recognizing the main model purpose is for measurement of interaction effects with two uniquely different test techniques. Every effort was made in the design to ensure that any differences in the aerodynamics between test techniques is an effect of propulsion/airframe coupling, <u>not</u> test technique bias. This is not meant to infer that the model is simple, since this program represents the first time that two propulsion simulators of this type will be tested in a realistic wind tunnel model. We believe that this conceptual design provides an excellent basis for the detailed model design and fabrication in Phase 2, and eventual successful testing in Phase 3.

1.0 INTRODUCTION

Many of the configurations proposed for advanced supersonic V/STOL aircraft are very compact in nature. This results primarily from the design goal to minimize control forces and forward lift engine size by concentrating the major components of the aircraft near the center of gravity. Integration of the propulsion system with the airframe for these configurations can result in potentially significant aerodynamic flowfield interactions. These interactions may arise from geometrically close-coupled wing/canard/inlet arrangements along with minimum length nacelles and supercirculation induced by vectoring exhaust nozzles.

The data obtained with conventional wind tunnel test techniques can be questionable in the presence of large flowfield interactions, since these techniques cannot achieve simultaneous simulation of all of the flowfields involved. This can be achieved with the Compact Multi-Mission Aircraft Propulsion Simulator (CMAPS), developed by the Air Force Aeropropulsion Laboratory (AFAPL), Reference 1. The CMAPS, Figure 1-1, is a miniature low bypass ratio turbofan engine powered by a high pressure air turbine.

The most beneficial application of the CMAPS will obviously be on those aircraft that have potentially large flowfield interactions between the inlet, nozzle, and airframe. Since testing a CMAPS equipped model may be more complex and expensive than testing a conventional model (flow-through and jet-effects), the need to identify the types of configurations which require CMAPS evaluation is critical. An aerodynamically "close-coupled" V/STOL configuration represents an effective means of evaluating the requirement for simultaneous inlet and exhaust nozzle flow simulation, and thus the potential need for the CMAPS testing technique.

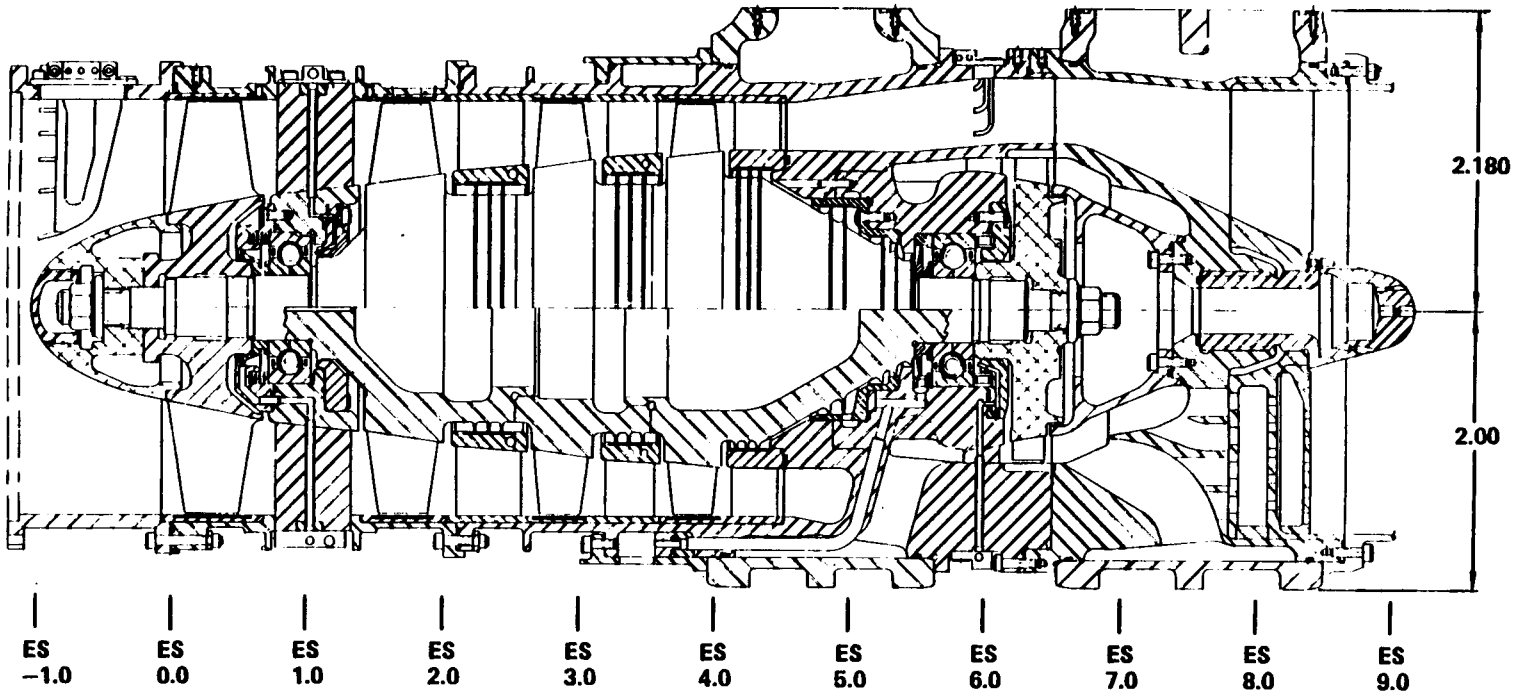

FIGURE 1-1
COMPACT MULTIMISSION AIRCRAFT PROPULSION SIMULATOR (CMAPS)

GP13-0503-41

Based on the foregoing considerations, a three phase NASA program of 29 months planned duration has been initiated to measure airframe/propulsion system interactions on close-coupled supersonic V/STOL configurations using the propulsion simulator and conventional model techniques. A secondary objective is to begin development of installation and test techniques for propulsion simulator equipped wind tunnel models.

The approach to accomplish these objectives is to design, fabricate, and test two model configurations characterized by a close-coupled and a closer coupled airframe/propulsion arrangement - each in simulator and conventional test modes. Key characteristics of the test configurations are shown in Figure 1-2. The basic model (close-coupled) of the baseline configuration (i.e. external airframe components) will be provided by the Air Force. It was developed under prime contract to the Air Force Wright Aeronautical Laboratories (AFWAL) by MCAIR in the Advanced Nozzle Concepts (ANC) program, Reference 2. The very close-coupled model is a modification of the basic configuration with shortened inlet length (canard removed).

Preliminary (conceptual) design of the test model was completed in Phase 1 during the first seven months of the program. The essential products of Phase 1 are the design layouts of the model in the different test modes, and the supporting analyses. The layouts have been transmitted per Reference (3). The supporting analyses and other necessary documentation are the subject of this report.

The remainder of the report includes description of the aircraft test configurations; overall testing approach; model common components; test mode concepts; instrumentation; and error analysis.

BASELINE
CLOSE-COUPLED

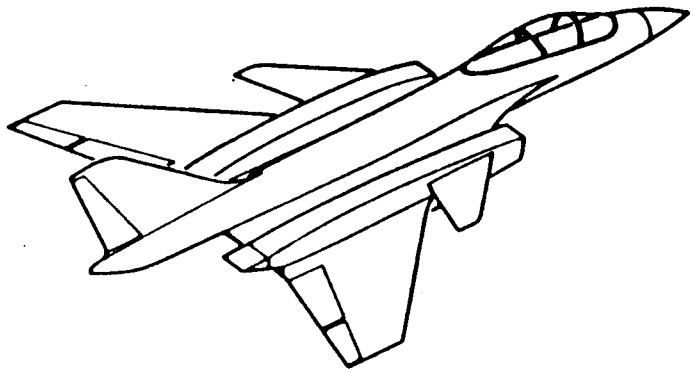

ALTERNATE
ULTRA CLOSE-COUPLED

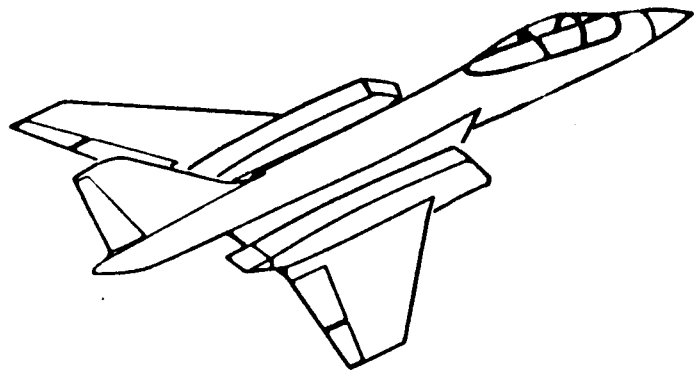

AIR-TO-AIR CONCEPT

- 2-D ALBEN VECTORABLE NOZZLES (AR 4)
- 2-D NORMAL SHOCK INLET WITH DROOP LIP
- WIDE-SPACED PODDED NACELLES
- CLOSE-COUPLED, ALL MOVABLE CANARDS
- ADVANCED MANEUVERING WING

CHANGES FOR ALTERNATE

- ROUND SHORT INLET WITH LOWER SLOT
- CANARDS REMOVED
- INNER WING EXTENSION SHORTENED

FIGURE 1-2
STUDY AERODYNAMIC CONCEPTS

2.0 AERODYNAMIC CONFIGURATION DESCRIPTION

The baseline aerodynamic configuration for the study was selected in proposal studies (Reference 4) to be consistent with several NASA program requirements, as follows:

(1) Twin engine propulsion system with non-axisymmetric and deflectable exhaust nozzles.

(2) Aerodynamic configuration and propulsion system integrated to maximize supercirculation lift induced by thrust vectoring.

(3) Configurations with high probability of demonstrating aerodynamic coupling of inlet and exhaust nozzle flowfields, including a baseline close-coupled configuration and one even more close-coupled in nature.

(4) Realistic design of a supersonic V/STOL fighter/attack aircraft utilizing a wing/canard configuration.

In addition, other desirable requirements included engine cycle compatibility with the CMAPS and commonality with other programs to minimize cost.

The aerodynamic concept selection involved (1) choosing an aerodynamic concept to meet the configuration requirements above (Items 1, 2 and 3) and (2) conducting sizing studies of various propulsion systems in the aerodynamic concept to assess the realism for meeting V/STOL fighter/attack requirements (Item (4) above), concluding in selection of a specific V/STOL system for test simulation.

2.1 AERODYNAMIC CONCEPT DESCRIPTION - The aerodynamic baseline configuration selected for the study was derived from a concept developed for the Air Force sponsored ANC program, Reference 2.

The selected configuration, Figure 2-1, is characterized by wide-spaced, podded nacelles, a canard/wing arrangement, twin vectorable 2-D nozzles at the wing trailing edge, and close-coupled airframe (canard/wing) and propulsion system (inlet/nozzle) components. The nozzle concept is a General Electric Aerodynamic Load Balanced Exhaust Nozzle (ALBEN), with fully continuous vectoring capability up to $\pm 30°$.

A major design objective for this aerodynamic concept was to provide a combination of the movable canard and vectorable nozzles to achieve maneuvering drag reductions. This was accomplished by tailoring the canard/wing arrangement to achieve a maximum unstable static margin of 15%$\bar{c}$ at subsonic speeds. With this relaxed stability level, the vehicle pitching moment characteristics are such that a nose-up moment is produced with the canard deflection for minimum maneuvering drag. Positive nozzle deflection (nozzle deflected downward) is then used for trim, producing a beneficial lift/drag increment from supercirculation. The estimated thrust vectoring payoff in drag is illustrated by comparing trimmed polar estimates with and without vectoring, Figure 2-2. At a typical maneuvering lift coefficient of 0.8, the drag reduction is about 100 counts, or 10% of aircraft drag (thrust loss due to vectoring included).

Maximizing the degree of coupling between the airframe and propulsion system components was a strong consideration in selection of the baseline configuration for the program. Of course, it is possible to only qualitatively assess the level of coupling, since the wind tunnel data are yet to be obtained. There is little question that the inlet/canard interactions will be significant, since the canard is located at the side of the inlet. Similarly, the nozzle/wing interactions should be maximized due to the location of the vectoring nozzle at the wing trailing edge.

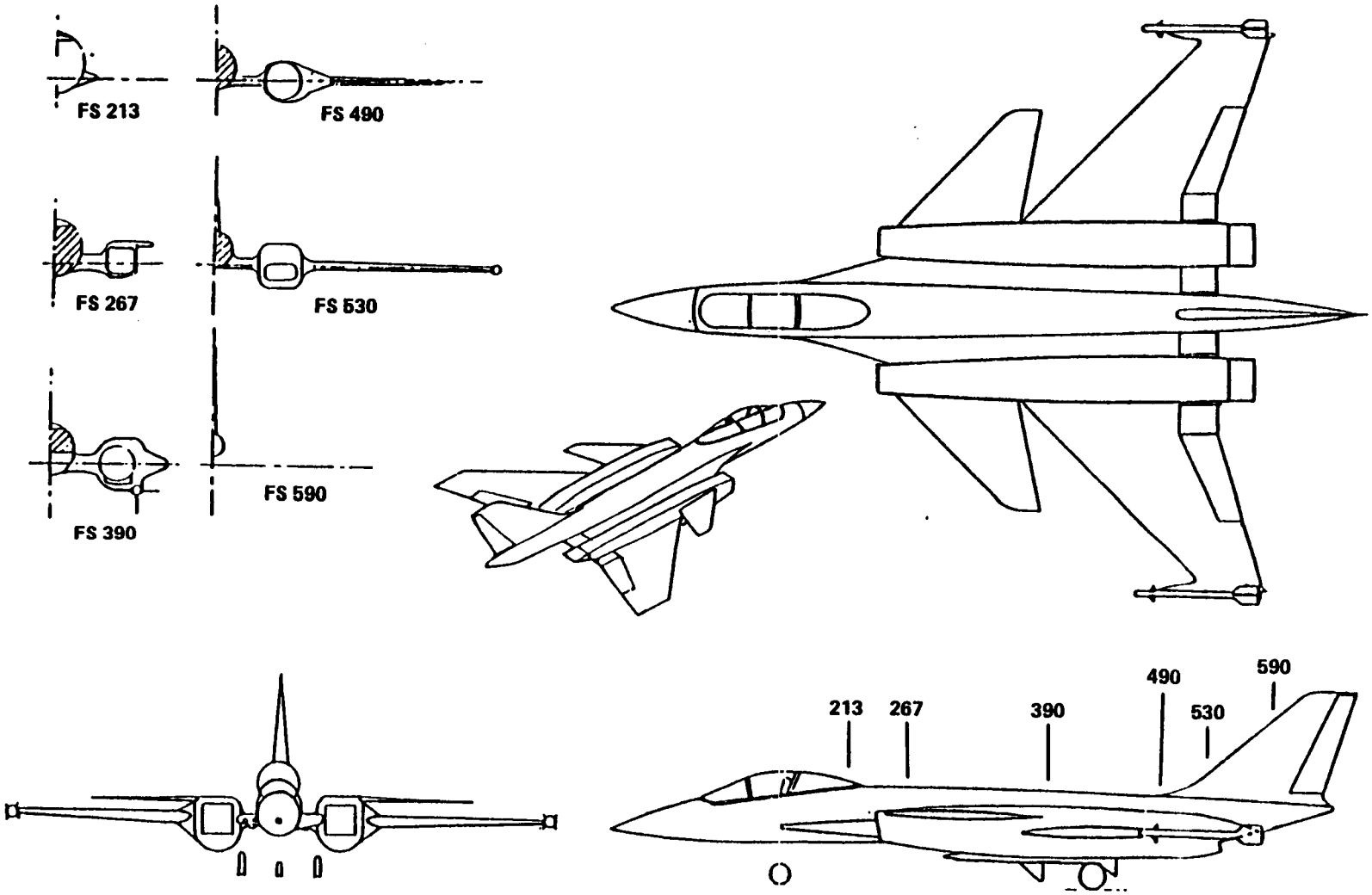

FIGURE 2-1
STUDY BASELINE AERODYNAMIC CONFIGURATION

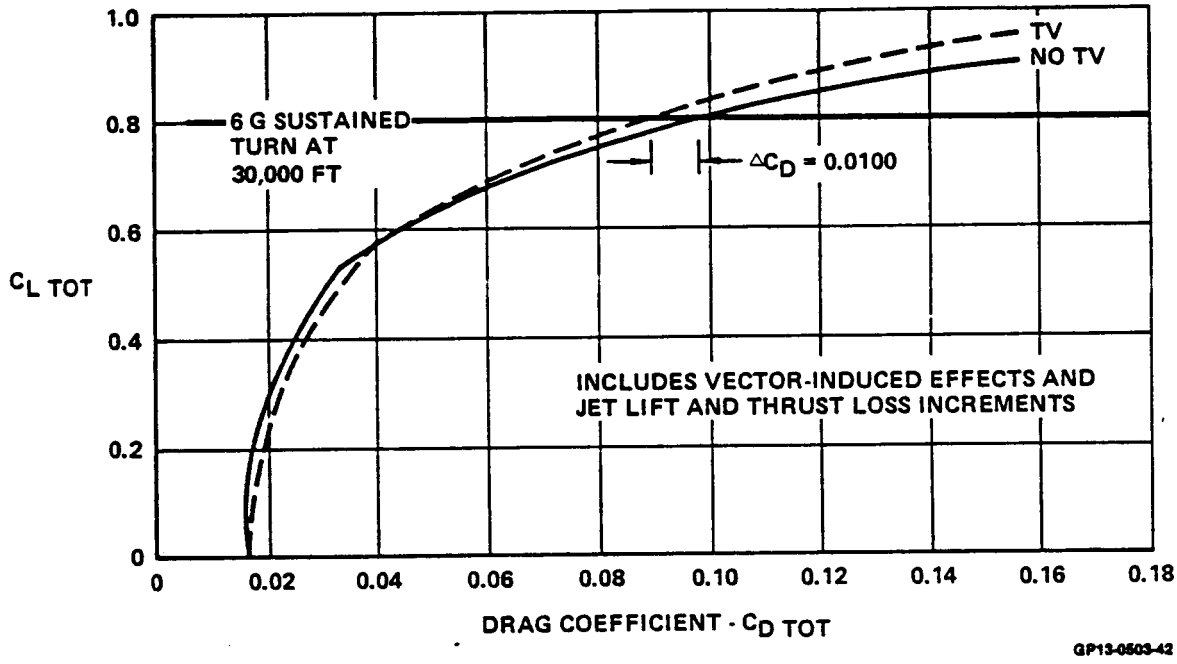

FIGURE 2-2
EFFECT OF THRUST VECTORING ON TRIMMED POLAR
ANC Estimate Air-to-Air Vehicle 15% Unstable
Mach 0.9 Max A/B ($C_T = 0.14$)

The level of geometric coupling fore to aft is dictated by the nacelle length. In the baseline configuration, the nacelle length was established by the size requirements of the close-coupled canard and wing. The related length of the inlet duct is equivalent to approximately four engine face diameters. The resulting nacelle length is 54% of the overall aircraft length. Comparing to the F-15, which is generally regarded as a "far-coupled" installation, the inlet duct length is about seven engine face diameters, and the nacelle length is approximately 65% of overall aircraft length. Since both the study baseline configuration and the F-15 are nearly equal in overall length, the nacelle of the close-coupled baseline is about 20% shorter than the F-15.

To achieve a more closely coupled configuration, the inlet duct was shortened to about one engine face diameter in length. This ultra close-coupled configuration is shown in Figure 2-3. The nacelle length is about 30% shorter than the baseline. Considering propulsion system requirements alone, the decreased duct length is practical since the duct is straight. The only other change to achieve the modified configuration is to remove the canard. The shorter nacelle length precludes a nacelle-mounted canard, unless the wings are changed.

Testing of both the selected baseline and modified configurations should provide an excellent approach for achieving the high level of propulsion/airframe coupling considered necessary to fulfill program objectives.

2.2 SIMULATED V/STOL CONFIGURATION - The viability of the selected baseline aerodynamic configuration as a supersonic V/STOL fighter was assessed in proposal studies through sizing analyses on a deck launched intercept (DLI) mission. Three different V/STOL propulsion systems were evaluated as candidates. One was selected as a study baseline to allow development of the aerodynamic performance at inlet/nozzle flow conditions which are

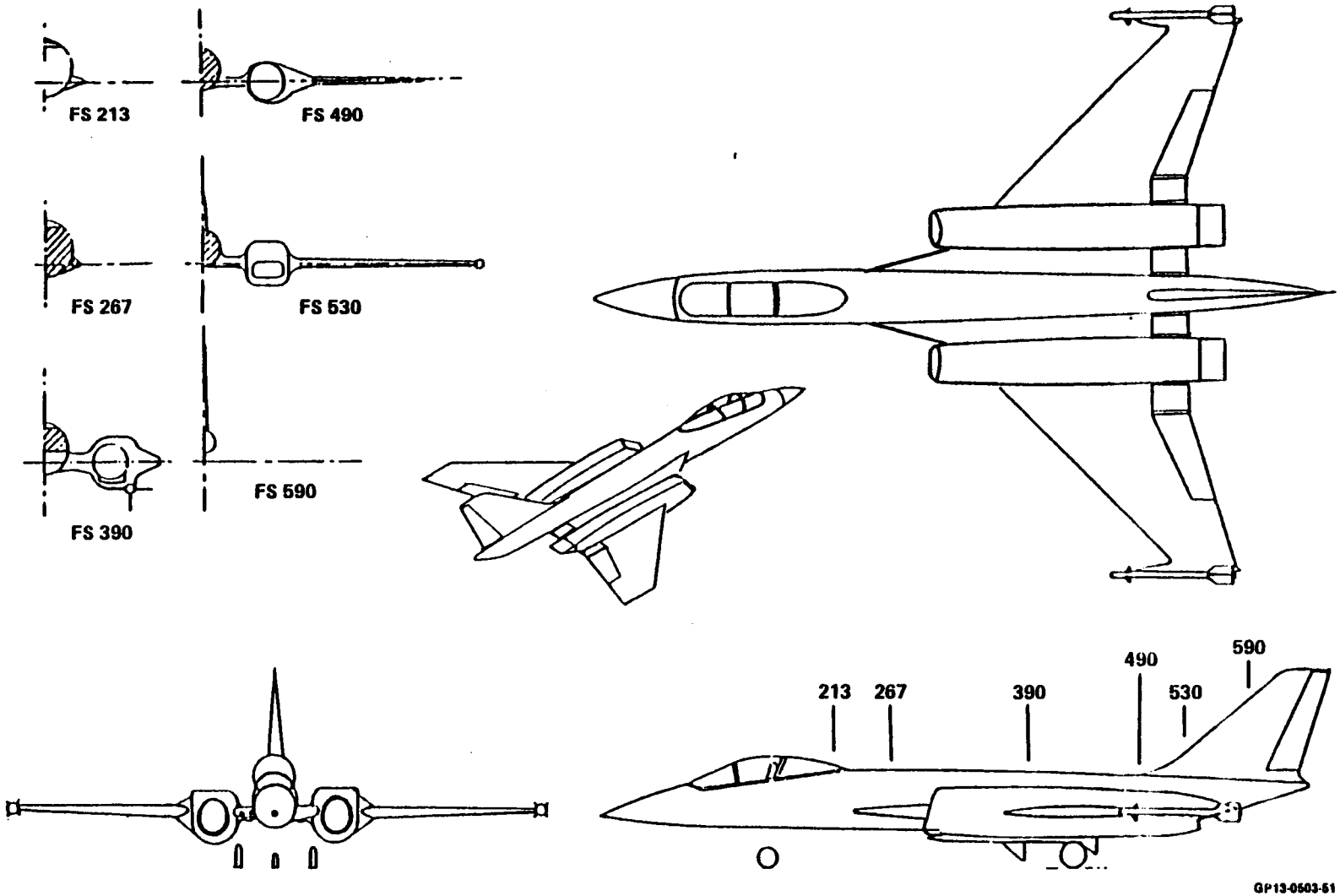

FIGURE 2-3
STUDY ULTRA CLOSE-COUPLED (MODIFIED) CONFIGURATION

consistent with a representative V/STOL system. Selection criteria were twofold; (1) compatibility of the required model scale for the V/STOL candidate with model hardware available from the ANC program, and (2) capability of the CMAPS to match the operating characteristics of the candidate lift/cruise engine.

Based on the sizing studies and other noted considerations, a lift plus turbofan lift/cruise configuration, Figure 2-4, was selected as the study V/STOL concept for test simulation. The scale of a CMAPS-equipped wind tunnel model of this V/STOL configuration would be set by matching the maximum airflow of the CMAPS to the maximum engine airflow (normally the sea level static condition). Specifically, the model scale factor is determined as follows:

$$\text{Scale Factor} = \sqrt{\frac{\text{Max CMAPS Compressor Corrected Airflow}}{\text{Max Engine Corrected Airflow}}}$$

Application of this relationship to the turbofan lift/cruise concept results in a model scale of 9.62%.

A comparison of the key geometric parameters of the scaled V/STOL configuration with the existing ANC model is provided in Figure 2-5. The model airframe parameters (i.e. wing, canard, fuselage, nacelle) are somewhat larger than would be required for the properly scaled V/STOL concept, as is the inlet capture area. The nozzle throat areas are essentially correct. It is planned to modify the ANC model inlet for the NASA program to reduce the capture area to the properly scaled value (5.46 in^2).

An external geometry comparison of the modified (smaller inlet area) model and the lift + lift/cruise V/STOL configuration at 9.62% scale, Figure 2-6, shows that the ANC model is an excellent representation of the V/STOL concept. The propulsion system components are properly scaled in the model, as well as the relative location of the canard/inlet and wing/nozzle.

		Characteristics		
		Wing	Canard	Vertical Tail
S (ft^2)		448	85	88
AR		3.5	3.0	1.0
λ		0.25	0.25	0.33
b (ft)		39.6	16.0	9.4
C_R (in.)		217.1	102.0	169.2
C_T (in.)		54.2	25.2	56.4
$\bar{c}$ (in.)		152.0	72.0	122.4
$\bar{y}$ (in.)		95.0	38.4	46.8
Λ_{LE}		45°	45°	50°
Airfoil Section	C_R	64A006	64A006	64A005.5
	C_T	64A003	64A003.5	64A003.5

Total Fuel = 10,866 lb
Total Wetted Area = 2,197 ft^2
$S_{max} - A_C$ = 35.3 ft^2 Fuselage Less Wing

Armament and Radar
(1) 25 mm Gun and 400 Rounds Ammo
2 MRM + 2 SRM
28 in. Radar

	Landing Gear	
	Nose Gear	Main Gear
Tire Size	18 x 4.4 6 Ply	24 x 7.7 4 Ply
Stroke	10 in.	10 in.
Pressure	120 psi	200 psi

	Propulsion
Engines	(2) P & WA Mixed Flow Turbofans
	(2) Advanced Direct Lift Engines
L/C FNSLSI (ea)	19,630 lb
DLE FNSLSI (ea)	10,800 lb · 90°F Day
Nozzles	L/C: ADEN · DLE: Eye Lid
Inlet	Normal Shock, A_C = 4.2 ft^2

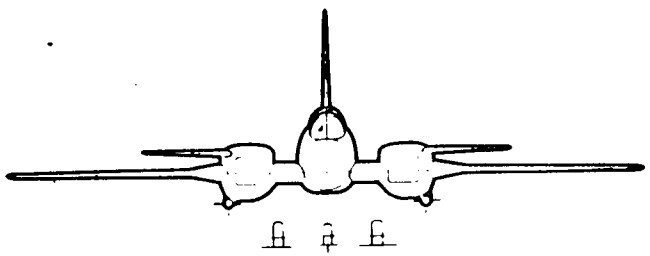

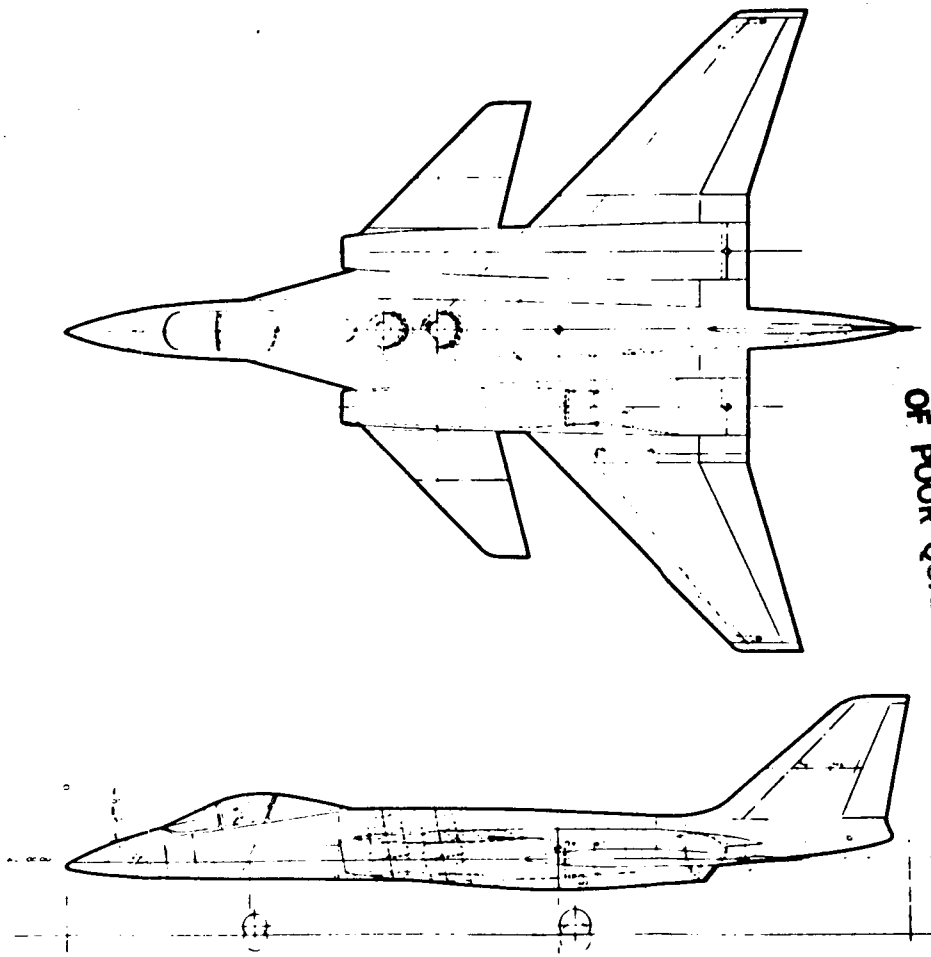

FIGURE 2-4
SUPERSONIC V/STOL CONFIGURATION LIFT PLUS TURBOFAN LIFT/CRUISE CONCEPT

	SUPERSONIC V/STOL L + L/C TURBOFAN AT 9.62% SCALE	ANC AIR-TO-AIR MODEL
OVERALL FUSELAGE LENGTH	5.63 FT	5.88 FT
NACELLE LENGTH	2.59 FT	2.83 FT
WING SPAN	3.81 FT	4.28 FT
WING AREA	4.15 FT^2	5.22 FT^2
CANARD AREA	0.79 FT^2	1.02 FT^2
INLET CAPTURE AREA	5.27 $IN.^2$	5.67 $IN.^{2*}$
NACELLE MAXIMUM AREA	16.7 $IN.^2$	18 $IN.^2$
NOZZLE THROAT AREA (DRY)	2.89 $IN.^2$	2.83 $IN.^2$
NOZZLE THROAT AREA (A/B)	5.08 $IN.^2$	5.15 $IN.^2$

*Modified to 5.46 $in.^2$ for NASA Program

GP13-0503-20

FIGURE 2-5
COMPARISON OF KEY GEOMETRIC PARAMETERS FOR SUPERSONIC V/STOL SYSTEM AND ANC MODEL

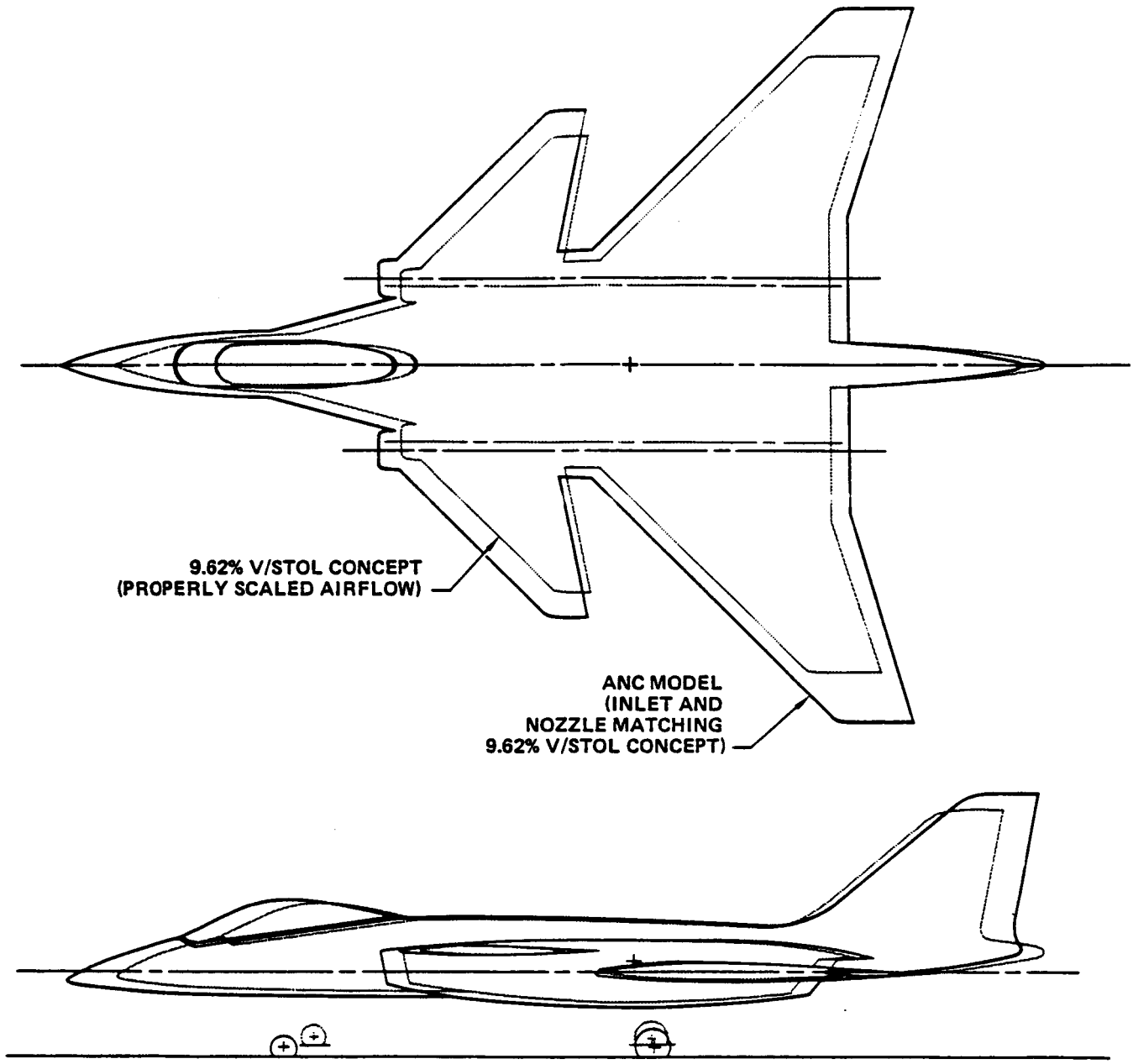

FIGURE 2-6
EXTERNAL GEOMETRY COMPARISON BETWEEN ANC MODEL AND 9.62% V/STOL CONCEPT

3.0 OVERALL TESTING APPROACH

The overall testing approach and associated data requirements were established early in the program to ensure a proper groundwork for fulfilling the major program objective. Basically, the major objective is to measure propulsion/airframe interactions using the propulsion simulator and conventional model techniques.

3.1 BASIC DATA REQUIREMENTS - The basic data requirements are set by the need to measure the inlet/airframe and nozzle/airframe interactions, and to assess the extent to which these interactions are coupled together. Here, the term basic data requirements refers to the "end product" data by which the interactions are quantified. If inlet/nozzle flow coupling exists, the inlet/airframe interactions measured by the conventional flow-through model with a "constant nozzle condition" will not agree with the interactions measured with the simulator and a "variable nozzle condition." Likewise, the nozzle/airframe interactions measured by the conventional jet-effects model with a "constant inlet condition" will not agree with the interactions measured with the simulator and a "variable inlet condition." The basic data requirements for the two test techniques, in terms of total vehicle aerodynamic coefficients, are therefore as illustrated in Figure 3-1. If the level of disagreement between conventional and simulator equipped models (left and right hand sides of Figure 3-1) is significant, simulator testing may be required.

Utilizing the basic set of data (Figure 3-1), the two types of testing can be compared either in terms of propulsion/airframe interactions or overall aerodynamic performance. The interaction comparisons are between either of the conventional modes and the simulator mode, and are quantified as illustrated in Figure 3-2.

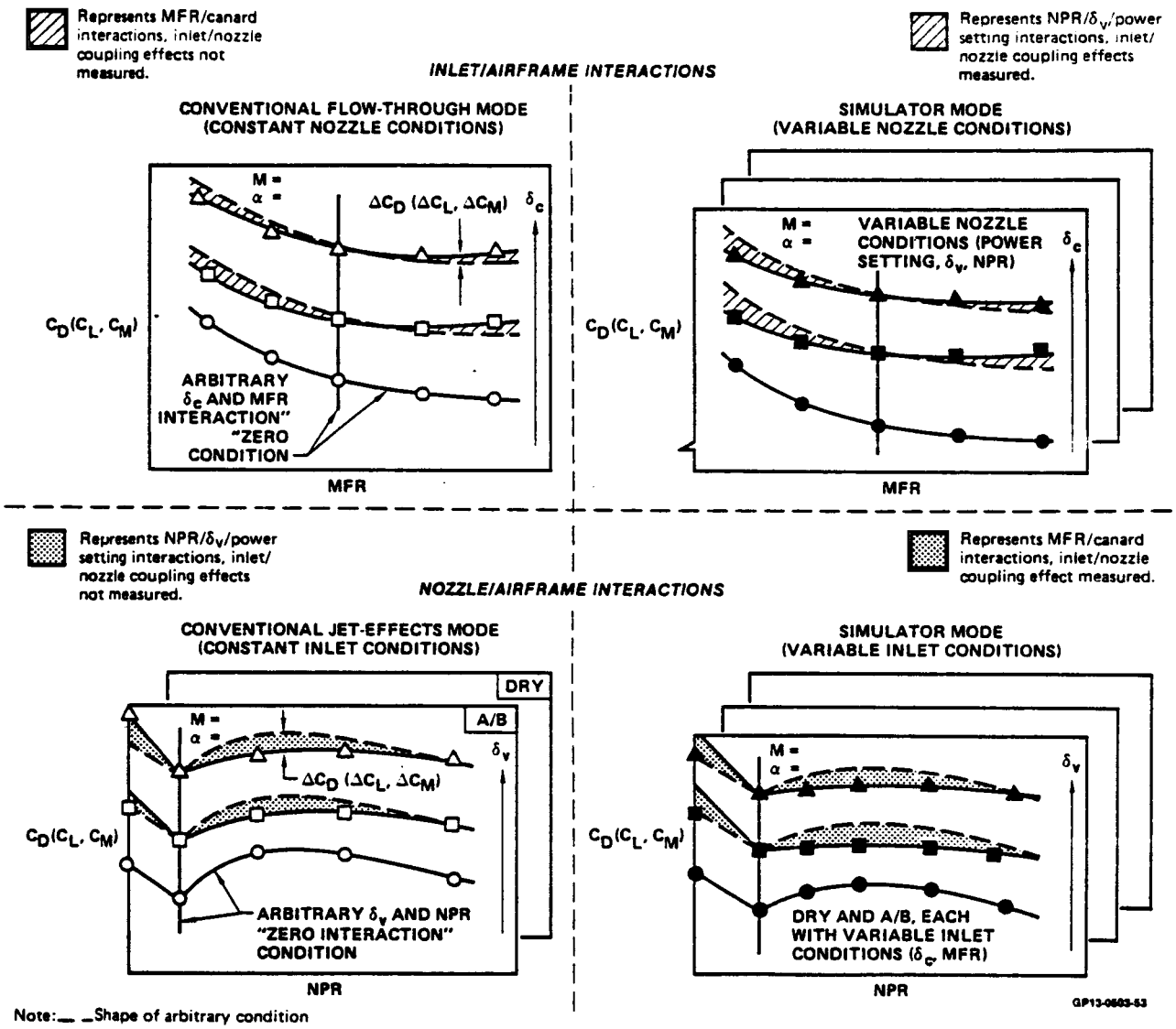

FIGURE 3-1
BASIC DATA REQUIREMENTS FOR MEASUREMENT OF PROPULSION/AIRFRAME INTERACTIONS

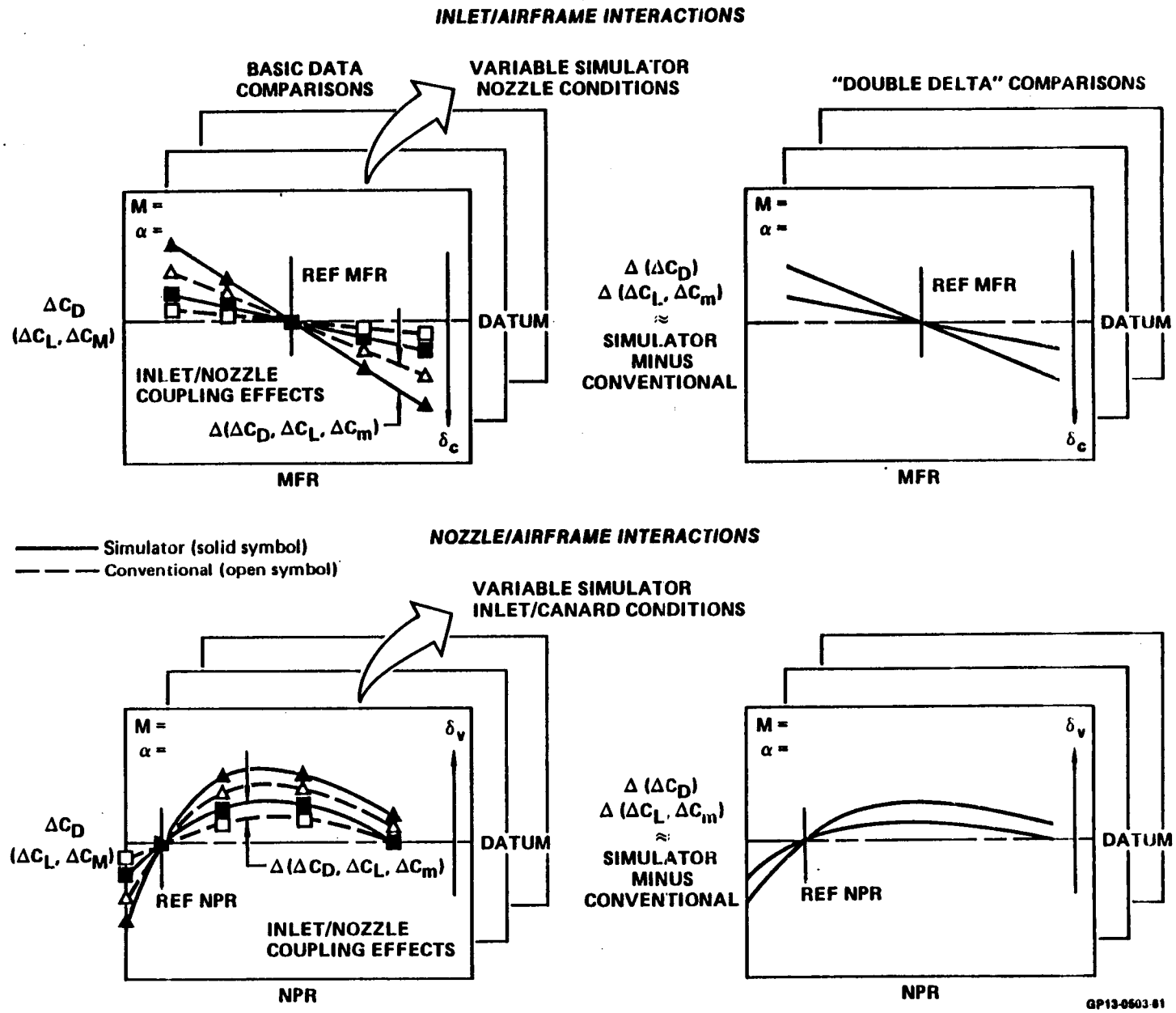

FIGURE 3-2
COMPARISON OF PROPULSION/AIRFRAME INTERACTIONS

The full impact of any differences in the interactions is probably most visible from overall aerodynamic performance comparisons. This involves combining the flow-through and jet-effects data, using appropriate inlet and nozzle "reference conditions", for comparison to the simulator data. Here, comparison of trimmed drag polars is of most interest, as illustrated in Figure 3-3.

It should be noted that all test mode data comparisons are not expected to take the relatively simple form illustrated in Figures 3-1 through 3-3. Other comparisons will also be of interest, such as those between vectoring induced lift, drag, and moment increments, external pressure distributions, and pitching moment characteristics. In the foregoing discussion, the fundamental approach for comparisons was presented; the actual data elements will be dictated by the observed data levels and trends.

3.2 OVERALL MODEL CONCEPT - Valid and meaningful measurement and comparison of the interactions and overall performance implies at least two major requirements for the model approach: (1) test technique biases must not enter into the comparisons and (2) appropriate inlet and nozzle reference conditions must be established.

3.2.1 Elimination of Test Technique Bias Sources - There are two major possible sources of bias errors. These are due to support system and metric arrangement differences between test modes. The obvious solution to eliminate these bias sources is for the support system and metric break locations to be common in all test modes. This is the model approach to be used in the program.

a. Support System Selection - Selection of a common support system concept for all test modes is dictated by several requirements. Of these, three predominate:

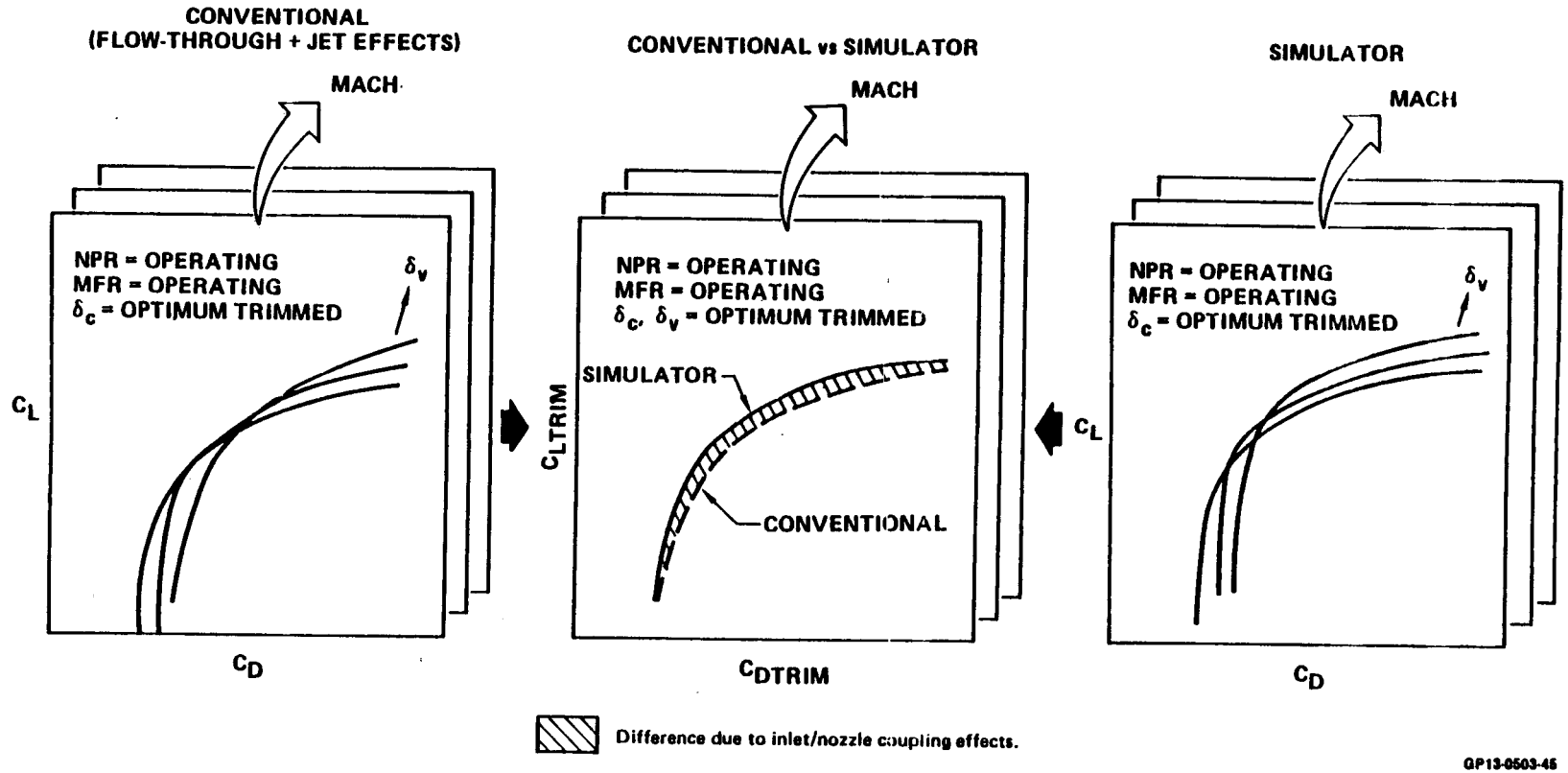

FIGURE 3-3
COMPARISON OF OVERALL AERODYNAMIC PERFORMANCE

(1) Adequate volume to contain drive, bleed, and instrumentation lines for two CMAPS units, plus strength to sustain loads at angles of attack up to 25° at high q levels.

(2) Minimum interference, particularly in the nacelle and wing regions, where aerodynamic interactions are of most interest. This must take into consideration the requirement for future low speed testing up to 90° angle of attack.

(3) Feasibility for adaptation to other types of configurations.

There were four fundamentally different types of support systems considered, as illustrated in Figure 3-4. They were (1) wing tip, (2) upper fuselage mounted strut, (3) lower fuselage mounted strut, and (4) rear entry sting.

Wing tip mounting was not considered feasible because the high volume requirements for CMAPS air would have distorted the wing considerably all along the span. This would conflict with proper measurement of interactions involving wing supercirculation effects due to vectoring. Further, flexibility to adapt a wing tip support to other configurations makes this approach unattractive.

The upper fuselage mounted strut is attractive for high angle of attack testing. However, for the selected test configuration, which has the inner wing attached low on the fuselage, CMAPS air routing from the upper fuselage to the low inner wing was virtually impossible without excessive fuselage distortion and model complication.

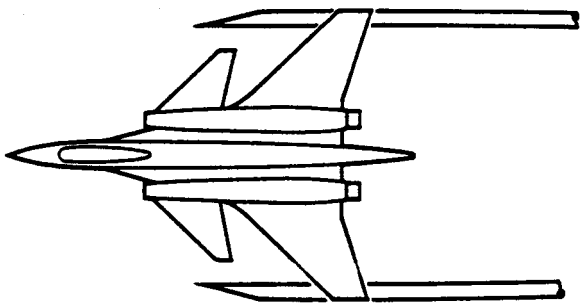

WING-TIP SUPPORT

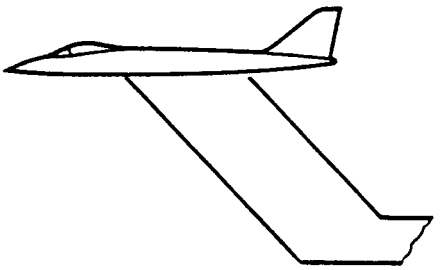

LOWER FUSELAGE
MOUNTED STRUT

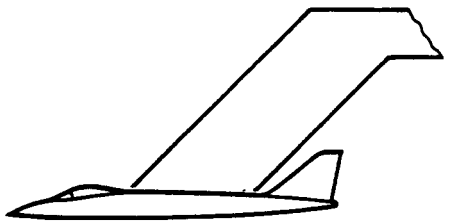

UPPER FUSELAGE
MOUNTED STRUT

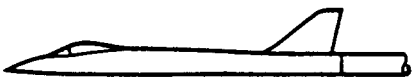

REAR ENTRY STING

FIGURE 3-4
TYPES OF SUPPORT SYSTEMS

GP13-0503-46

The lower fuselage mounted strut was given strong consideration. In fact, it is the support system being used for tests of this model in the ANC program. It is compatible with the fuselage/wing arrangement of the test configuration, and does not interfere with the vertical tail. The major drawbacks are that the fuselage interference effects at high angle of attack may become excessive.

A direct rear entry sting is the type of support system used for most force and moment testing on conventional flow-through models. It is probably the best system for high angle of attack testing; and it is generally regarded as the lowest interference support system, although very often the aft fuselage must be distorted for sting entry. In fact, this is the major disadvantage of the direct rear entry sting on the selected test configuration. Excessive aft-fuselage distortion would be required to accommodate the support of the model plus volume for air lines and instrumentation.

The selected support system is a compromise between the lower fuselage mounted strut and the direct rear entry sting. Details of the aerodynamic design are shown in Figure 3-5. Adequate volume and strength are provided in the same maximum thickness (2.25" near the model) that is required for the lower fuselage mounted strut. However, elimination of the vertical "blade" portion of the strut acts to reduce interference at high angles of attack. The major disadvantage compared to the other candidates is probable increased interference at low angles of attack. However, the interference effects should be confined largely to the lower aft fuselage area, which is removed from the wide-spaced nacelles and outer wing regions where the interaction effects will predominate.

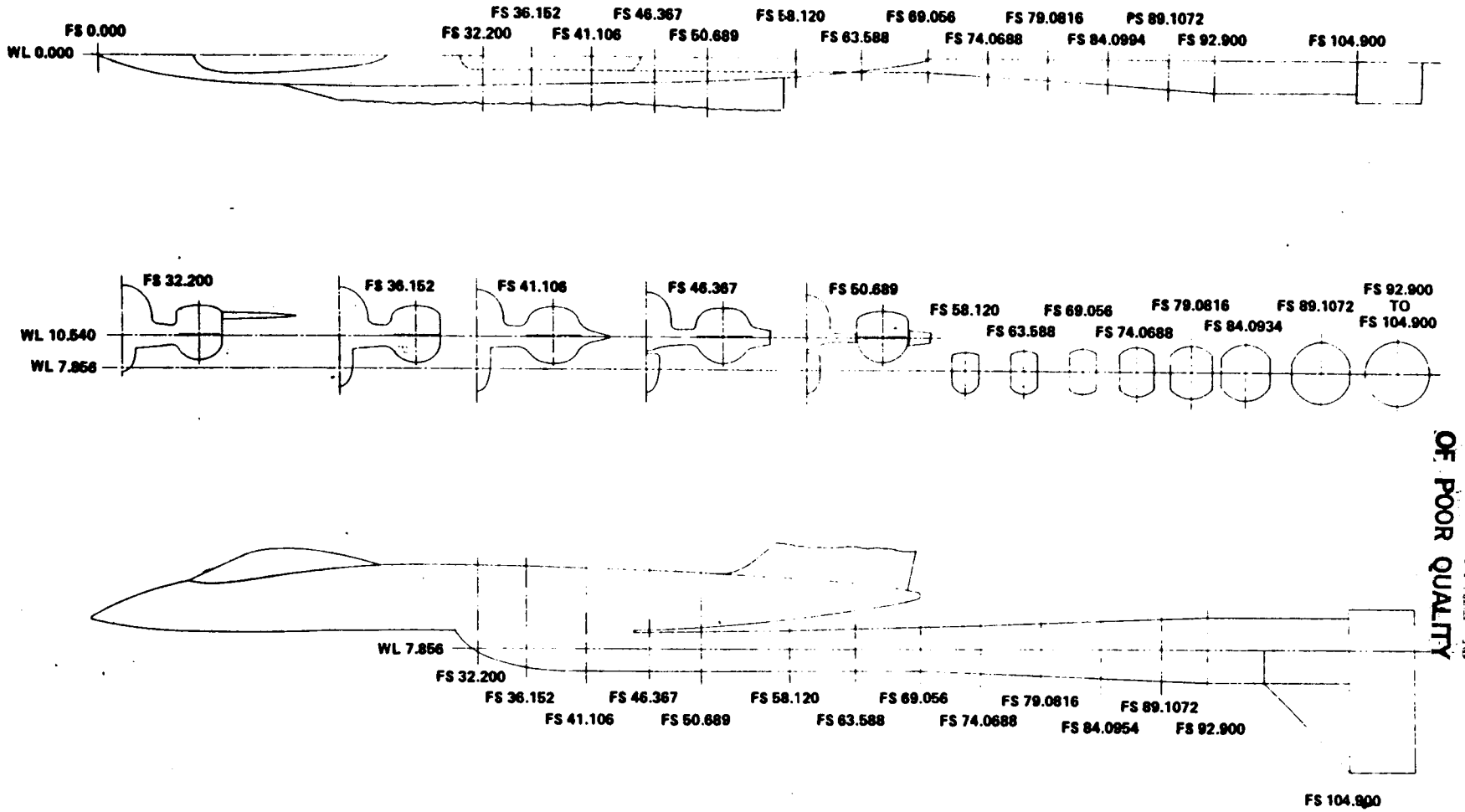

FIGURE 3-5
AERODYNAMIC DESIGN OF SUPPORT SYSTEM

GP13-0003-36

b. Metric Arrangement Selection - The main requirements of metric arrangement selection were for measurement of external aerodynamic interactions on the complete configuration, and non-metric mounting of the simulator units and nozzles (i.e. no exit gross thrust on the metric portion of the model). These requirements dictated that the airframe "skin" components be metric in all test modes. A partially metric jet-effects mode, which is common practice, could have been a candidate. However, if aft-body flowfield changes (e.g. due to vectoring) reached the non-metric forebody and were not measured, then the comparisons between simulator and conventional modes would reflect test technique bias, not true interaction effects.

The selected metric arrangement concept is characterized by a single balance system with three metric break locations common to all test modes. The concept is shown in Figure 3-6. The external aerodynamic forces are measured by a single internal balance attached to the aircraft skin, except for the nozzle boattail, and by 52 pressure taps located on the nozzle boattail surface. The CMAPS and nozzle (external and internal surfaces) are therefore non-metric in the simulator mode, the jet-effects internal ducting and nozzle are non-metric in the jet-effects mode, and the internal duct aft of the simulator face station and choke are non-metric in the flow-through mode.

There were two major reasons for choosing the single balance system. First and most important, this approach fully satisfied the program objective to measure external aerodynamic interactions. Second, compared to a multiple balance system, it is the most simple, cost effective, and lowest risk approach. This program represents the first time that two CMAPS units will be tested in a compact wind tunnel model. Internal model volume is at a premium; packaging too much hardware inside the model could result in an unreasonable amount of model development time and high risk.

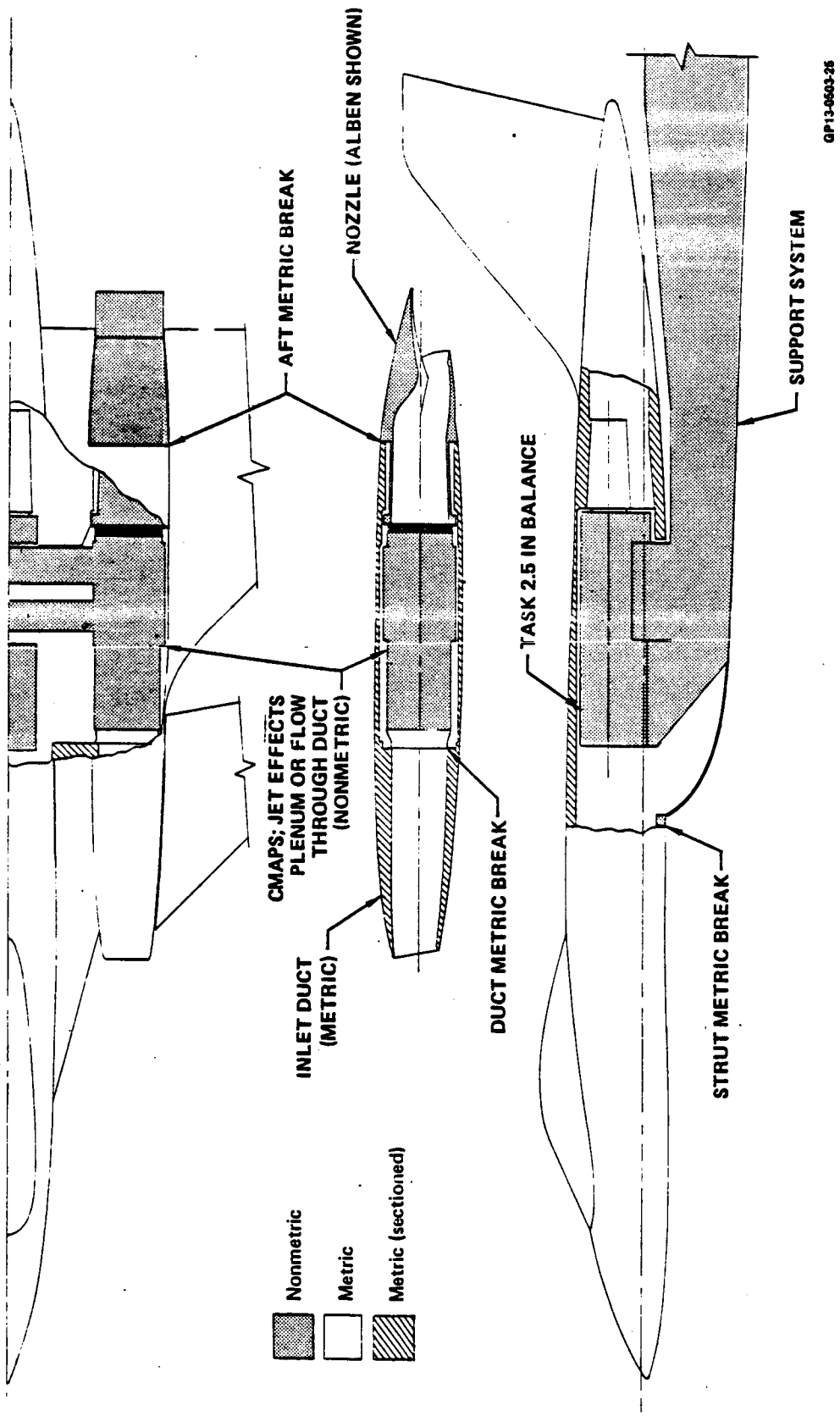

FIGURE 3-6
METRIC ARRANGEMENT CONCEPT

In the proposed metric arrangement (Figure 3-6), there are three metric breaks and three associated seals common to all testing modes. The three seal locations are at the simulator compressor face station, (duct metric break), at the beginning of the nozzle boattail (aft metric break), and between the strut and lower fuselage (strut metric break). The strut and aft metric break concepts are not new, and have been successfully employed in recent nozzle research investigations (e.g. References 2 and 5). The duct metric break is somewhat unconventional, since usual practice for conventional flow-through testing is a completely metric internal duct. However, the only practical location for the duct metric break in the simulator mode is at the simulator inlet. Here, a seal tare and a duct exit momentum tare must be determined. The duct metric break for the two conventional modes was also chosen to be at this same location. The idea is to eliminate possible bias errors due to determination of the tares at two different locations. Further details concerning the metric break configurations are presented in Section 4.0.

3.2.2 Reference Inlet and Nozzle Conditions - Specified reference conditions are required primarily for overall performance determination using data from the two conventional test modes. In common practice, the flow-through model, tested with various size chokes at the duct exit and variations in the aerodynamic control surfaces, provides the basic aerodynamic polars, trim characteristics, and drag variations with mass flow ratio (MFR). Increments from the jet-effects model (often partially metric) are applied to the flow-through data to account for operating nozzle geometry and nozzle pressure ratio (NPR). In order to apply the increments properly, a common nozzle condition must be tested on the two conventional models. The common nozzle condition is usually a flow-through model choke tested at the low NPR corresponding to a flowing inlet condition.

One problem is often neglected in this type of conventional testing. The chokes used to obtain the effects of inlet MFR on the flow-through model also produce a variable plume shape and possible variation in the flow over the nozzle boattail with MFR. If the model is fully metric, these plume effects can be misinterpreted as due to MFR variations and can cause errors in the predicted full scale performance at some MFR conditions.

Based on the foregoing considerations of bias sources and reference conditions, a testing approach concept was selected where "multipurpose" reference conditions are established which are used not only for measurement of overall performance, but for elimination of bias errors as well.

Selection of the proper reference conditions presented some unique possibilities. The concept of a single configuration common to all three test modes became attractive, particularly since the same metric arrangement is used in all modes. The need for an inlet/nozzle configuration common to the two conventional test modes is readily understandable, since there must be a method for combining the two sets of data into overall performance. In the selected testing approach, this same configuration is also tested in the simulator mode. This provides a "check" configuration to eliminate bias from model build-up. After the initial build-up in the tunnel of each mode, the common reference configuration is tested in a series of check runs over the Mach number and angle of attack range. These check runs are then compared with runs of the common configuration on the other modes. If the check run data does not agree (within some established tolerances), reasons for the discrepancies must be found and corrected.

There are not many choices for inlet and nozzle reference configurations which can be common to all three test modes. The inlet must be non-flowing (e.g. faired), since inlet flow cannot be simulated in the jet-effects mode. And since the inlet must

be non-flowing, this locks in a non-flowing reference nozzle. This is because there can be no simulation of nozzle flow in the flow-through mode if the reference inlet is also non-flowing.

The choice of the geometry for the reference non-flowing inlet was between an internally blocked or externally faired inlet. The blocked inlet would be high in drag, simulating a zero mass flow ratio condition. Based on past experience, the faired inlet has a more representative drag level. This is considered advantageous in a thrust/drag accounting system, otherwise, increments from the reference performance basis are large, resulting in increased uncertainty at the normal operating drag level. Based on these considerations, the faired inlet was chosen as the non-flowing reference inlet condition. The selected fairing shapes for the baseline and ultra close-coupled configurations are shown in Figure 3-7. The fairing shapes represent simple forward extensions of the local cowl moldline.

There are also several factors to consider in choosing the exact configuration for the non-flowing reference nozzle. If the non-flowing condition were the only requirement, almost any nozzle geometry could be used. It is best, however, to make the reference nozzle compatible with the nozzle requirements for the other testing modes. The ALBEN is not a good choice, because the flow-through mode must have an easily variable throat size to achieve MFR variations. Further, as previously discussed, it would be best to remove the effect of choke size on the external aerodynamics so that only the effects of inlet variations will be measured in the flow-through mode. This is possible if the nozzle is extended far downstream of the normal vehicle exit plane, with variable chokes at the exit. The nozzle extension at a no-flow condition is then used on the other test modes to serve as the reference nozzle geometry. This was the selected approach for the reference nozzle condition. The aerodynamic shape of the extensions are shown in Figure 3-8.

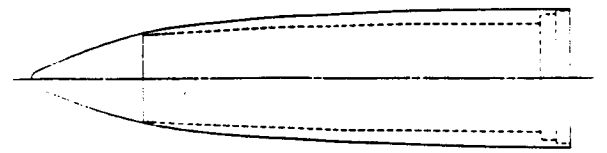

PLAN

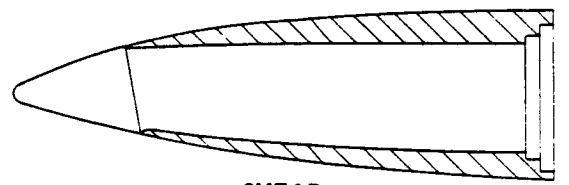

SHEAR

BASELINE INLET

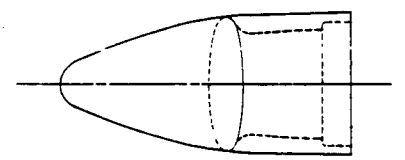

PLAN

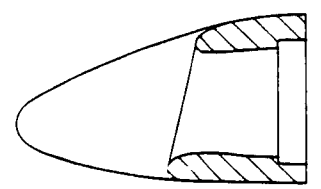

SHEAR

GP13-0603-32

ULTRA CLOSE-COUPLED (MODIFIED INLET)

FIGURE 3-7
AERODYNAMIC DESIGN OF REFERENCE INLET CONFIGURATIONS

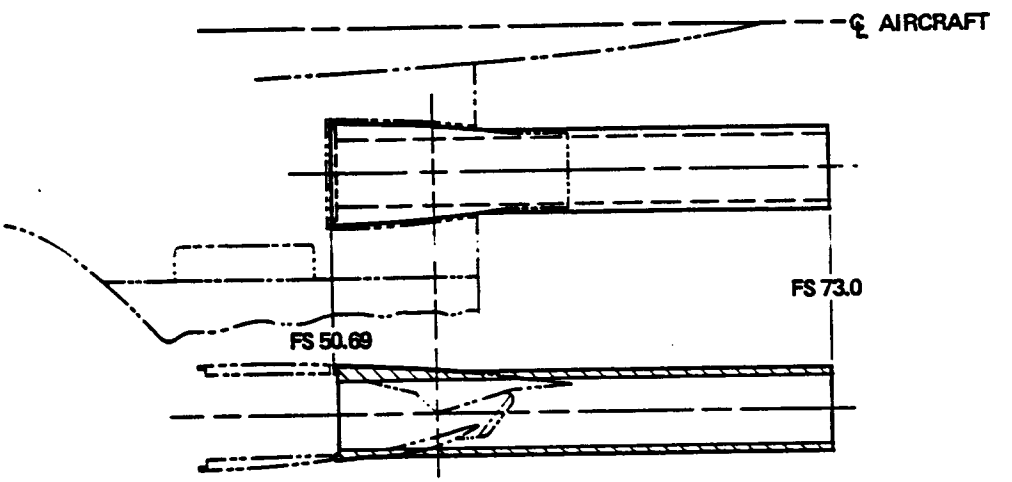

GP13-0603-52

FIGURE 3-8
REFERENCE NOZZLE GEOMETRY

The reference nozzle extensions are non-metric. The outer shape conforms to the ALBEN up to the lower flap hinge point, thus making the absolute drag level in the flow-through mode nearly representative of the actual full scale configuration. The circular internal flow path was chosen for ease of fabrication. Chokes of various sizes are placed at the exit of the extensions for flow-through testing. The extensions have the further advantage that they may be attached easily to an ejector system for low speed flow-through testing, thus making it possible to achieve the proper inlet mass flow ratio. Further discussion of the preliminary design for the nozzle extensions and ejector system is provided in Section 5.2.

3.3 SUMMARY OF TESTING APPROACH - The overall testing approach and data utilization features three key elements; (1) check runs on the common configuration, (2) comparisons of inlet/airframe and nozzle/airframe interactions between test modes, and (3) comparisons of overall performance in terms of trimmed drag polars. These elements are illustrated in Figure 3-9.

The check runs are made on the common reference configuration in each testing mode. Assuming no correctable model build-up biases are revealed by these tests, the results provide an indication of the differences due to random errors between the test modes (although without simulated propulsion flows). The polars for the common configuration also provide the reference basis for the overall performance build-up. Data from the "operating" conventional and simulator modes, with actual inlet and nozzle flows and simulated airframe variations (δ_C, δ_V), are combined with the reference configuration data to give the overall performance comparisons. The operating modes also provide the data for direct comparison of inlet/airframe and nozzle/airframe interactions.

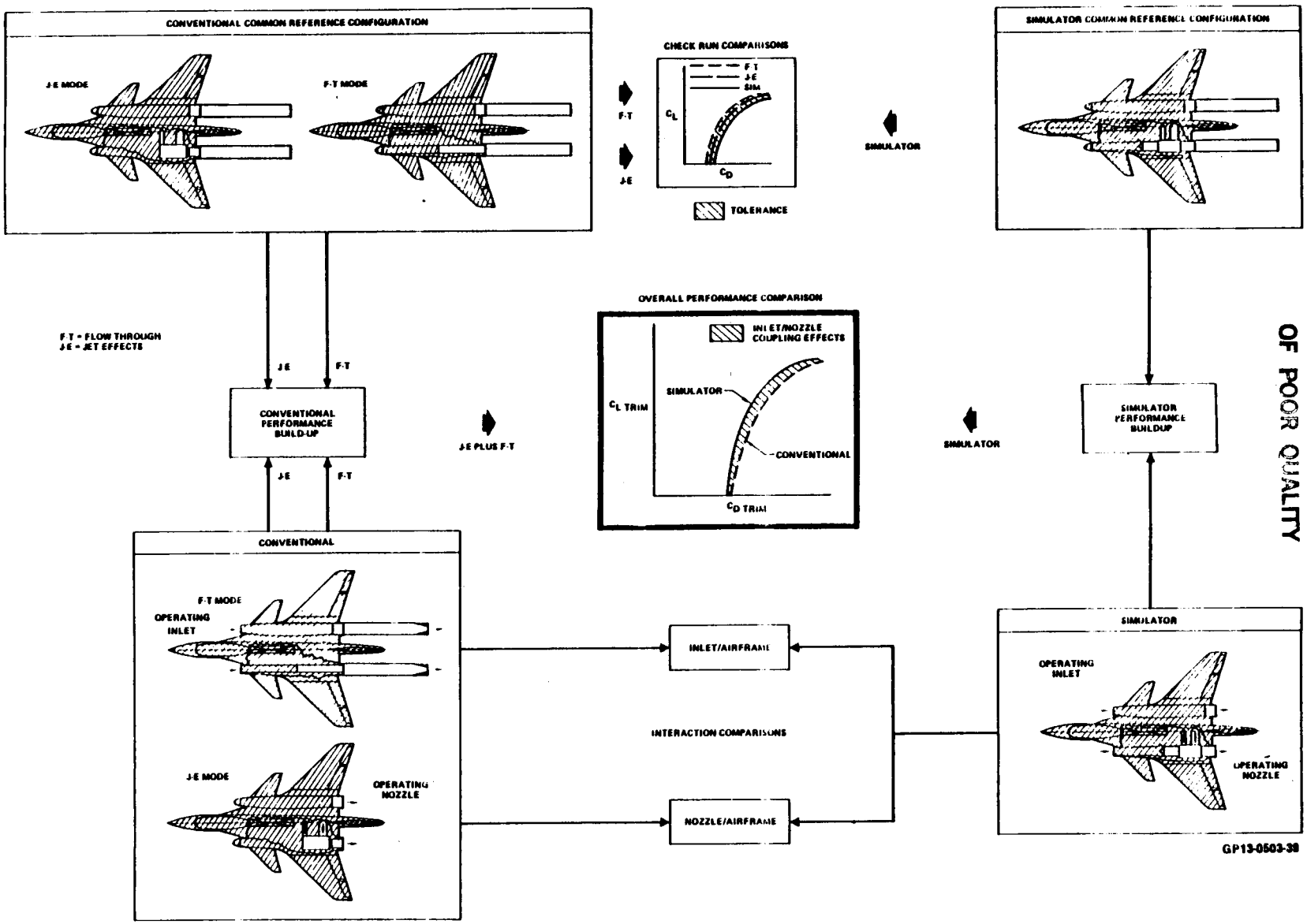

FIGURE 3-9
TESTING APPROACH SUMMARY

4.0 DESCRIPTION OF COMMON MODEL COMPONENTS

Achievement of hardware commonality in the preliminary model design received considerable emphasis in Phase 1. The key common model features, other than the fuselage/wing/canard/tail components are: (1) test mode conversion hardware, (2) metric break seals, (3) model support/tunnel installation, (4) force balance, (5) balance thermal control, (6) inlets, and (7) nozzles.

4.1 TEST MODE CONVERSION HARDWARE - A key to implementing commonality was in design of the hardware to convert from the internal "propulsion package" of one mode to another. The test mode conversion concept is shown in Figure 4-1. The only components of the model not common are the CMAPS, flow-through duct, and jet-effects air supply plenum. When converting to flow-through, the CMAPS units are replaced with a section of straight duct; when converting to jet-effects, the CMAPS units are replaced with the high pressure jet-effects plenum. All nacelle hardware forward of FS 36.33 is common, including the duct metric break seal, instrumentation ring, and inlet. All nacelle hardware aft of FS 45.08 is also common, including the duct bellows, transition duct, and nozzles. The duct bellows is needed primarily for the simulator mode-acting to prevent vectored nozzle induced bending moments from loading the simulator.

The real key to the test mode conversion concept is the common support hardware. This common hardware, as seen in the plan-view portion of Figure 4-1, ensures consistent positioning of the internal non-metric and metric model components. The supports consist of the forward side mount, bleed line manifold, and the nozzle support. The forward side mount and bleed line/manifold provide consistent alignment of the duct seal, which should eliminate bias in the tare correction for this seal. The forward side mount removes torque loads and is flexible in the axial direction to allow for thermal growth. Consistent positioning at

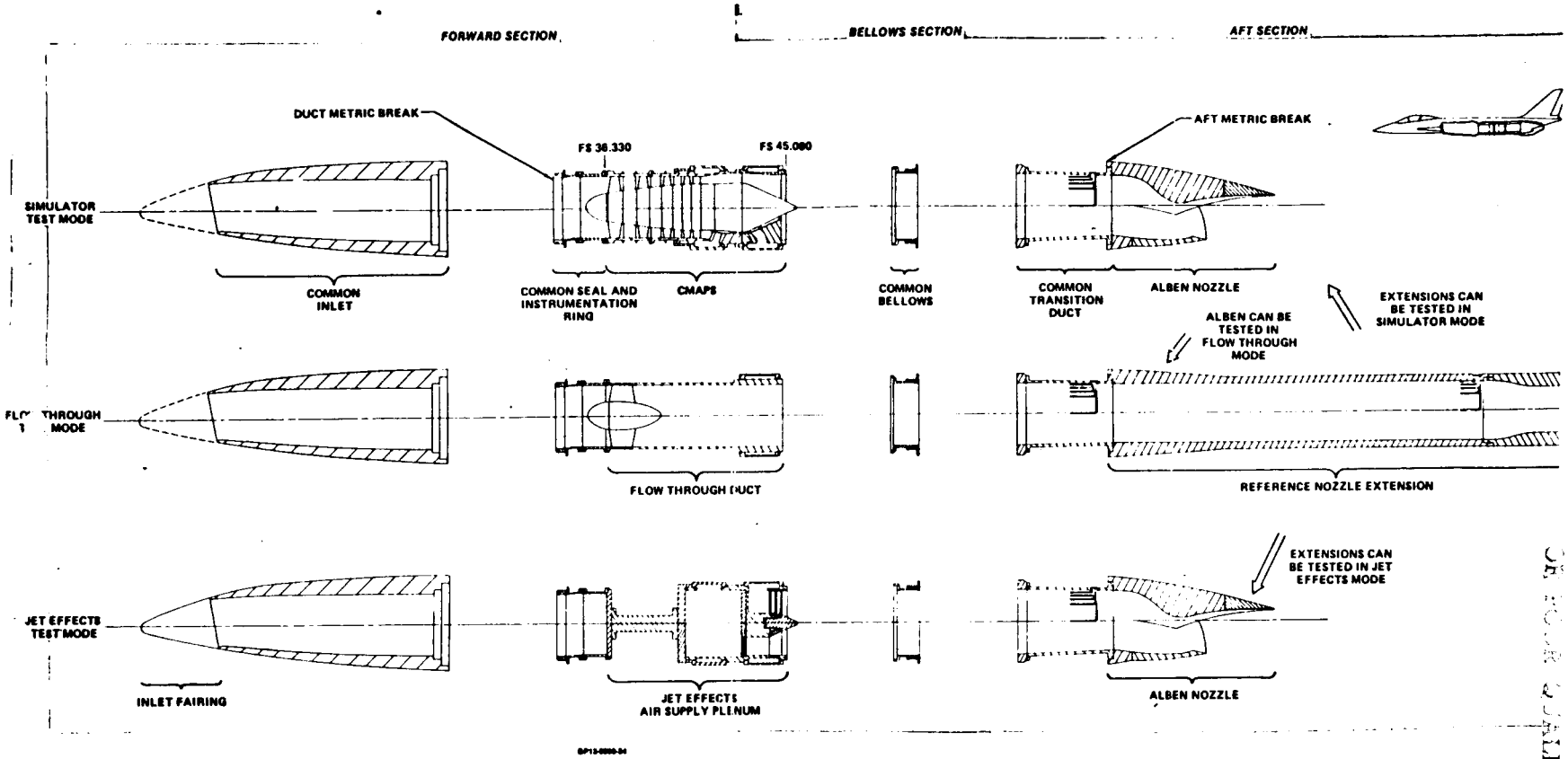

FIGURE 4-1
TEST MODE CONVERSION CONCEPT
Sheer View

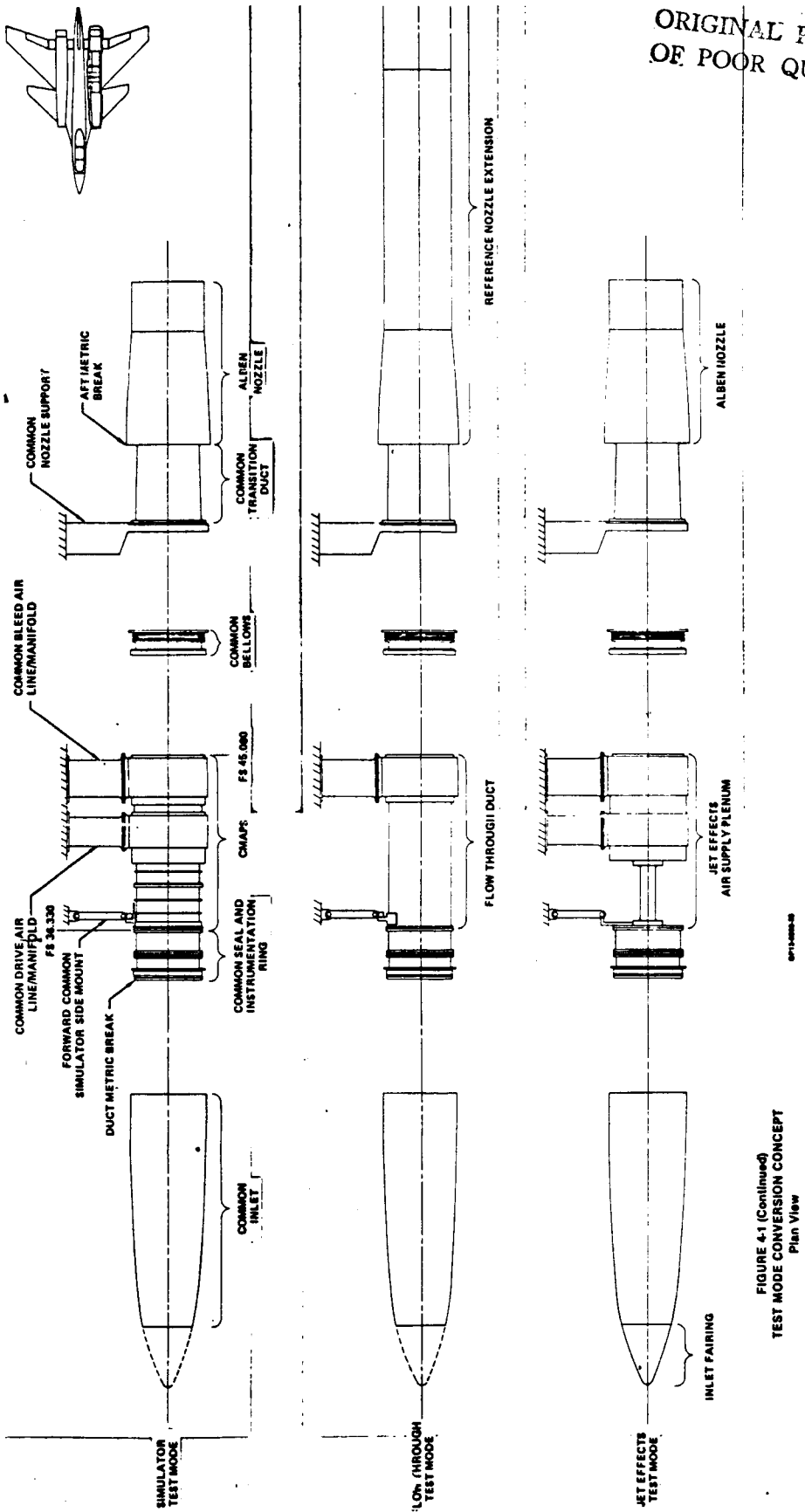

FIGURE 4-1 (Continued)
TEST MODE CONVERSION CONCEPT
Plan View

the aft metric break is provided by the common nozzle support and transition duct. This should eliminate differences in the small step at the aft metric break caused by balance deflection at angle of attack. A difference in step height at this metric break between test modes could cause a drag bias. The nozzle support also transmits the nozzle thrust and moment loads into the non-metric balance housing.

4.2 METRIC BREAK SEALS - In this model concept, the airframe components are metric and the CMAPS units and nozzles are mounted non-metrically to the strut. Accordingly, there are three distinct bridging locations between metric and non-metric hardware. These are at the (1) strut and lower fuselage (strut metric break), (2) beginning of the nozzle boattail (aft metric break), and (3) simulator compressor face station (duct metric break). Details of the metric break design, including the seals, are shown in Figure 4-2.

A thin flexible teflon seal will be used at the strut metric break. The seal is positive in that no flow enters the internal cavity through this juncture. This seal has a negligible installation effect, as evidenced in recent static loadings at AEDC prior to test of the model under the ANC program. Loadings in axial force, normal force, and pitching moment were made with and without the seal installed. There were no measurable seal effects, either to reduce balance output sensitivity or increase random error.

The aft metric break is bridged by a floating teflon seal. This is not a positive seal, but simply a restrictor intended to stabilize pressure inside the model cavity. At the start of the nozzle boattail, where the seal is located, a sizeable pressure differential can exist between top and bottom at angle of attack. Therefore, to avoid flow within the cavity, some seal or restrictor is required. The teflon seal is attached in a groove to the metric aftbody and is backed by foam in the groove (see

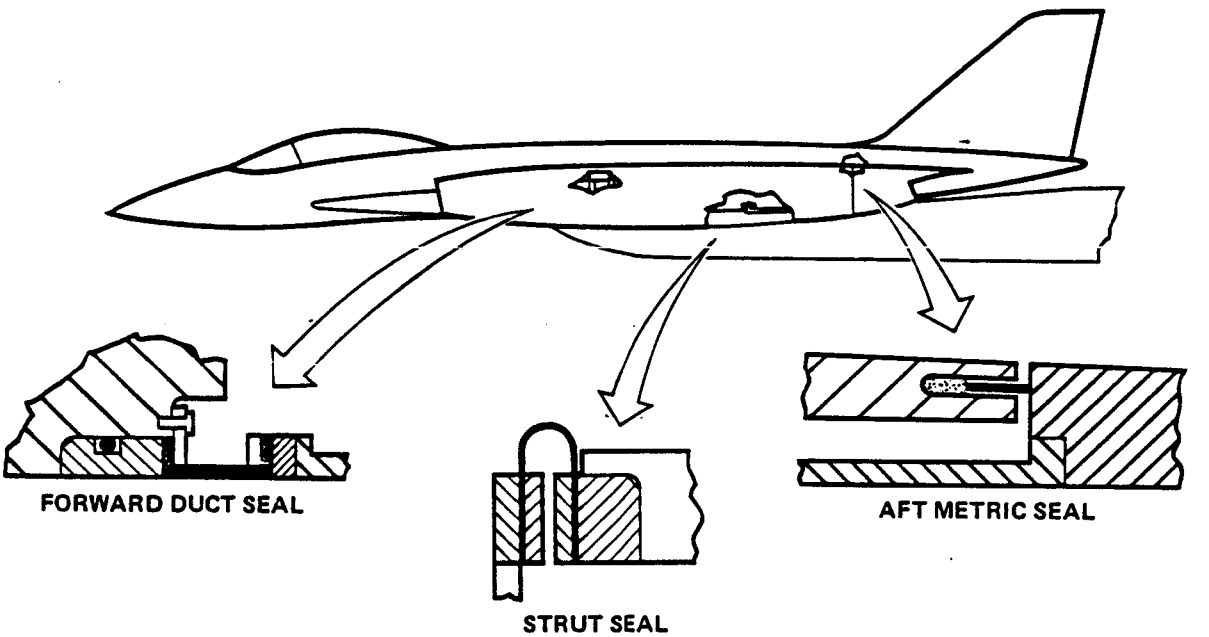

FIGURE 4-2
SEAL ARRANGEMENT

GP13-0503-21

Figure 4-2). This has the effect of "spring loading" the seal slightly against the flat surfaces of the non-metric nozzle. The non-metric, downstream side of the seal must ride on a flat surface (i.e., as opposed to another groove) because the non-metric nozzle deflects relative to the metric aftbody under vectoring loads. This seal design has also been shown to have a negligible installation effect based on the recent static check loadings of the ANC model.

The duct metric break is bridged by a Butyl rubber seal. This positive seal arrangement is the same type used on the 8.5% Simulator Demonstration Model and the 7.5% F-15 Inlet/Airframe Model (References 6 and 7). The tare force of this seal depends upon the pressure differential across it and the relative deflection between the metric and non-metric duct on either side of it (imposed by model aerodynamic loads). Successful calibrations of these effects from the two referenced programs provide experience for establishing this tare force.

Two design features have been incorporated to further ensure minimum, repeatable corrections due to the duct seal tare. One is to minimize deflection at the duct metric break, and the other is to ensure identical seal positioning in all test modes. The latter feature is provided by the mounting arrangement, as addressed in Section 4.1. To minimize the vertical downward offset which results from balance deflections at high α (large pitching moments), a .050 inch upward vertical offset is incorporated in the basic design. The variation in offset with angle of attack will thus be as shown in Figure 4-3. At low α, where the air loads produce very little deflection, a small upward offset (.05 in. maximum) will exist. As the model is pitched to nominal maneuvering α (10°-12°) and additional deflections occur, near zero offset will occur. At even higher α test conditions, a small negative downward offset (.05 in maximum) will exist between the inlet duct and simulator. The maximum offset over

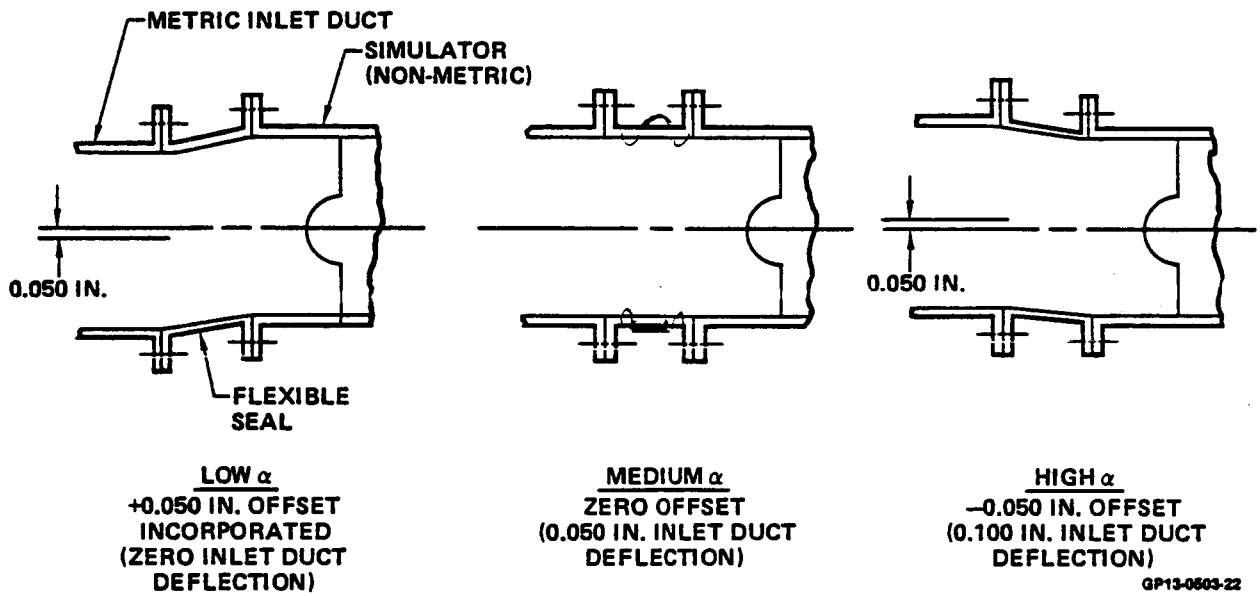

FIGURE 4-3
DEFLECTION VARIATION AT DUCT METRIC BREAK

the test angle-of-attack range is therefore limited to the .050 inch deflection. A deflection of this same value, experienced on previous models, caused no problems.

4.3 MODEL SUPPORT/TUNNEL INSTALLATION - The emphasis of this program is to evaluate the airframe/propulsion system interactions in the conventional wing borne flight mode. An installation in the Ames 11-foot Unitary Plan Wind Tunnel has been defined to conduct this evaluation. There is also interest in assessing low speed interaction effects at angles of attack up to 90°, where vectored thrust must be used for control. Testing at these conditions would be conducted in a future test program in the Ames 12-Foot Pressure Wind Tunnel. A conceptual installation for the 12-foot tunnel testing has also been defined.

4.3.1 Ames 11-Foot Tunnel Installation - The support system was designed consistent with (1) a test Mach number range from 0.3 to 1.4, (2) a constant tunnel Reynolds number of 2.5×10^6 per foot, (3) angle of attack capability from -5° to +25°, and (4) minimum buoyancy effects from the support system.

The test Mach number range covers the operating range available in the 11-foot tunnel. The test Reynolds number was selected as a compromise between the desire to operate at the highest dynamic pressure possible and model and support system strength considerations. The tunnel dynamic pressure and total pressure corresponding to this Reynolds number is shown in Figure 4-4. Angle of attack capability up to 25° should cover the conditions of primary interest for conventional V/STOL flight attitudes.

A tunnel installation was defined consistent with these operating requirements. The installation, Figure 4-5, consists of the Ames 40 inch extension and 10° canted adapter, and a new tapered adapter, offset adapter, and sting support. The maximum bending moment for the installation is within the 800,000 in-lb moment limit of the tunnel sector.

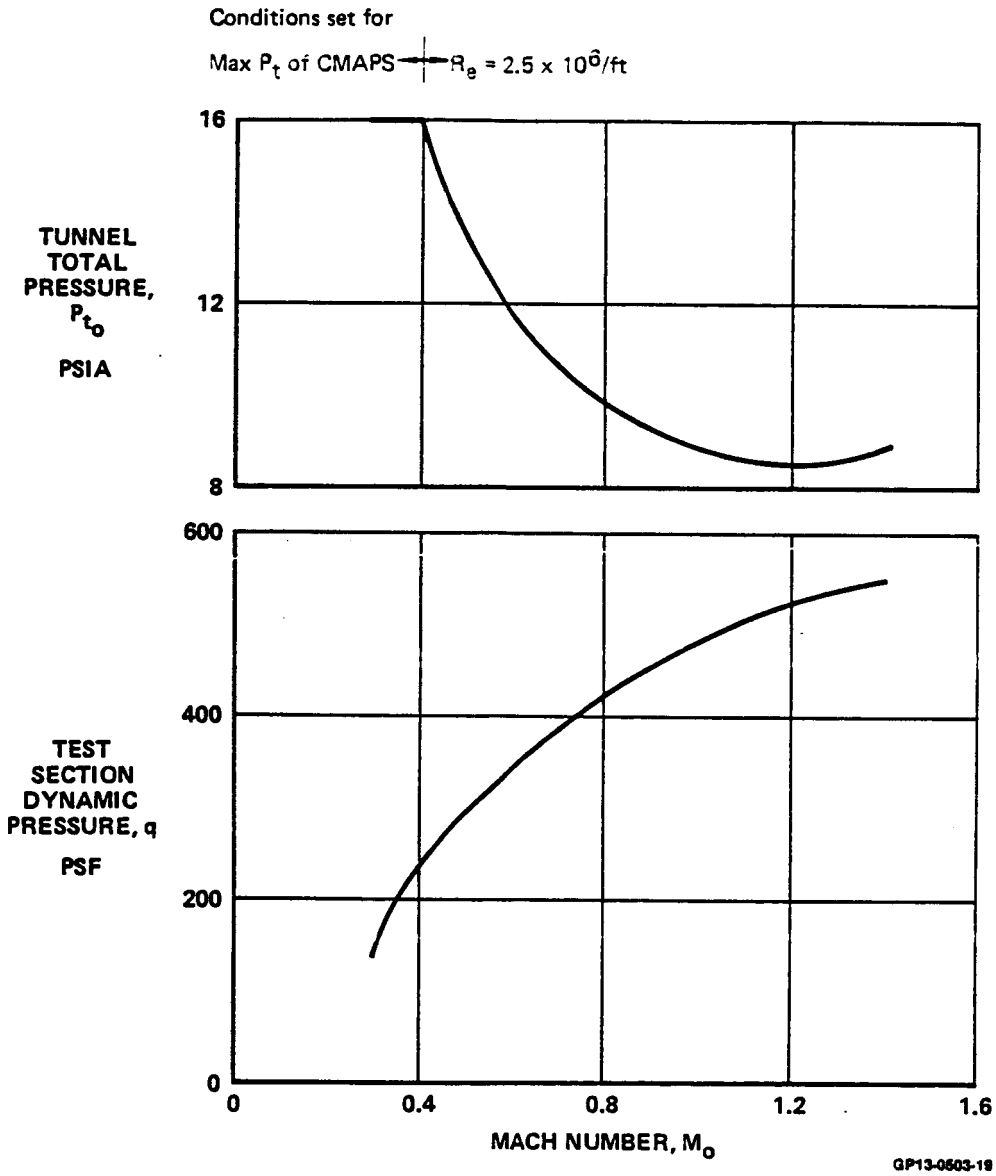

FIGURE 4-4
PLANNED TEST OPERATING CONDITIONS IN NASA/AMES 11 FT UNITARY TUNNEL

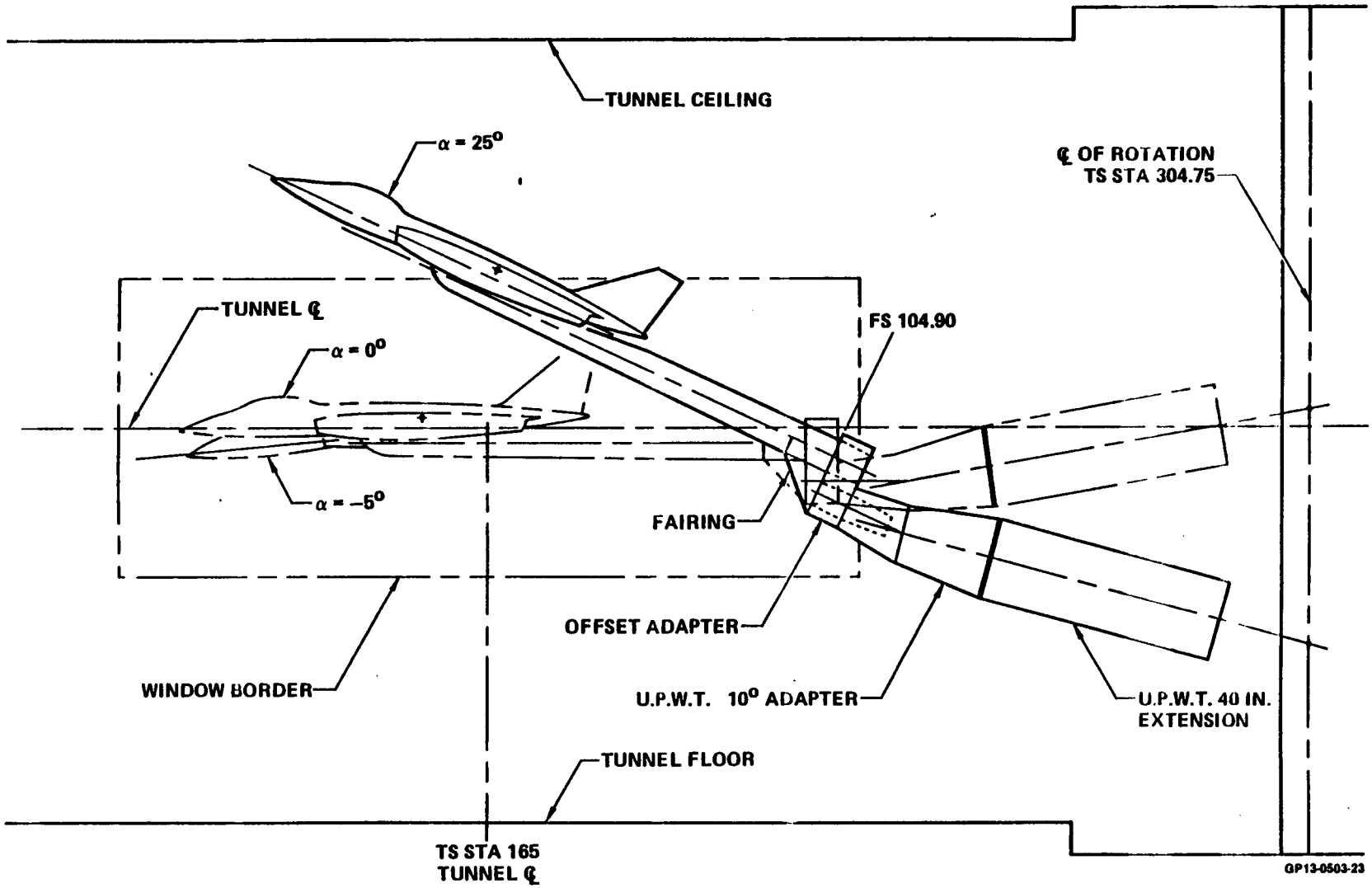

FIGURE 4-5
MODEL INSTALLATION IN THE NASA/AMES 11 FT UNITARY WIND TUNNEL

The model sting length was selected to minimize the buoyancy effect of the offset adapter on the model. The effect of the adapter was analyzed using a MCAIR-developed program for analyzing subsonic and transonic flow about 3-D bodies (Program AFTEND). The analysis was performed for two different sting lengths. The shorter sting length is compatible with both the 11-foot tunnel installation and high angle-of-attack testing (40° to 90°) in the 12-foot low speed tunnel. The longer sting represents an estimate of the required length to minimize the effect of the adapter, as determined from AEDC sting interference test results, Reference 8. For comparison, a baseline sting installation without the offset adapter was also analyzed. Results are shown in Figure 4-6 in terms of incremental pressure coefficient (ΔC_p) from the baseline for the short and long stings.

The offset adapter with the short sting produces a C_p rise of approximately 0.02 on the model aftbody up to the metric break, which converts to a drag error for both nozzles of about 6 counts. In this calculation, the .02 ΔC_p value was applied to the projected area from the aft metric break to the nozzle exit. The C_p increase with the short sting was considered unacceptable. There is no discernible pressure rise from the adapter felt on the model with the longer sting. Based on this analysis, and in concurrence with the NASA project engineer, the longer sting has been selected for the program.

4.3.2 Ames 12-Foot Tunnel Installation - NASA-Ames is currently planning to modify the 12-foot tunnel; the extent of this modification is not totally defined. However, a conceptual installation has been defined using the current AMES pitch system, Figure 4-7. With this installation, angle of attack testing up to 90° would be conducted in two steps. For angles of attack from 0° to 40°, the installation consists of an existing NASA adapter, a new tapered adapter, and the 0° offset adapter used in the 11-foot installation. For the testing to 90° angle of attack, another tapered adapter will be provided between the 0°

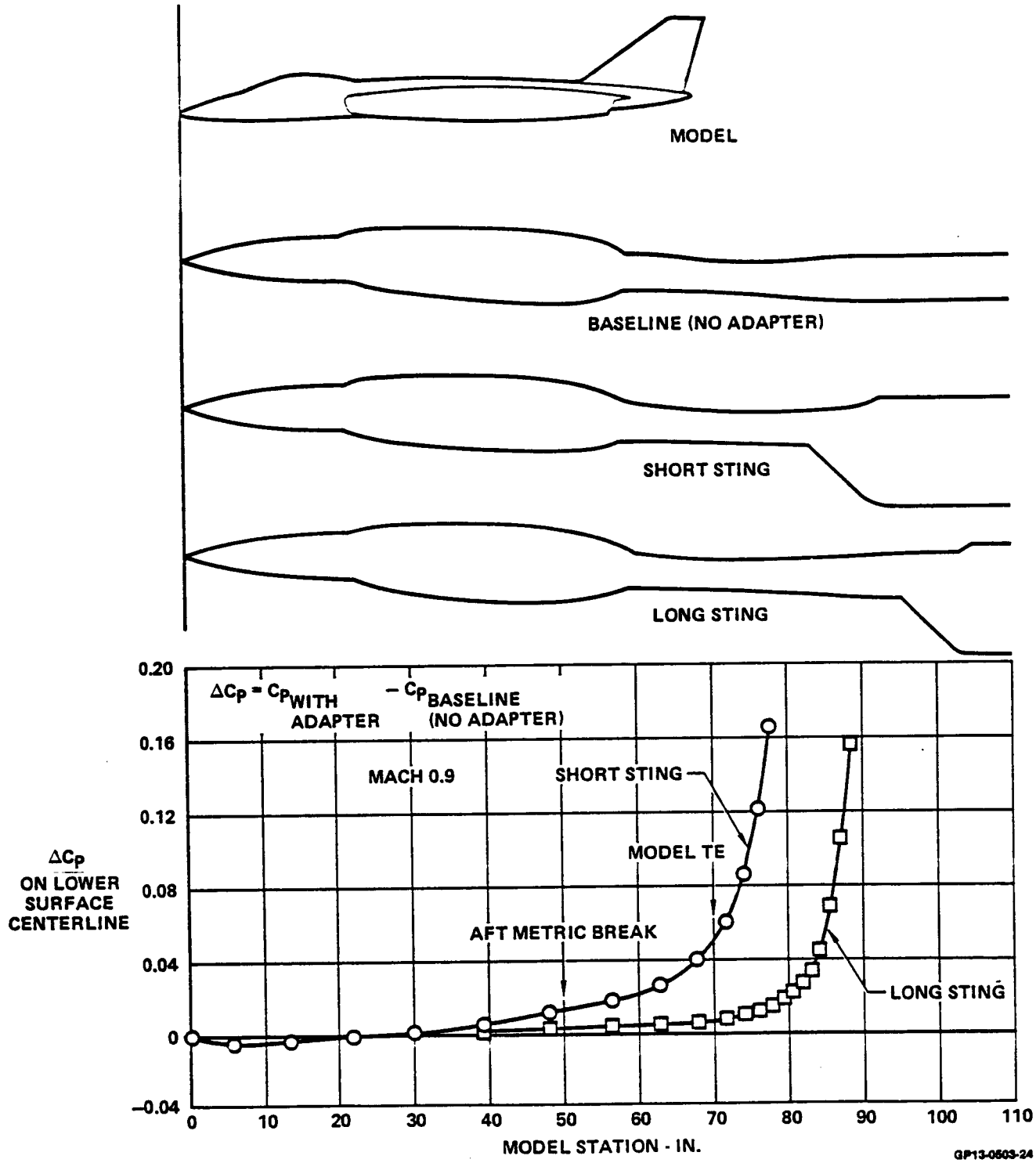

FIGURE 4-6
STING LENGTH EFFECT ON ADAPTER INDUCED PRESSURE INCREMENTS

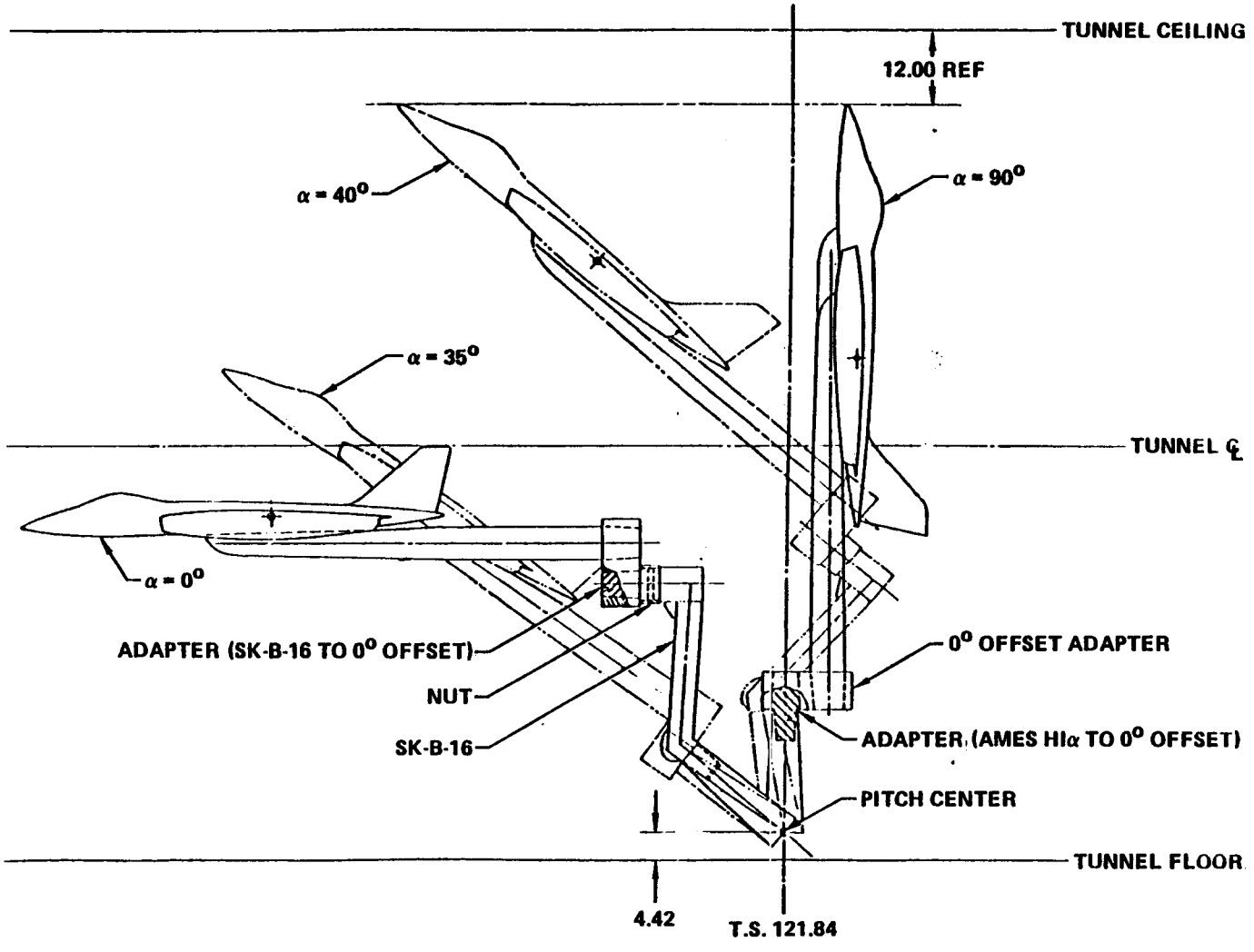

FIGURE 4-7
CONCEPTUAL MODEL INSTALLATION IN AMES 12 FT PRESSURE WIND TUNNEL

GP13-0503-18

offset adapter and the Ames high angle of attack pitch system. It should be noted that the model sting shown for the 90° testing is shorter than the sting selected for the 11-foot installation.

4.4 FORCE BALANCE - A Task Mark XXXII, 2.5 inch balance owned by NASA will be used in this program. Its selection was based on maximizing the axial force accuracy, consistent with normal force/pitching moment and deflection limits. The axial force limit of the balance is 250 lb, which is consistent with the expected maximum axial force loads for the testing (near 200 lb at Mach 1.4, maximum α(16°)). The maximum allowable normal force/pitching moment envelope for the Mark XXXII is compared to the estimated model loads in Figure 4-8 for Mach 0.9 and 1.4. Also shown are the allowable deflection limits at the duct and aft metric breaks, ΔY = 0.100 and 0.080 inches respectively. The deflection limits are based on test experience from applicable inlet and nozzle research programs, References 5 and 6. At Mach 0.9, the baseline model configuration testing at the higher angles of attack ($\alpha \geq 20°$) will be limited to negative canard deflection settings (canard leading edge down), due primarily to the duct metric break deflection limit. At Mach 1.4, the balance load capacity limits the test angle of attack as a function of canard deflection.

The available test envelope is large enough to cover the conditions of primary interest. The angle of attack/canard deflection test envelope is summarized in Figure 4-9.

4.5 BALANCE THERMAL CONTROL - The force balance in the model will be subjected to a wide range of temperatures in the three test modes. In the simulator mode, the CMAPS units have three significant heat sources: (1) turbine drive air with a fixed temperature of about 200°F, (2) turbine bleed air with a temperature varying from about 50° to 165°F, and (3) compressor

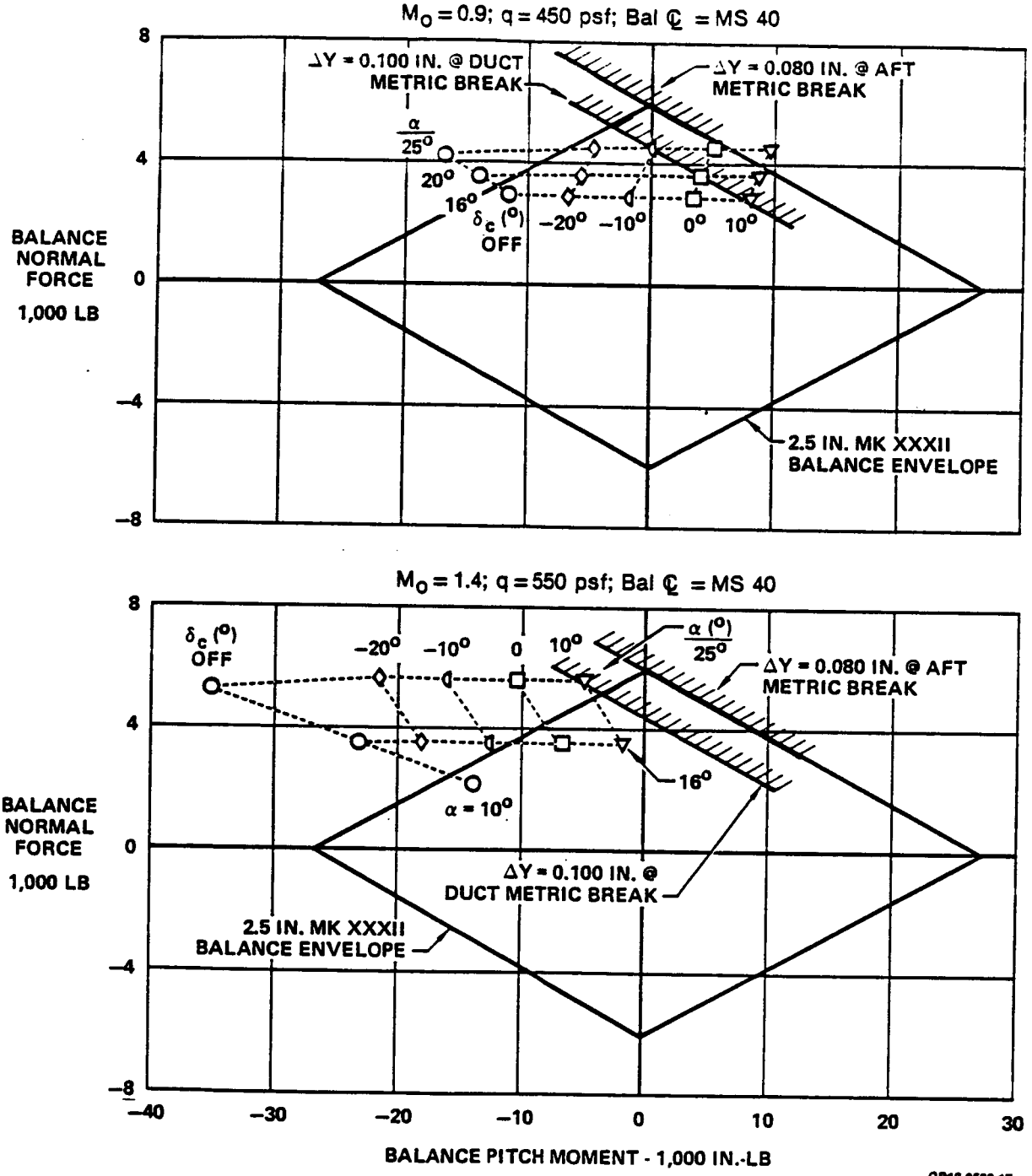

Note: (1) Canard "Off," Simulates Ultra Close-Coupled Configuration

FIGURE 4-8
MODEL LOADS AND BALANCE NORMAL FORCE/PITCHING MOMENT ENVELOPE

- BASELINE CONFIGURATION

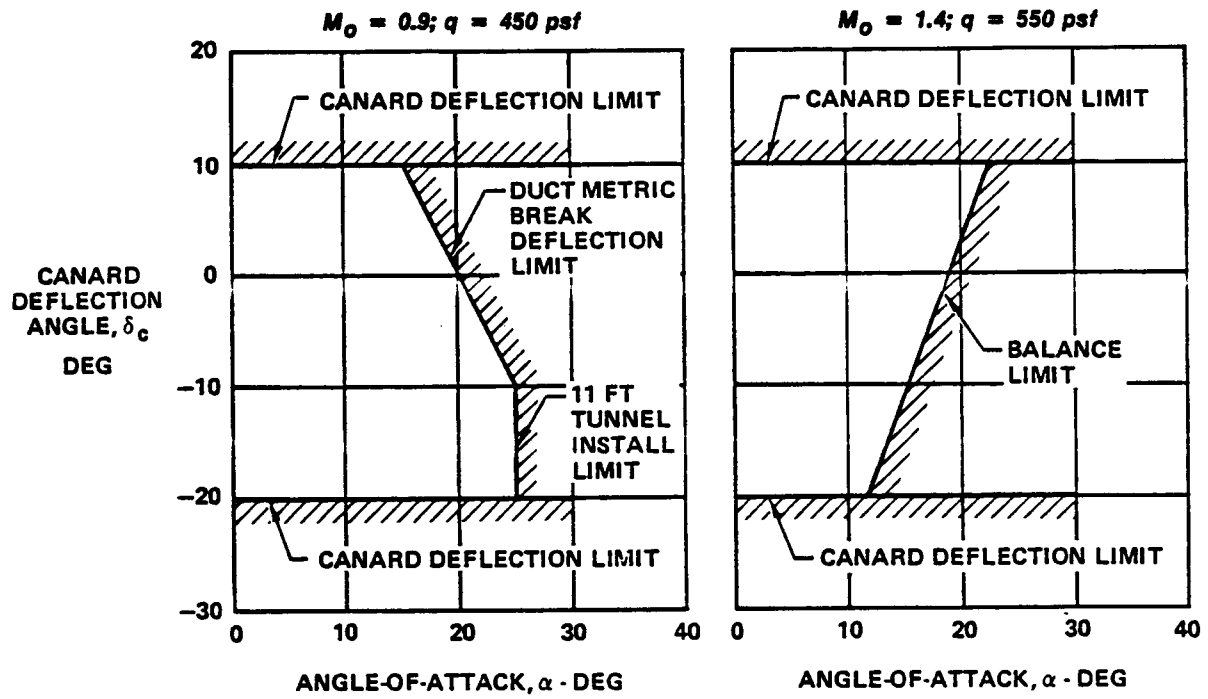

- ULTRA CLOSE-COUPLED CONFIGURATION (CANARD "OFF")

$\alpha_{MAX} = 18^o$ $\alpha_{MAX} = 11^o$

GP13-0503-1

FIGURE 4-9
ANGLE-OF-ATTACK/CANARD
DEFLECTION TEST ENVELOPE
2.5 In. MKXXXII Balance Bal ℄ = FS 40

discharge air temperature that can approach 400°F. In the jet-effects mode, turbine drive and bleed air temperatures of the simulator mode are duplicated, although the high temperature compressor discharge air is not. In the flow-through mode, the balance is subjected only to the tunnel temperature ($\sim$ 120°F). Bias errors can be introduced into the force balance output as a result of the differing temperature environments, particularly if thermal gradients occur.

These errors can be eliminated if the balance is thermally controlled in all modes to the same constant temperature levels, with minimum thermal gradients. A three-dimensional thermal model of the balance and surrounding model structure was developed as a means to design the thermal control system. The model consists of approximately 300 nodes; a schematic of the node locations are shown in Figure 4-10.

The thermal control system was designed under the following criteria:

(1) Maintain a balance operating temperature of 160°F in all test modes, consistent with the nominal upper limit of Task balance operation;

(2) Minimize steady-state balance axial temperature gradients to within 2°F, consistent with recent experience on an F-15 jet-effects model; and on the ANC program;

(3) Provide steady state temperatures in a reasonable amount of time ($\sim$ 1-2 hr).

The thermal control system designed to these criteria is shown in Figure 4-11. Two heaters (#1 and #2) are located on the forward and aft sections of the balance housing. Another heater (#3) is located on the forward end of the balance taper insert. The fourth heater (#4) is located beneath the balance. Very thin

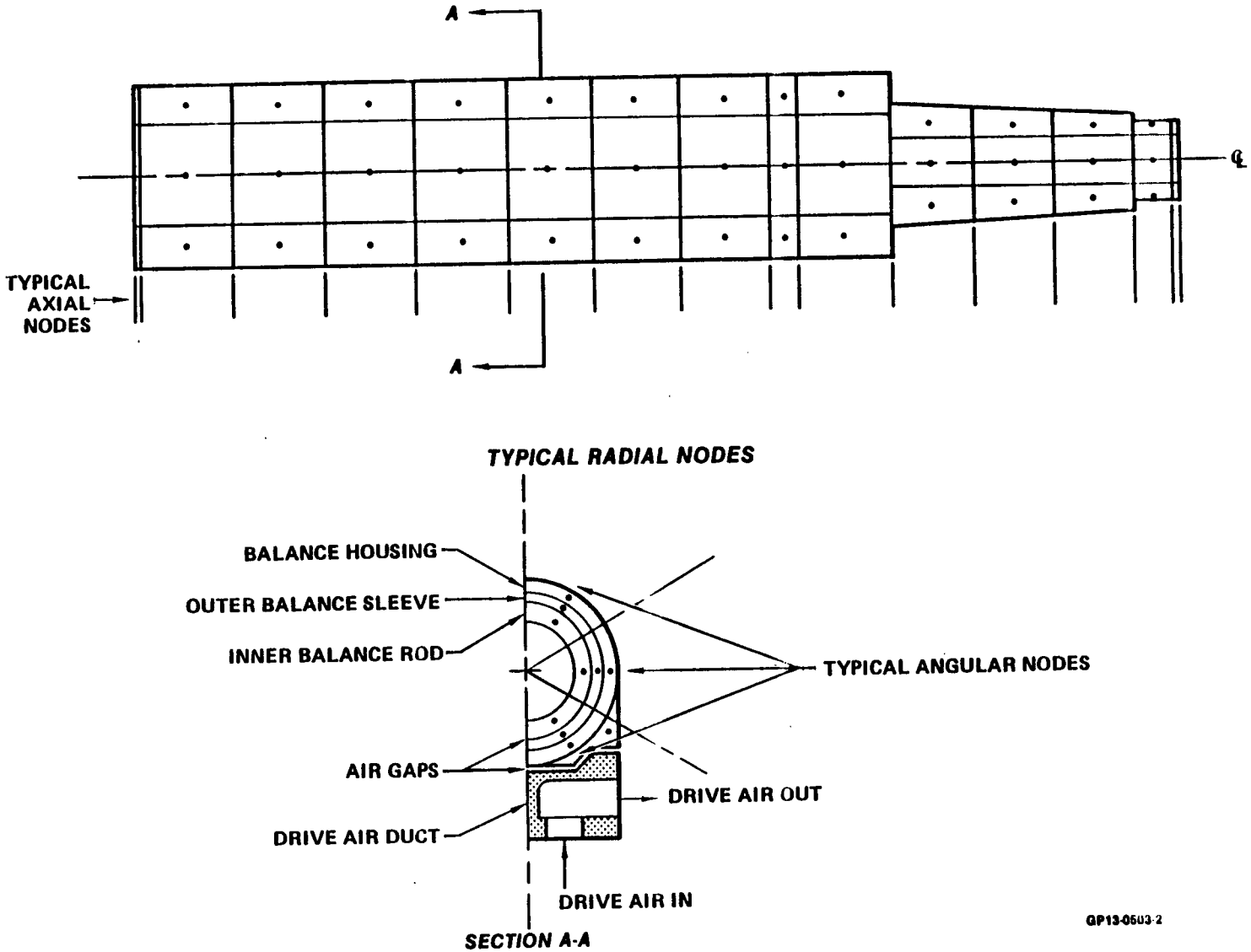

FIGURE 4-10
BALANCE THERMAL NODE DIAGRAM

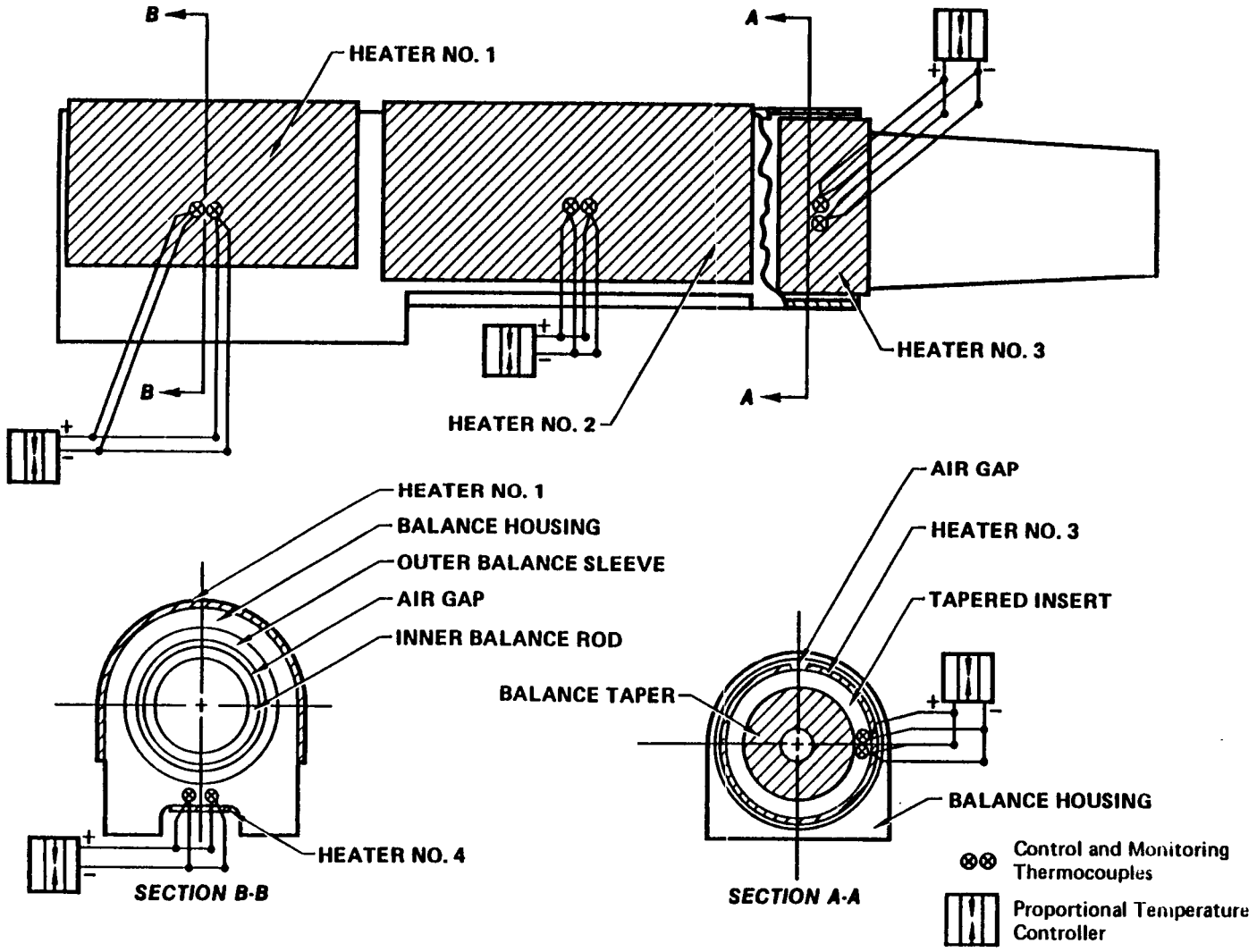

FIGURE 4-11
BALANCE THERMAL CONTROL SYSTEM

GP13-0503-3

(.030 inch) custom heaters, manufactured by the Watlow Corporation, will be used for this application. Two thermocouples are provided for each of the four heaters. One provides feedback to the proportional temperature controller, set to maintain 160°F on a specific location of the balance housing (or tapered insert). The other is for temperature monitoring and back-up purposes. Use of the proportional temperature controllers, in conjunction with the thin blankets, will permit heater power densities of up to 25-30 watts/in^2 for this application.

The thermal model was used to predict balance temperatures with this thermal control system for both transient and steady-state operating conditions. The transient analysis, representing balance heat-up from 80°F with the tunnel off, indicated the balance could be driven to 160°F in about one hour. This is consistent with the design criteria. Maximum power density required for this length of heat-up time was about 1/3 of the system's capability. This converts into either a high safety factor or a potentially more rapid heat-up period. The power density requirements for steady-state operation with the model and tunnel operating are much less.

Three steady-state cases, two for the simulator mode and one for the flow-through mode, were analyzed to ensure that the temperature gradient requirements were attained. The two simulator test cases correspond to the range of CMAPS turbine bleed air temperature (50 to 165°F) from recent CMAPS testing. A maximum axial temperature gradient of about 2°F is predicted for the three test cases, as shown in Figures 4-12 and 4-13. This is within acceptable limits. The angular and radial temperature distributions for these same three conditions are within about 4°F, as shown in Figure 4-14.

Detailed design and procurement of the heaters and controllers will be accomplished in the Phase 2 detailed design activity.

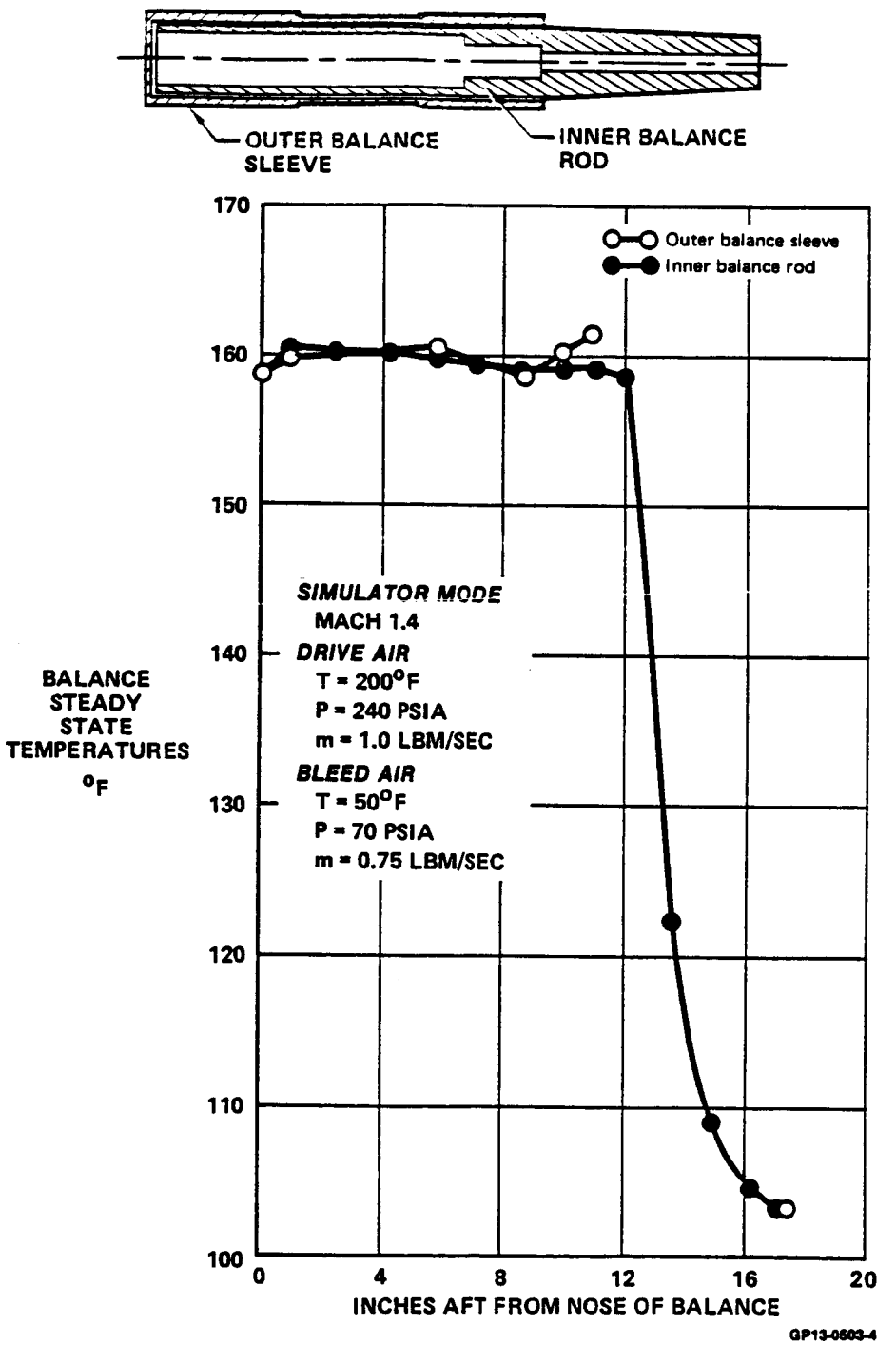

FIGURE 4-12a
BALANCE AXIAL TEMPERATURES - SIMULATOR MODE; T_{BLEED} = 50°F

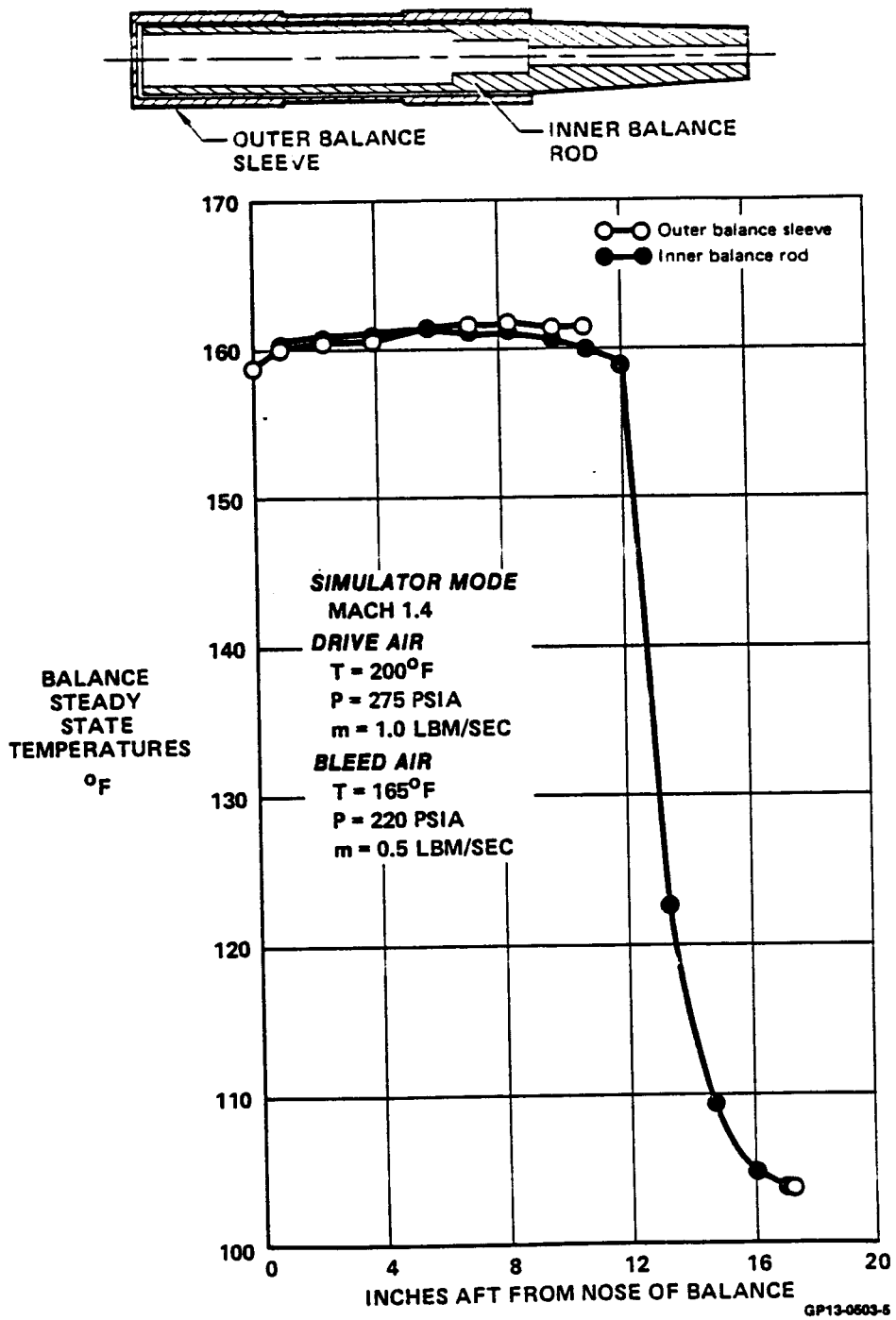

FIGURE 4-12b
BALANCE AXIAL TEMPERATURES - SIMULATOR MODE; T_{BLEED} = 165°F

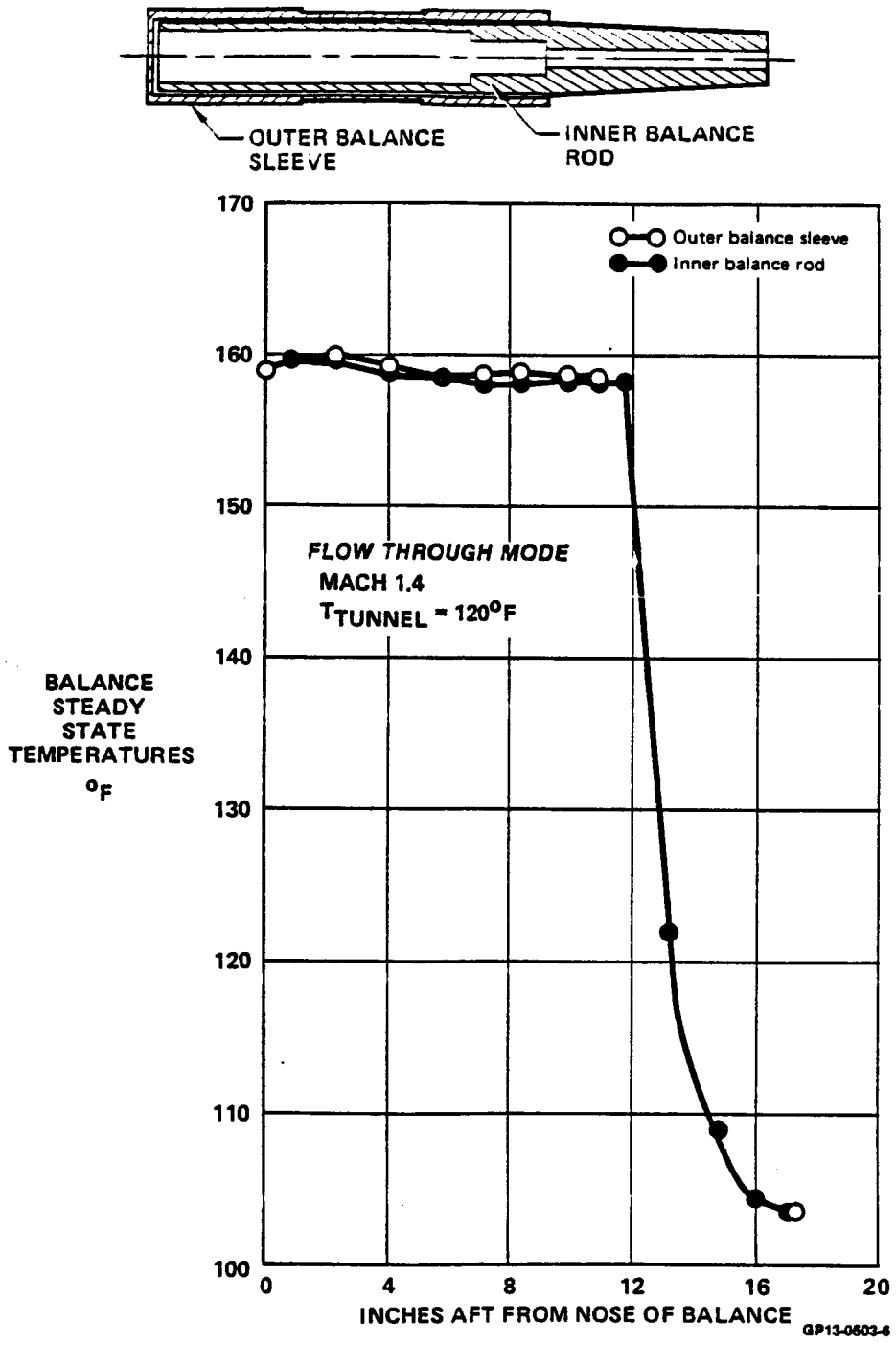

FIGURE 4-13
BALANCE AXIAL TEMPERATURES - FLOW THROUGH MODE

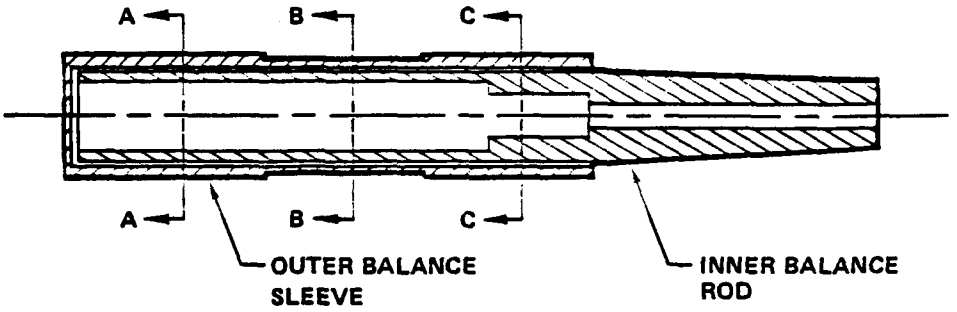

SIMULATOR MODE (MACH 1.4; $T_{DRIVE\ AIR}$ = 200°F; $T_{BLEED\ AIR}$ = 165°F)

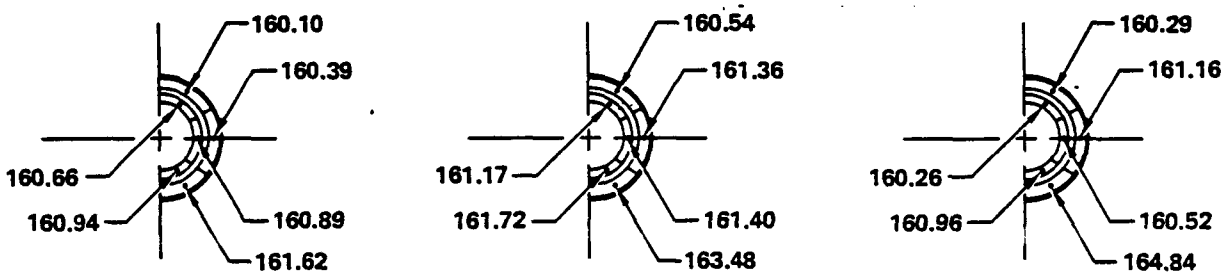

SECTION A-A SECTION B-B SECTION C-C

SIMULATOR MODE (MACH 1.4; $T_{DRIVE\ AIR}$ = 200°F; $T_{BLEED\ AIR}$ = 50°F)

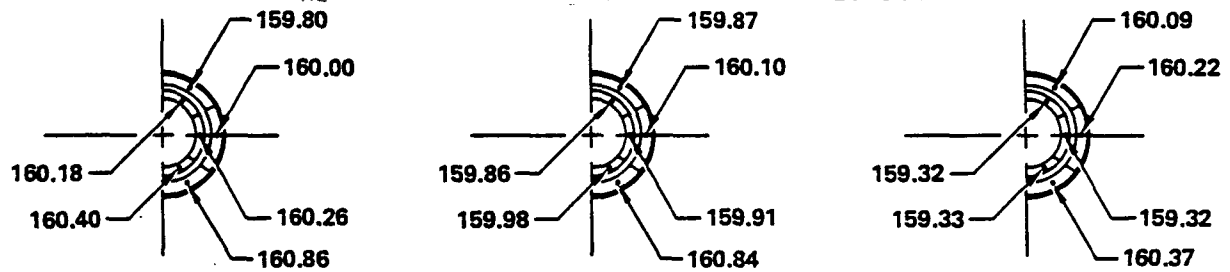

SECTION A-A SECTION B-B SECTION C-C

FLOW THROUGH MODE (MACH 1.4; T_{TUNNEL} = 120°F)

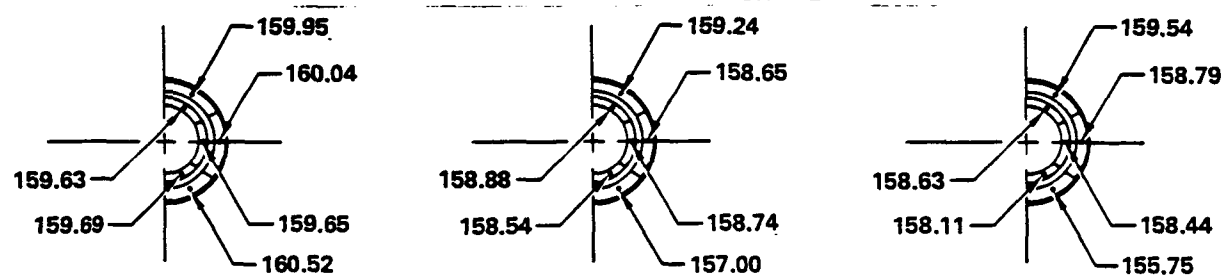

SECTION A-A SECTION B-B SECTION C-C

FIGURE 4-14
BALANCE ANGULAR AND RADIAL TEMPERATURES

GP13-0503-7

4.6 INLET DESIGNS - Two different inlets have been designed for the baseline and ultra close-coupled configurations.

4.6.1 Baseline Inlet - The baseline inlet is a rectangular, normal shock design with a 15° scarf angle. The inlet concept is shown in Figure 4-15. It was sized for operation at 95 percent of critical mass flow ratio with the maximum simulator airflow (1.65 lbs/sec). A rotating cowl lip is incorporated into the design to reduce lip separation at static conditions and at high angles of attack. Lip rotation angles of 45° and 70° were selected for this design. It is expected that the 45° configuration will be used for low speed at moderate to high angles of attack. The 70° cowl deflection would be used for static operation and at low speed, high angles of attack (approaching 90°). Sideplates will be incorporated when the cowl is deflected. In addition, the cowl rotation point has been selected to provide a large flap knee radius to prevent separation. The rotating cowl lip design for this inlet is based on a similar design which was recently tested at MCAIR.

The need for specialized inlet devices, such as the rotating cowl lip, is illustrated by the test results on the 8.5% Simulator Demonstration Model, Reference 6. In this testing, there were numerous instances of simulator compressor stalls at static operation which were attributed to high flow inlet distortion levels. This distortion was due to separation off of the relatively sharp (F-15 type) lip at static conditions. The problems were resolved by subsequently using a bellmouth adapter as shown in Figure 4-16.

For this program, the rotating cowl lip was selected because of its demonstrated performance in the Reference 9 investigation and also in a recent MCAIR Independent Research and Development (IRAD) test program. The rotating cowl lip configuration tested in the recent MCAIR program is shown in Figure 4-17. The inlet performance improvement with the rotating cowl lip configurations

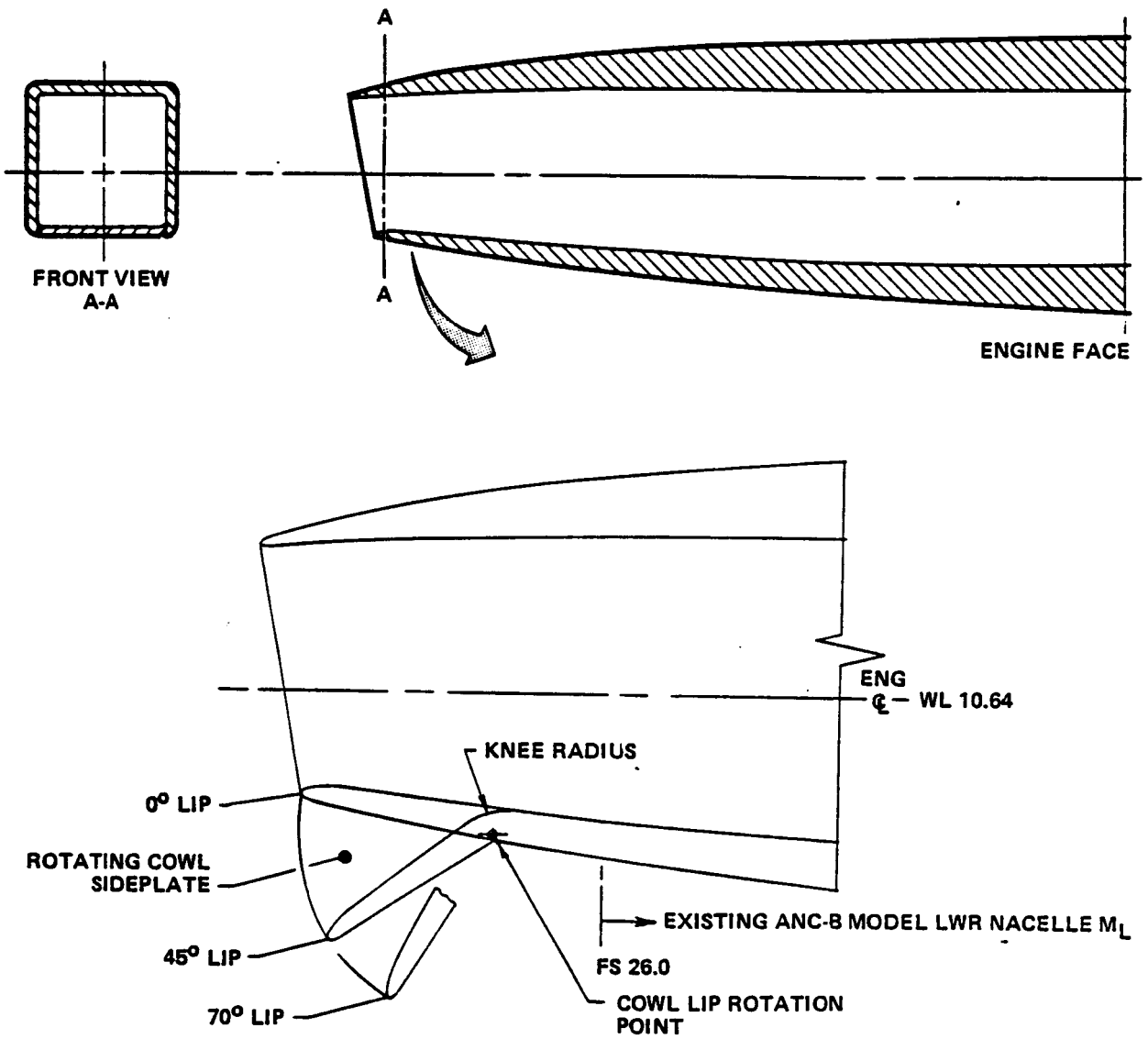

FIGURE 4-15
ARTICULATING COWL LIP FLAP SYSTEM FOR BASELINE INLET CONFIGURATION

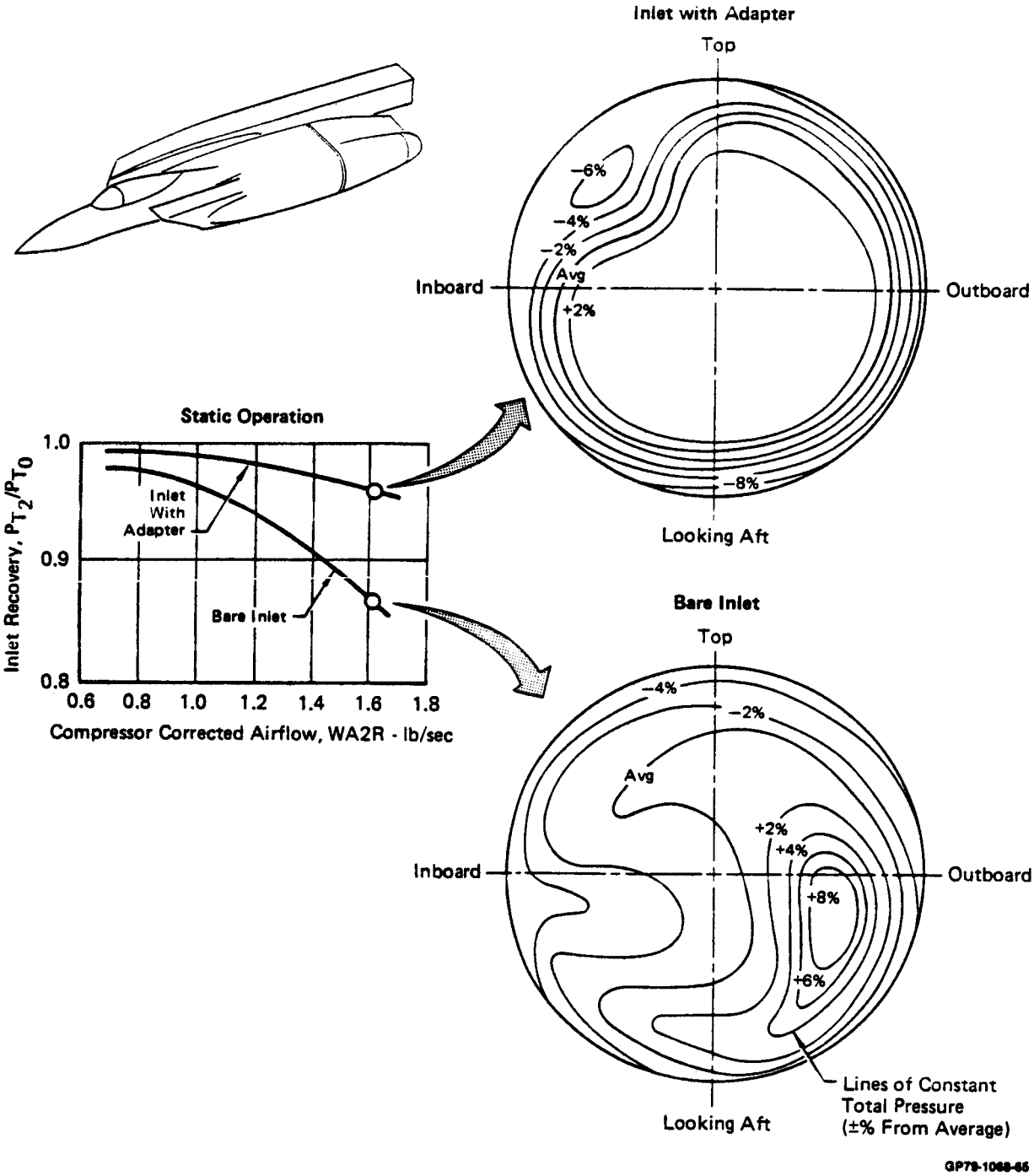

Figure 4-16.
INLET STATIC PERFORMANCE IMPROVEMENT WITH BELLMOUTH FOR 8.5% SIMULATOR DEMONSTRATION MODEL

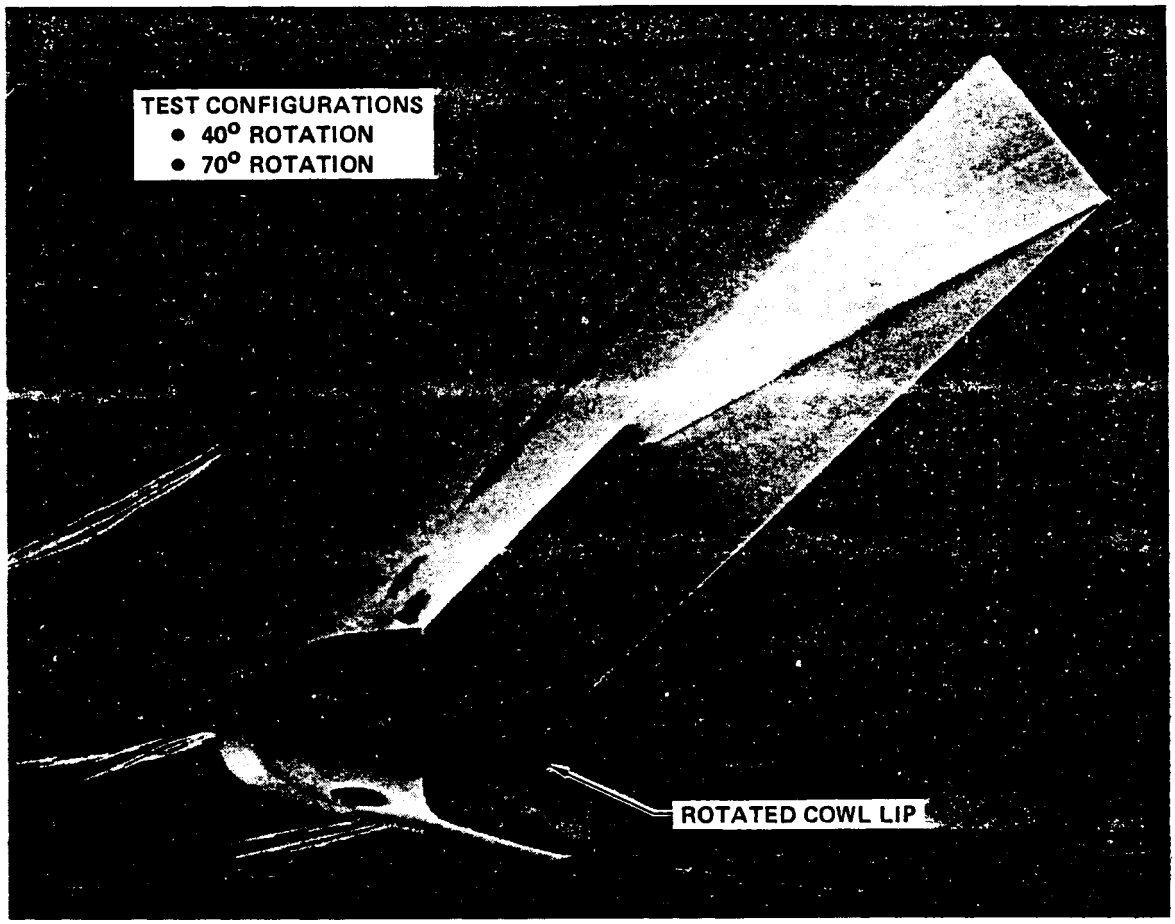

FIGURE 4-17
MCAIR ROTATING COWL LIP CONFIGURATION

was determined statically and at Mach 0.25 over an angle of attack range of 0° to 90°. As shown in Figure 4-18, the rotating cowl lips provide a significant performance improvement.

A comparison was made of inlet recovery, steady state distortion, and turbulence at static conditions for the following configurations:

- o 8.5% Sim. Dev. Baseline Inlet (F-15)
- o 8.5% Sim. Dev. Bellmouth Adapter
- o MCAIR 40° and 70° Rotating Lip Configurations

The performance differences are tabulated in Figure 4-19. Note that the MCAIR 70° rotating lip inlet has lower distortion than the bellmouth inlet and only slightly lower pressure recovery.

Since the V/STOL rotating cowl lip design are geometrically similar to those recently tested at MCAIR, the V/STOL inlet should have comparable performance and therefore result in satisfactory CMAPS operation.

An evaluation was also conducted to determine the need for an inlet bypass system to maintain stable inlet operation when the simulator is windmilling at supersonic test conditions. The operating characteristics at Mach 1.4 of a normal shock inlet similar to that on the baseline V/STOL configuration are shown in Figure 4-20. The start of inlet flow instability or "buzz" occurs below the mass flow ratio associated with the simulator windmilling airflow for all positive angles-of-attack tested. A bypass system is therefore not necessary providing the model is positioned at positive angle of attack during windmilling operation.

4.6.2 Ultra Close-Coupled Inlet Definition - The conversion of the baseline inlet configuration to a modified ultra-close-coupled configuration is accomplished with a minimum of hardware

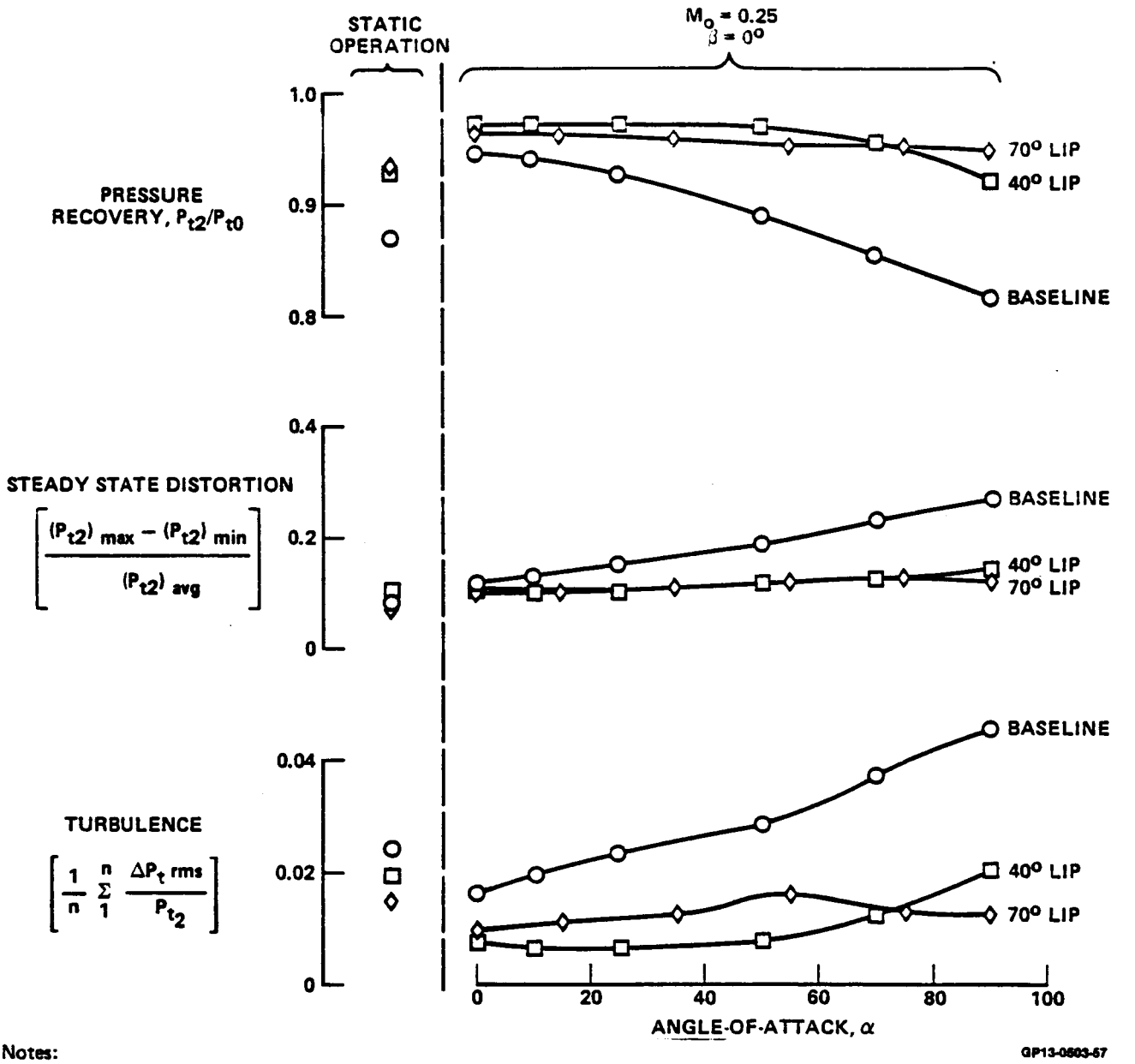

Notes:

1. Data from MCAIR IRAD test program.
2. ΔP_t rms is the root mean square deviation of the fluctuating portion of the dynamic total pressure.

FIGURE 4-18
IMPROVED INLET PERFORMANCE WITH ROTATING COWL LIP DATA AT DESIGN ENGINE AIRFLOW

Performance Parameter	Inlet Configuration			
	8.5% Sim Dev Baseline Inlet	F-15 (See Note 2)	8.5% Sim Dev Bellmouth Adapter	MCAIR 70° Rotating Lip
Inlet Recovery	0.870	0.881	0.960	0.933
Steady State Distortion	0.138	0.127	0.104	0.071
Turbulence	N/A	0.034	N/A	0.015

Notes:

GP13-0401-10

1. N/A - not available
2. F-15 inlet data from subscale inlet test. Baseline inlet for 8.5% sim dev program was based on F-15 design
3. Data at design engine airflow levels

Figure 4-19. Inlet Performance Comparison
Static Operation

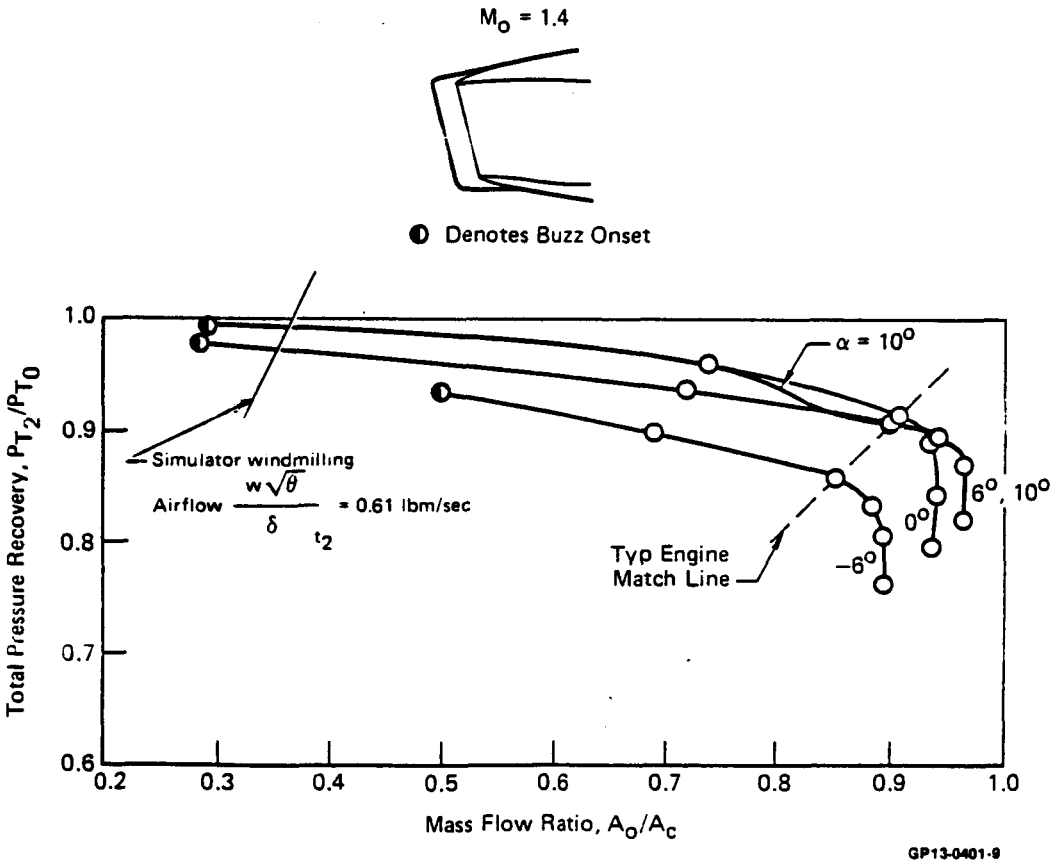

Figure 4-20. Typical Normal Shock Inlet Stable Range

changes. As illustrated in Figure 4-21, this modification involves (1) removal of the canard, (2) removal of the basic inlet duct, (3) insertion of a modified inlet duct, and (4) modification of the inner wing. All other aspects of the model hardware remain undisturbed as this modification is made. The balance and seal tare calibrations thus remain the same.

The short nacelle necessitates changes to the basic inlet design concept. In keeping with the optional design guidelines established by NASA, a subsonic inlet design has been selected, as detailed in Figure 4-22. Due to the short duct length, a circular inlet shape was chosen to avoid relatively large diffuser wall angles which would result when transitioning from a square to a circular duct over a very short distance. Based on similar designs, the inlet was sized to an inlet throat Mach number of 0.55 at the simulator design airflow.

The articulating lower cowl flap used in the baseline inlet design for improved performance at static and high angle of attack conditions is not being used in the short nacelle inlet. It was felt that the articulating flap was not compatible with the circular subsonic inlet concept. Therefore, three other design features are being used to "replace" the articulating flap function (good static/high angle of attack performance). First, in accordance with the results from Reference 10, a reverse scarf (lower lip extending past the upper lip) is incorporated. Tne increase in angle of attack capability obtained with a reverse scarf inlet design is shown in Figure 4-23. Second, generous inlet contraction ratios (capture area divided by throat area) have been selected for this inlet design. Based on the YC-15 design, contraction ratios of 1.78 and 1.34 have been chosen for the lower and upper inlet lips, respectively. The angle of attack performance improvement with increased inlet contraction ratio is shown in Figure 4-24. Finally, a leading edge slat has been provided over the lower 120° of the inlet to help prevent separation on the lower lip. As presently planned, the slat will

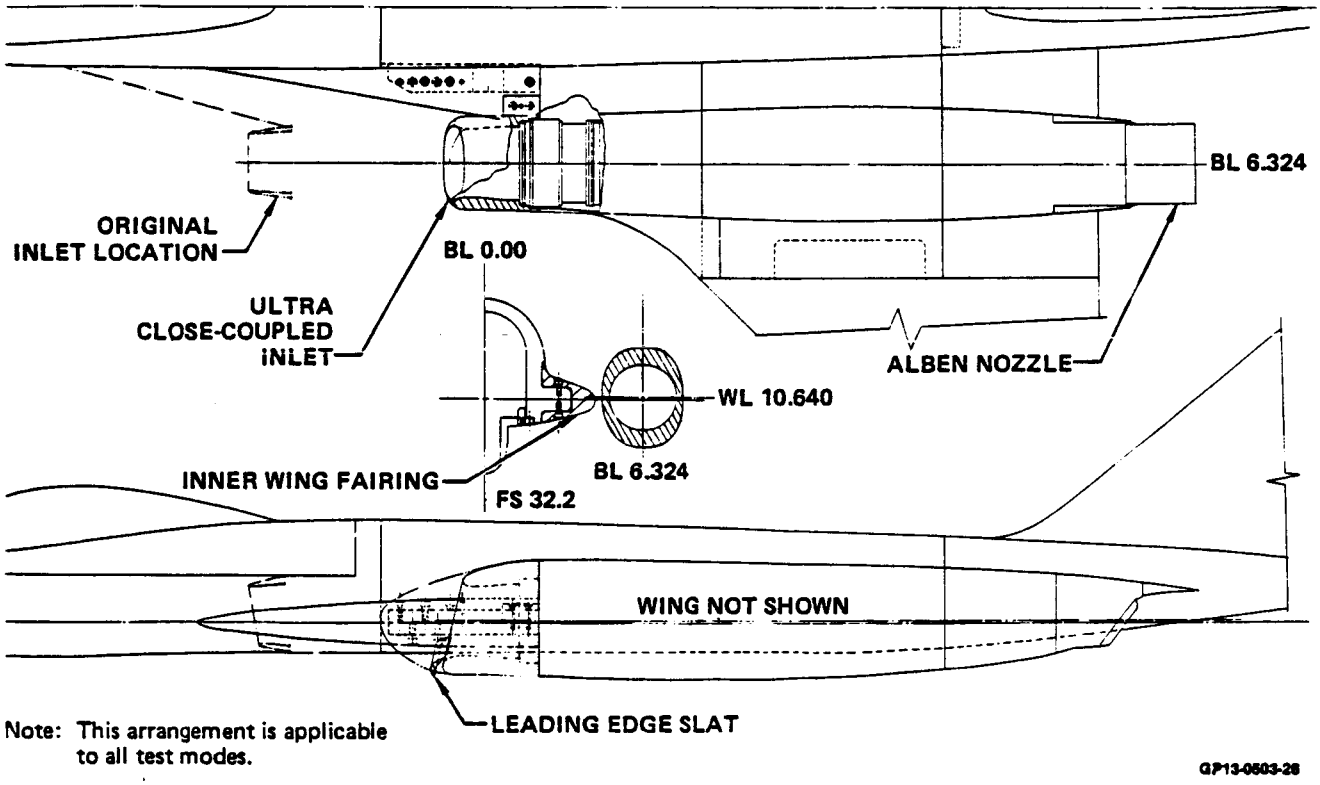

FIGURE 4-21
MODEL ARRANGEMENT OF CLOSE-COUPLED CONFIGURATION

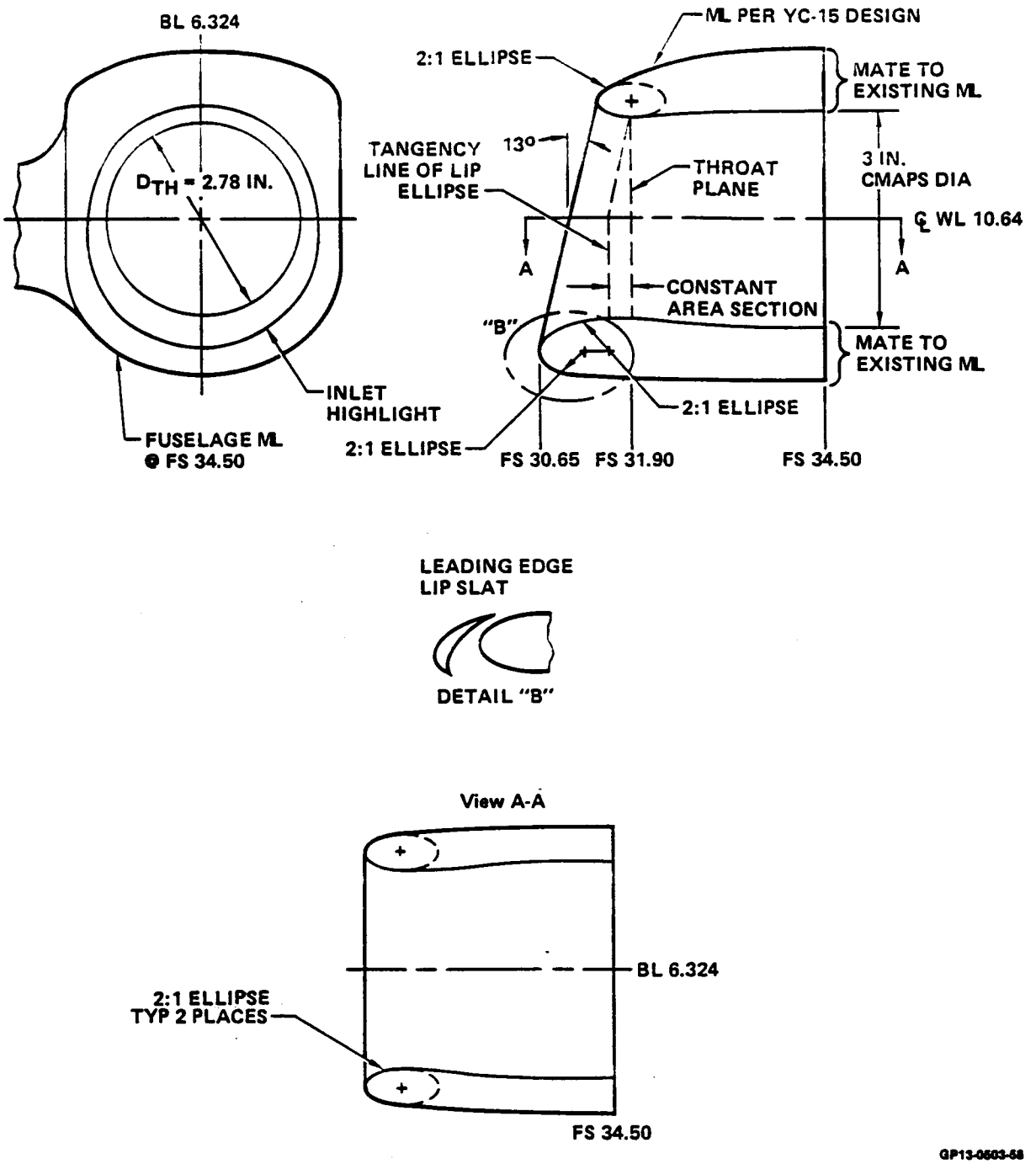

FIGURE 4-22
ULTRA CLOSE-COUPLED INLET CONFIGURATION

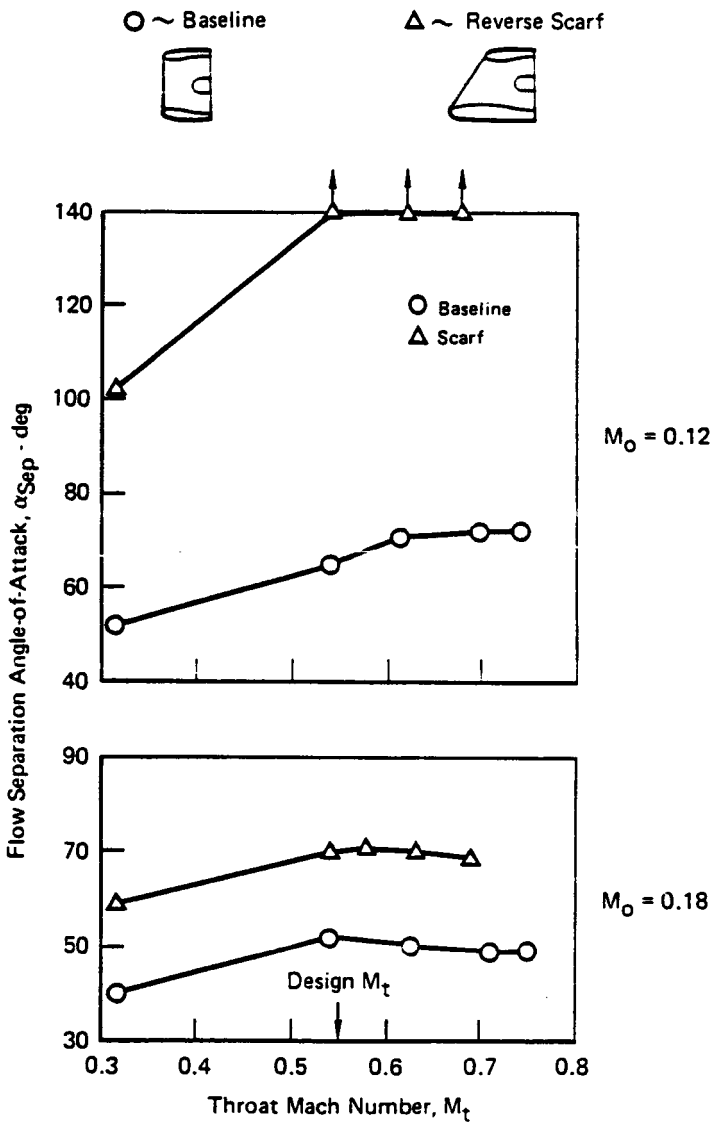

Figure 4-23. Effect of Reverse Scarf Inlet on Flow Separation Bounds

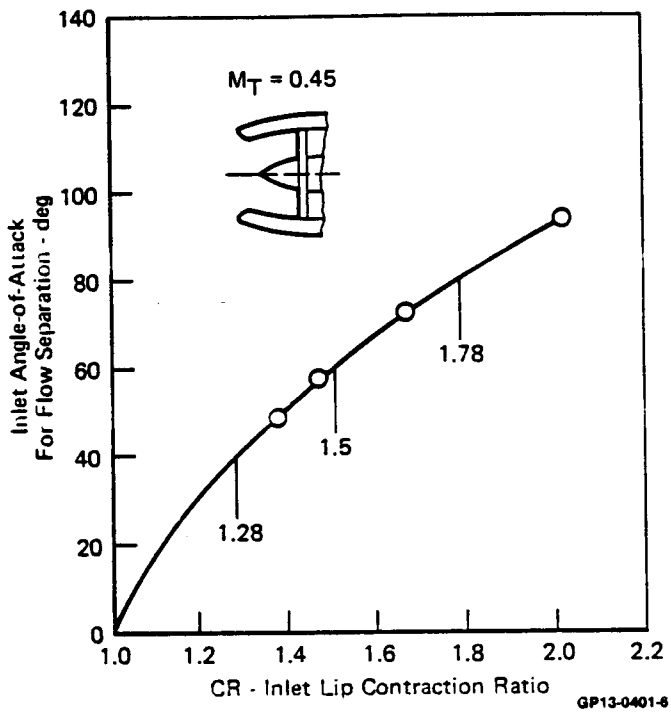

Figure 4-24. Effect of Inlet Contraction Ratio on Flow Separation Bounds

be used only at very high angle of attack. Performance improvement with a geometrically similar slot design is illustrated in Figure 4-25.

It is felt that this ultra close-coupled inlet design will provide the necessary performance levels at static and high angle of attack conditions to ensure safe simulator operation.

4.7 NOZZLE DESIGNS - The basic nozzle design for the program is the GE ALBEN concept. The ALBEN meets the program requirements and was selected for cost considerations since it is existing hardware from the ANC program. It can be tested in any of the three modes, although it will be used primarily in simulator and jet-effects testing. Nozzle extensions are used for the reference nozzle condition and in the flow-through mode. The aerodynamic design of the nozzle extensions is discussed in Section 3; their use in the flow-through mode is discussed in Section 5.

The ALBEN nozzle assembly simulates a full scale GE design with internal/external expansion, an aspect ratio of 3.8, fully variable throat area control, and thrust vectoring capability. This is a specialized type of single expansion ramp nozzle designed particularly for low weight. It utilizes an elliptically shaped canister or shroud to vary throat area, with the bottom section forming the lower nozzle lip. The upper portion of the shroud surrounds the upper ramp assembly creating a cavity that is pressurized with fan air. The pressure loading on the upper section of the shroud essentially balances the load on the lower section.

The ALBEN model can be vectored both at dry power and afterburning to 20° and 30° deflection. The model representation of the ALBEN is shown in Figure 4-26.

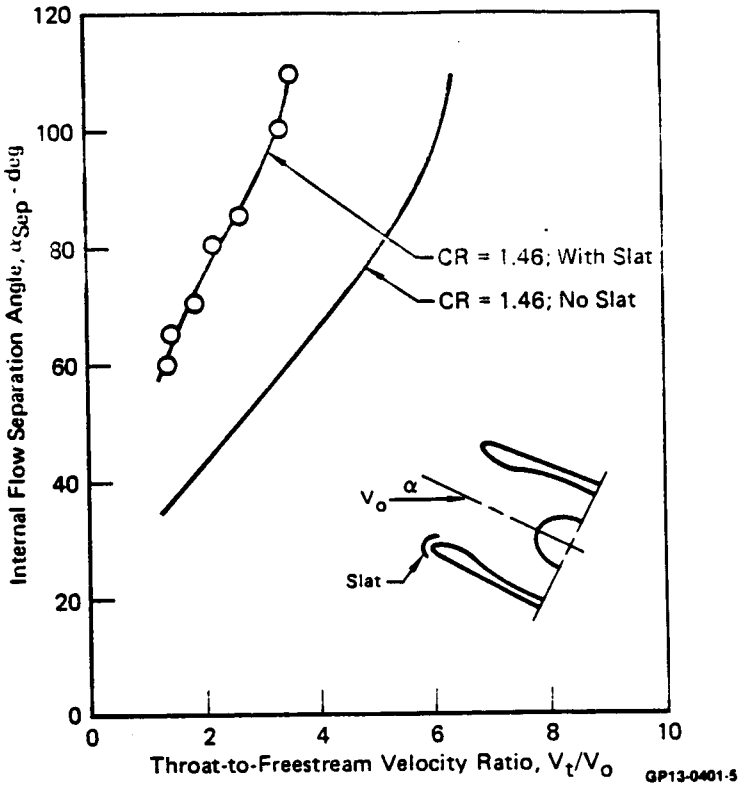

Figure 4-25. Effect of Leading-Edge Slat on Flow Separation Bounds

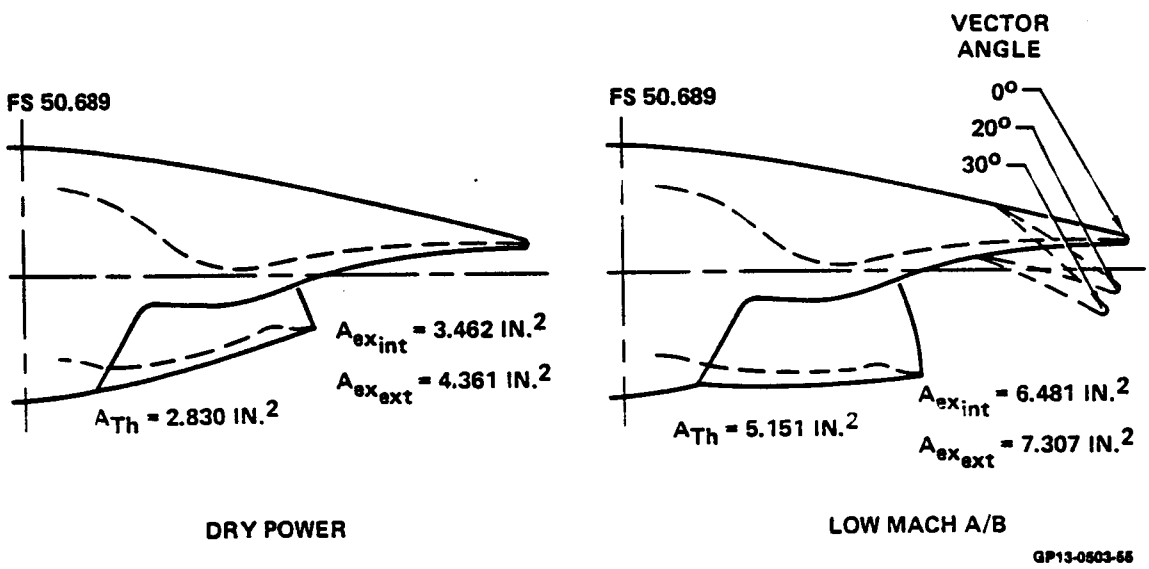

FIGURE 4-26
GE ALBEN NOZZLE ASSEMBLY
AR = 3.8:1

5.0 DESCRIPTION OF TEST MODE CONCEPTS

Successful completion of program objectives depends upon attention to detail in the design of all three test modes. Conceptual layouts and associated analyses have been accomplished for the key design aspects of the simulator, flow-through, and jet-effects testing modes.

5.1 SIMULATOR TEST MODE CONCEPT - The simulator mode is the most complicated of the designs, and requires extensive analysis to ensure the model and simulator are compatible. The only hardware components unique to this mode are the actual CMAPS units. The layout of the simulator test mode concept is shown in Figure 5-1. Extensive analyses of the pressure loss characteristics of the drive and bleed air system were conducted based on this design, and a "flexibility" analysis was done to assess CMAPS/model compatibility. The term flexibility refers to the CMAPS capability, in the model, to provide independent variation of airflow or engine pressure ratio while holding the other parameter fixed.

5.1.1 Drive Air System - The turbine drive air system must provide the simulator the required flow at a given pressure level. The design conditions for the drive air system are at maximum flow and pressure, as determined from data of References (6) and (11).

Turbine inlet flow (W4) = 5.5 lbs/sec/CMAPS unit
Turbine inlet pressure (PT4) = 1300 psia
Turbine inlet temperature (TT4) = 200°F
Compressor inlet pressure (PT2) = 16 psia

The proposed drive air system is composed of three different sections. A schematic is shown in Figure 5-2. The system consists of a 1-inch I.D. line from the NASA Flow Control Pallet to the model strut. Once inside the strut, the line size is reduced

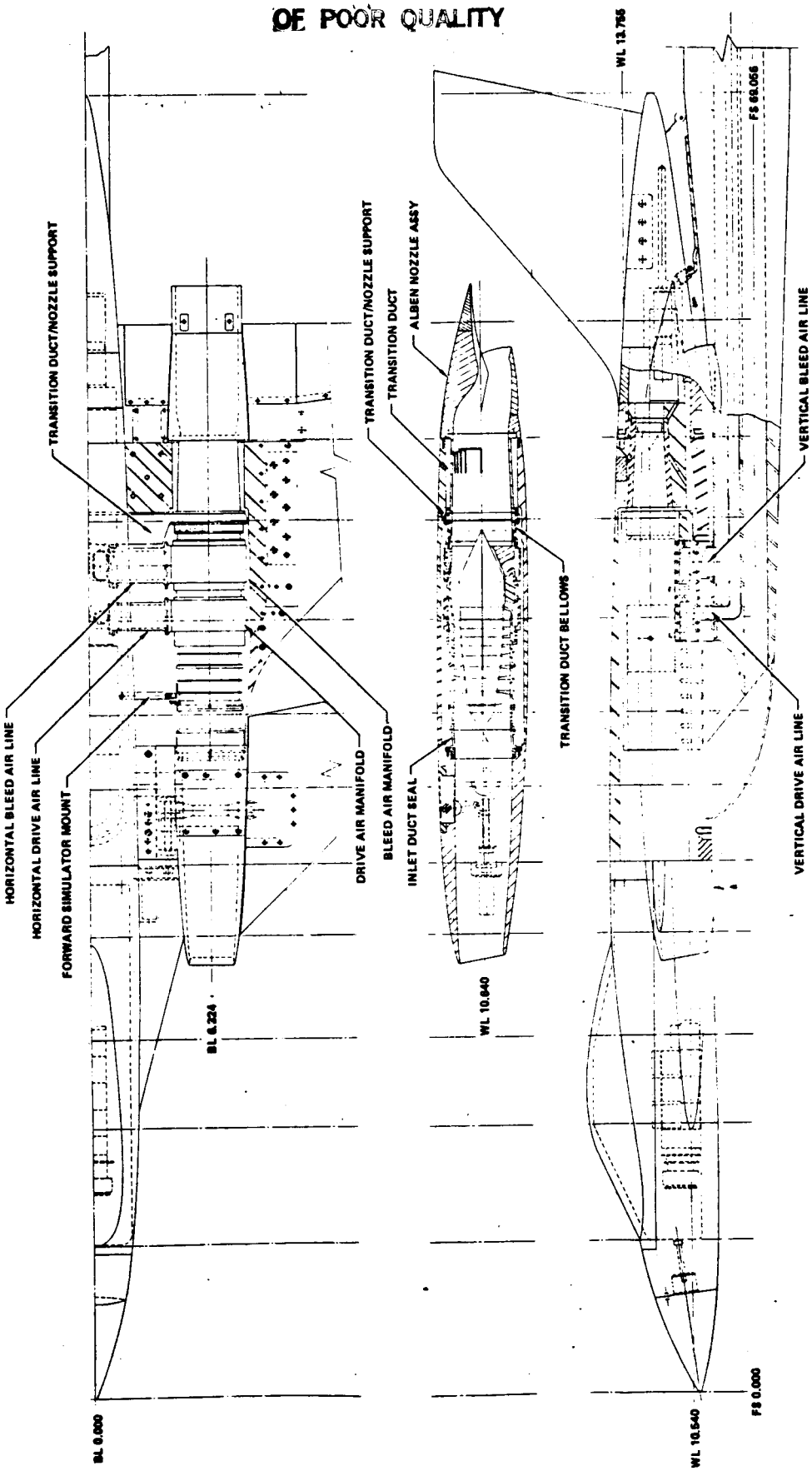

FIGURE 5-1
SIMULATOR TEST MODE DESIGN

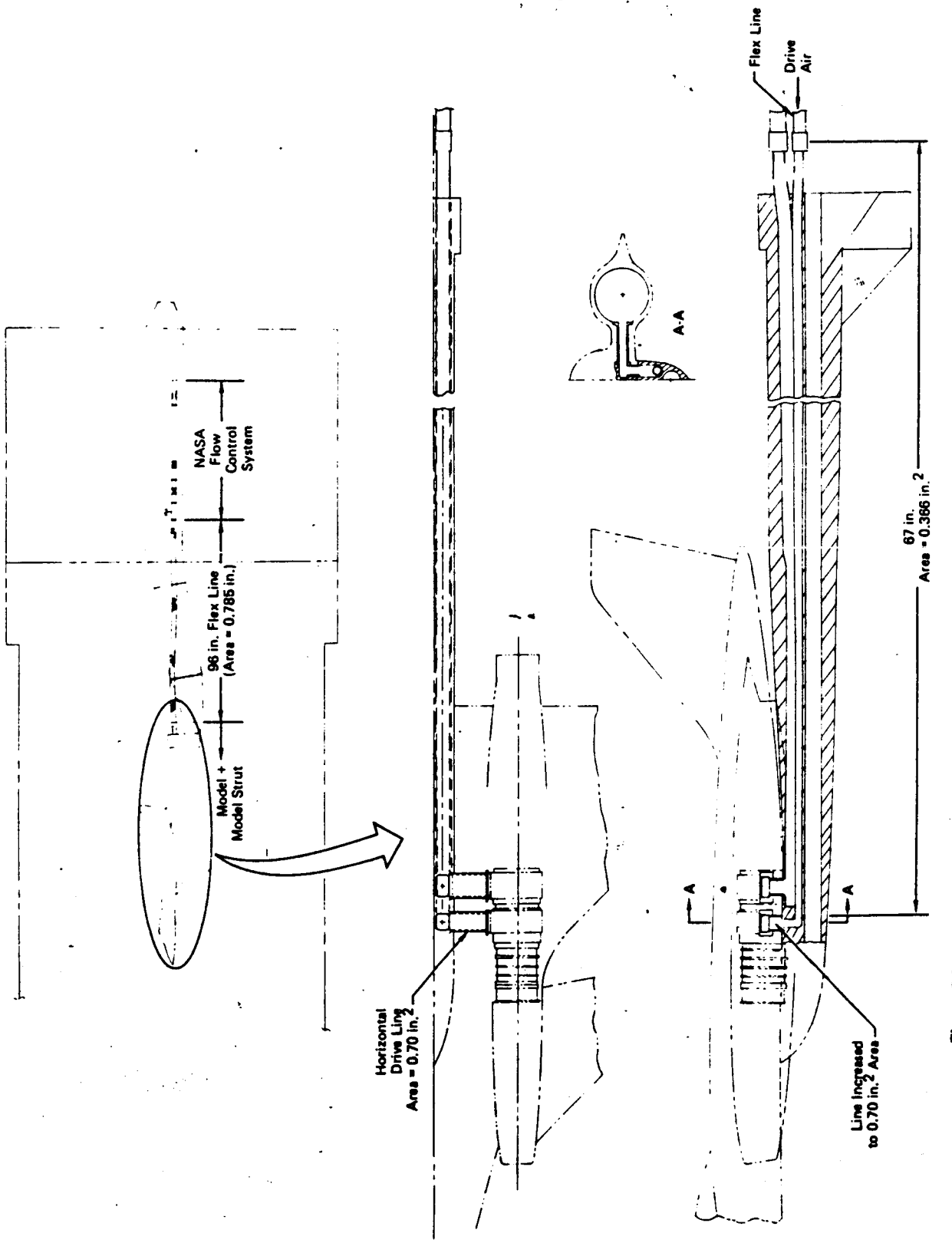

Figure 5-2. Turbine Drive Air System Schematic

to a .683 inch I.D. line (flow area of .366 in^2) to minimize strut size. The drive air line area is increased to .70 in^2 inside the model as soon as possible to reduce pressure loss. This .70 in^2 area is maintained up to the CMAPS drive manifold. It should be noted that this larger flow area is about the same as the area at the flange of the current CMAPS drive manifold shell.

Assuming an available supply pressure of 2000 psia at the exit of the NASA Flow Control Pallet, sufficient pressure should be available to the CMAPS units. With 2000 psia supply pressure, the available pressure at the CMAPS turbine inlet is estimated to be 1575 psia (1300 psia maximum required). The complete loss analysis is contained in Appendix A.

5.1.2 Bleed Air System - The capability of the CMAPS to vary engine pressure ratio (EPR) at a fixed compressor airflow is provided by mixing in the nozzle all or part of the turbine bleed airflow with the compressor airflow. For a given nozzle throat area and mixer area, the pressure drop or flow restriction in the bleed system directly affects the range of EPR available. As bleed system pressure losses increase, the amount of bleed flow that can be handled before choking occurs is correspondingly reduced. Consequently, the rest of the bleed flow must be dumped through the mixer, which in effect raises the minimum EPR attainable at a given compressor airflow. Larger reductions in bleed line area (or increased pressure loss) eventually result in a condition where it is no longer possible to power the CMAPS at maximum speed without stalling the compressor. Therefore, the design of the turbine bleed air line system is critical since it has a direct impact on the CMAPS performance. This is especially true for small throat area nozzles (typical of engine dry power operation), where the majority of the turbine bleed air must be routed back through the bleed air line.

To provide the greatest CMAPS flexibility, the bleed system was designed with the largest line areas possible considering the model and support system constraints. In the design shown in Figure 5-3, a bleed line area of 1.05 in^2 is maintained inside the model between the CMAPS bleed manifold and support strut. Once inside the forward section of the strut, the bleed area is increased to 1.23 in^2 to decrease pressure loss. The bleed area is further increased to 1.62 in^2 in the aft section of the strut. Aft of the model strut, a 2.0 in I.D. flexible line ducts the air to the NASA Flow Control Pallet located on the tunnel traversing strut. The bleed air then passes through the flow control/ measuring hardware on the pallet, and is exhausted into the tunnel.

With the system thus defined, the pressure drop through each component was calculated. A loss summary is shown in summary form in Figure 5-4. The bleed system losses are separated into three categories: (1) losses between the bleed manifold and model strut, (2) losses in the model strut, and (3) losses through the Flow Control Pallet hardware. About 60% of the total pressure loss occurs inside the model, where line size is restricted due to space limitations. An additional 20% is lost in the model strut, where strut size is a controlling consideration. Finally, about 20% of the pressure is lost within the pallet installation. The pressure loss analysis is described in Appendix B.

5.1.3 Flexibility Analysis - Extensive study has been conducted to estimate the flexibility envelope of the CMAPS units in the model. This work was done in cooperation with General Electric. The key "independent variables" which affect flexibility are:

(a) Turbine bleed system pressure loss
(b) Bleed venturi area (A_V)
(c) CMAPS mixer area (AE57)
(d) Nozzle throat area (A_8)

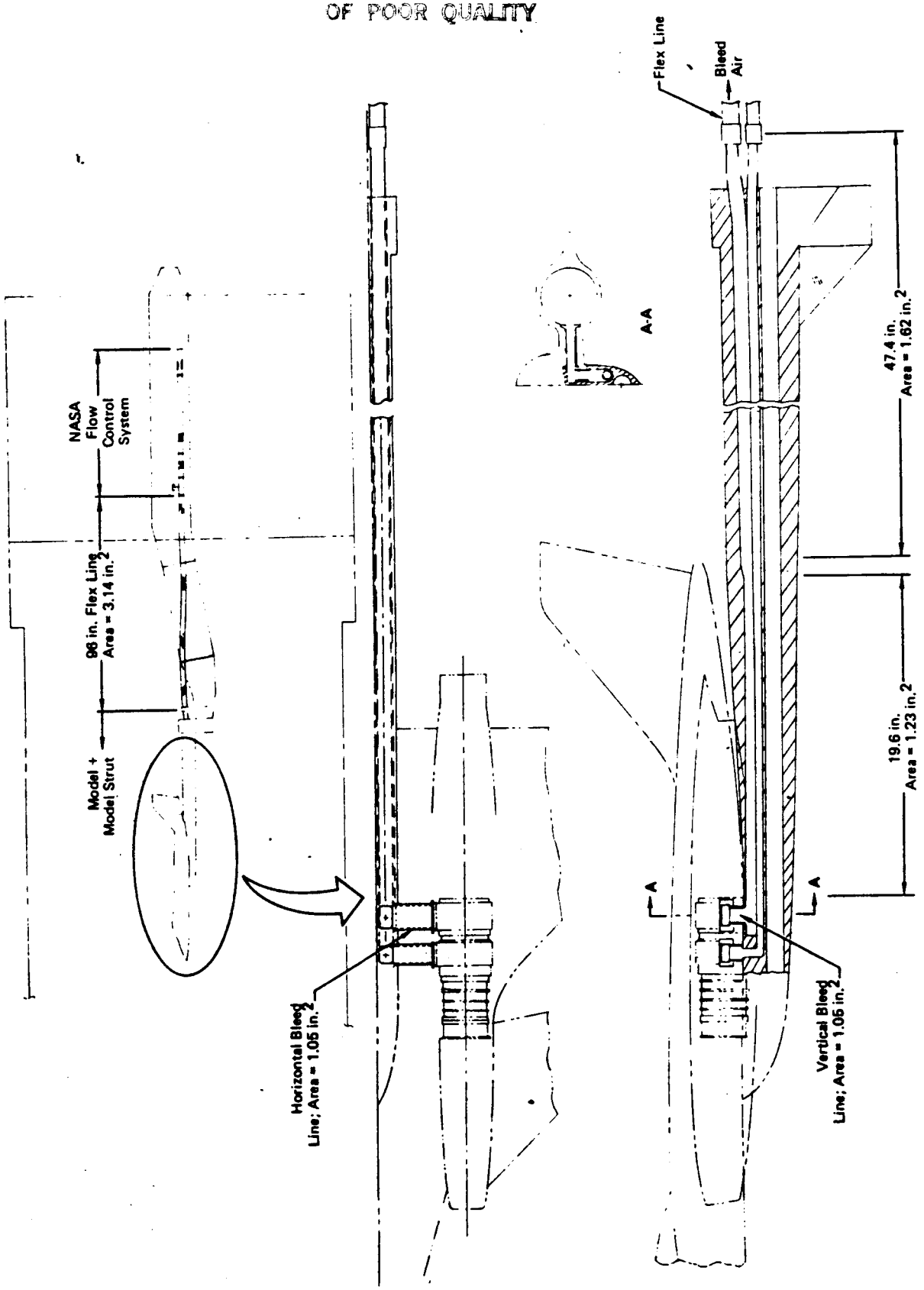

Figure 5-3. Turbine Bleed System Schematic

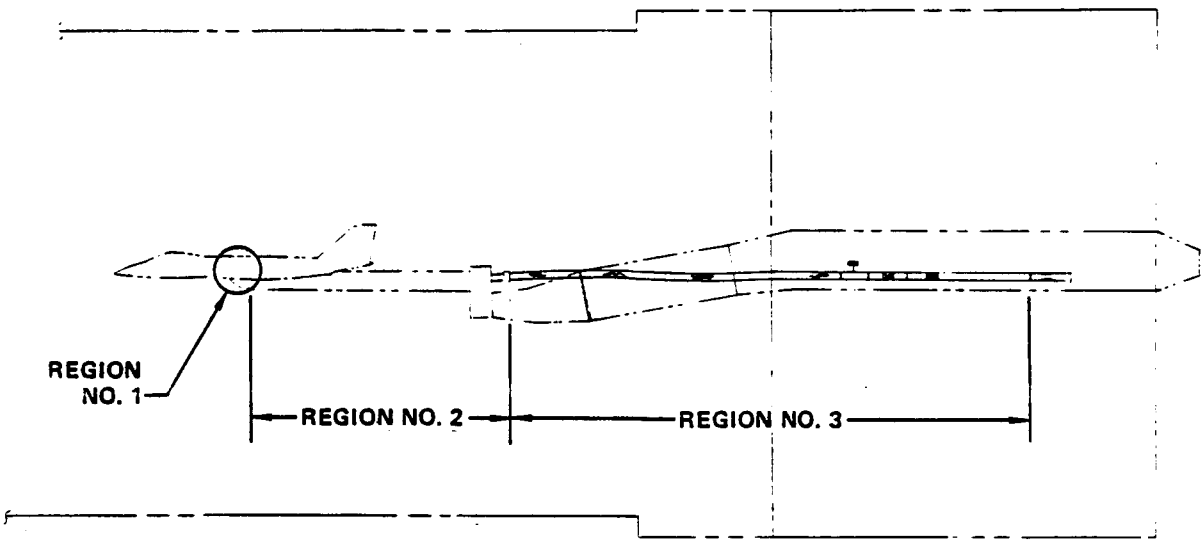

REGION	% OF TOTAL ΔP_t LOSS
NO. 1 INSIDE MODEL	62%
NO. 2 MODEL STRUT	18%
NO. 3 PALLET INSTALLED	20%

GP13-0503-58

FIGURE 5-4
TURBINE BLEED SYSTEM PRESSURE LOSS SUMMARY

In the detailed initial analysis presented in the March 1981 progress report, each of the above parameters was varied independently to assess their affects on CMAPS flexibility. Results indicated that reduction of bleed system pressure loss should be further evaluated, as well as a more optimum (smaller) mixer area. It was also determined that the larger of the two available venturis should be used. An increase in nozzle throat area was found to be effective, but was not considered due to the cost of new hardware.

Subsequent analyses has led to the final recommended system to achieve good CMAPS/model compatibility in terms of the flexibility envelope. The basis for comparison is the CMAPS flexibility obtained during the recent simulator development test at AEDC, Reference 1. A comparison of the key flexibility parameters for the CMAPS development system and the recommended NASA system, at the critical dry power condition, is given below:

Parameter	CMAPS Development System	Recommended NASA System
Turbine Bleed System Total Pressure Loss	20% (Bleed Manifold to Venturi)	42% (Bleed Manifold to Venturi)*
Bleed Venturi Area, A_v (in^2)	0.65	0.85
Dry Power Nozzle Throat Area, A_8 (in^2)	3.098	2.83
CMAPS Mixer Area, AE57 (in^2)	.1073	0.062

*Bleed air system defined in paragraph 5.1.2

The recommended parameter values above represent (1) an increased model bleed line area, compared to the earlier design, of about 10%, (2) the use of the larger of the two available NASA venturis, (3) reduced area mixer and (4) the use of the currently available ALBEN nozzle from the ANC program. The minimum CMAPS operating line for the recommended NASA system is shown in Figure 5-5, compared to the CMAPS development system. This prediction has been made using the GE CMAPS cycle analysis and the noted inputs. The recommended system is considered well within acceptable limits, with capability to achieve maximum CMAPS airflow (1.65 lb/sec) with adequate stall margin.

5.2 FLOW-THROUGH TEST MODE CONCEPT - The testing in the conventional flow-through mode is designed to measure the basic vehicle aerodynamics, including canard trim and inlet drag characteristics and any associated interactions. Conceptual design of the flow-through mode is shown in Figure 5-6.

The only model change required to convert from the simulator to the flow-through mode is to remove the CMAPS units and install the flow-through duct. The duct includes a dummy hub to simulate the simulator compressor hub. The nozzle extensions are normally installed in the flow-through mode, although the ALBEN can be tested if desired. The flow-through duct is mounted using the same attachment as the CMAPS to ensure identical positioning of the inlet duct seal. The nozzle extensions are cantilevered from the common transition duct/nozzle support.

Inlet mass flow ratio is controlled with chokes at the nozzle extension exit. A set of four chokes is sufficient to cover the range of inlet mass flow ratios available with the CMAPS units. The choke exit areas will range from approximately 2.5 to 5.2 in^2. Chokes of similar areas were utilized in the 8.5% Simulator Development Program and effectively covered the airflow range of interest. At Mach 0.6 and below, an ejector will be required to obtain the full range of inlet mass flow

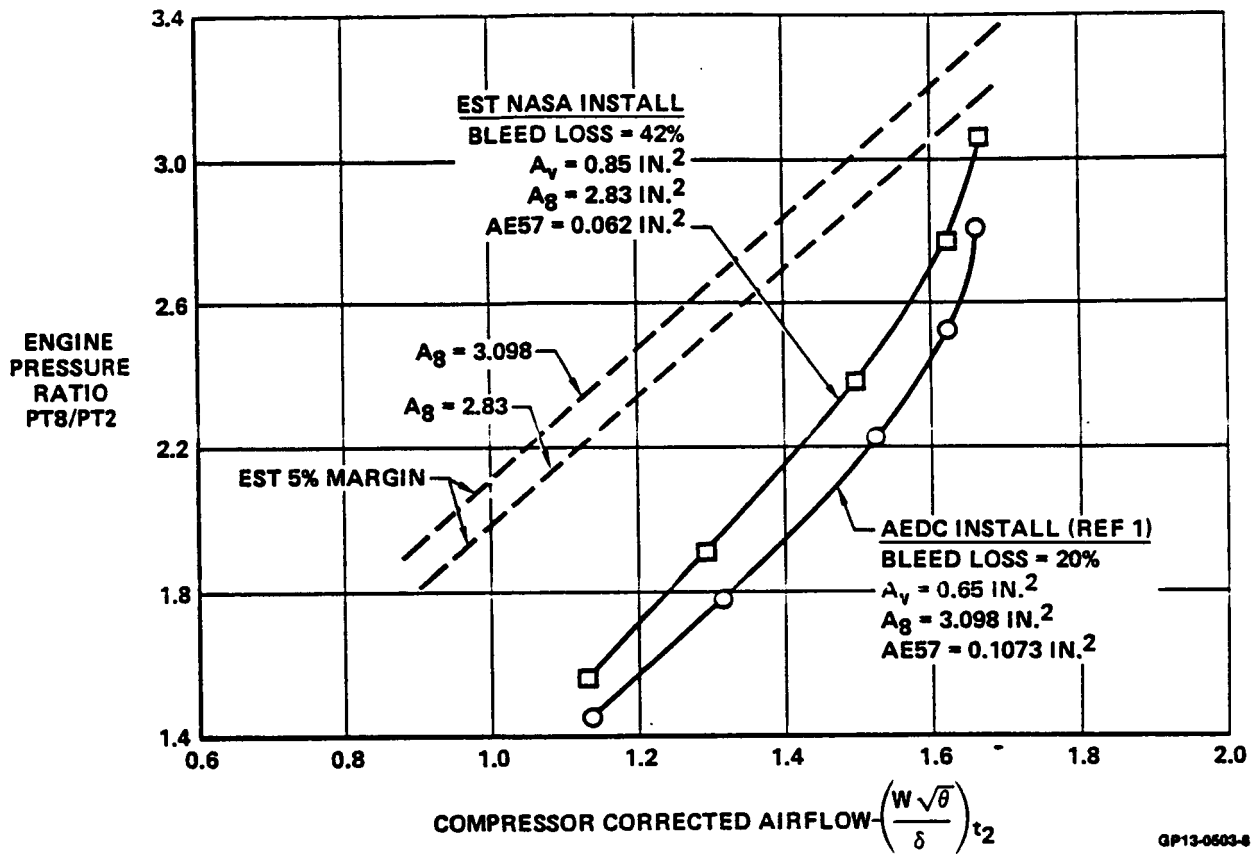

FIGURE 5-5
ESTIMATED SIMULATOR FLEXIBILITY ENVELOPE
M_O = 0.3; PT_2 = 15.2; P_{amb} = 15.1

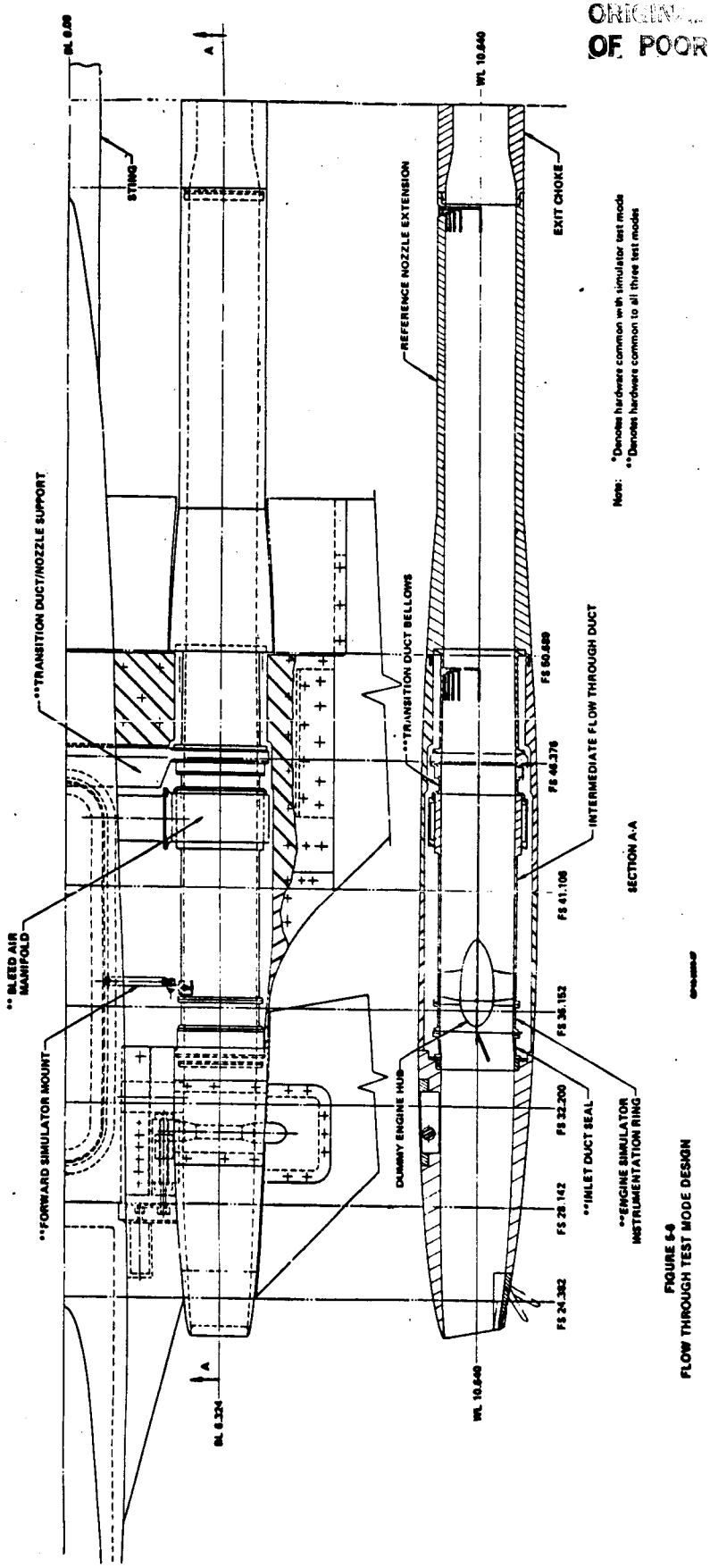

FIGURE 5-8
FLOW THROUGH TEST MODE DESIGN

ratios. It will be mounted on the tunnel support, as shown in Figure 5-7. Flexible lines will connect the ejector to the model. The CMAPS air supply will be adequate to power the ejector.

The recommended ejector for the lower speed testing is MCAIR owned and was previously used at NASA/Ames in an inlet development program, Reference (12). In this program, the ejector was used to pump up to 7.0 lbm/sec corrected airflow. The ejector flow/pressure requirements are presented in Figure 5-8.

5.3 JET-EFFECTS TEST MODE CONCEPT - Testing in the conventional jet-effects mode is designed to measure the incremental aerodynamics effects due to nozzle geometry (dry and afterburning), nozzle pressure ratio, and vectoring. Conceptual design of the jet-effects mode is shown in Figure 5-9.

The only model change required to convert from the simulator to the jet-effects mode is to remove the CMAPS units and install the high pressure air supply plenum assembly. Inlet fairings are also added.

In this mode, the non-metric plenum assembly is attached using the identical attachments as for the other two modes. The duct metric break seal and instrumentation ring forward of the plenum are retained, even though they do not serve a function. This is to ensure consistency in the duct metric break seal tare among the test modes. The bellows and transition duct aft of the plenum are also retained. The ALBEN nozzles mount to the transition duct/nozzle support, thus vectoring loads are transmitted directly to the balance housing.

The high pressure jet-effects plenum (Figure 5-9) is designed to provide the same total pressure levels and distribution at the nozzle charging station as the CMAPS. To accomplish this, the actual CMAPS mixers will be utilized as part of the air

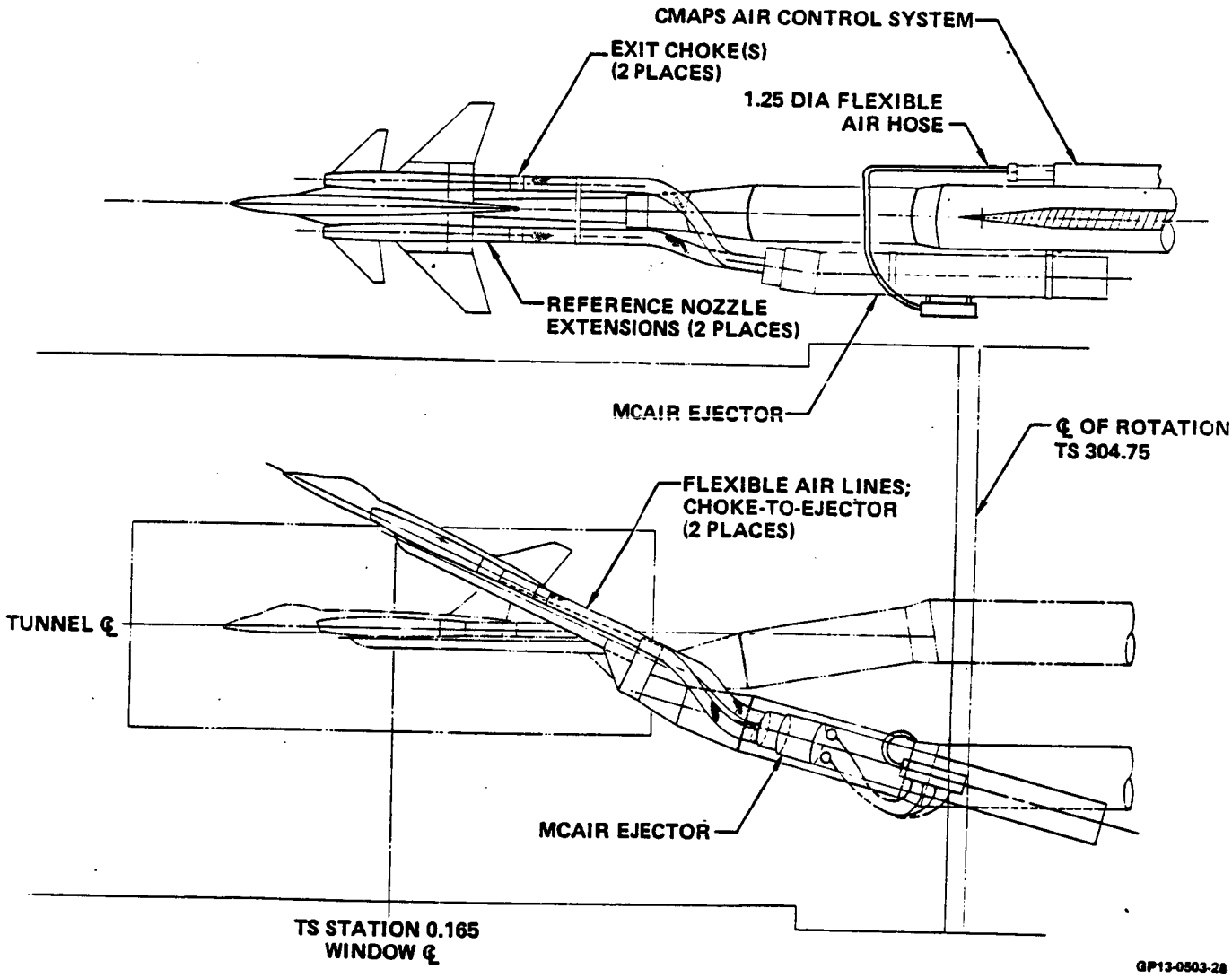

FIGURE 5-7
EJECTOR INSTALLATION FOR LOW SPEED FLOW THROUGH TESTING

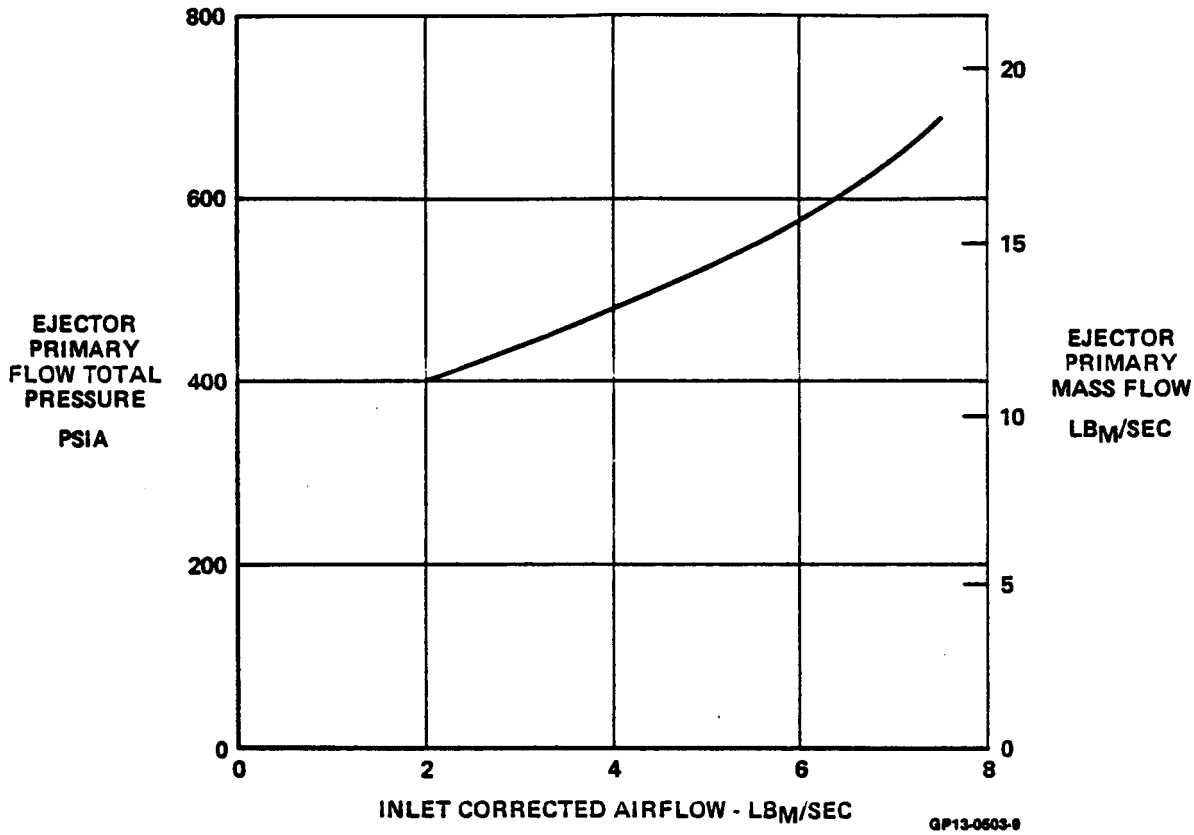

FIGURE 5-8
EJECTOR FLOW/PRESSURE REQUIREMENTS STATIC OPERATION
Static Condition

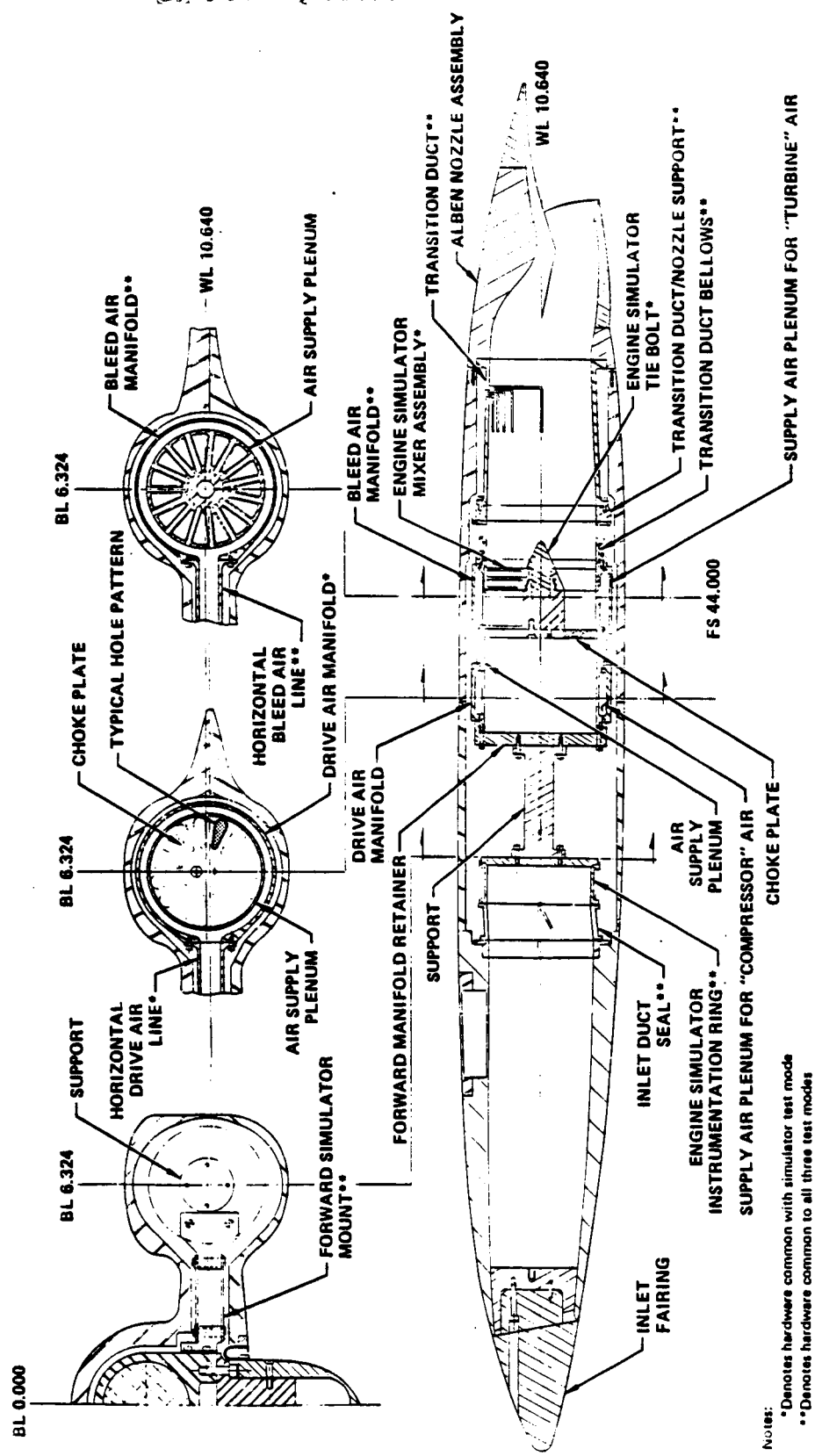

Notes:
*Denotes hardware common with simulator test mode
**Denotes hardware common to all three test modes

FIGURE 5-9
JET-EFFECTS TEST MODE DESIGN

supply plenum. Two separate high pressure air supplies are provided to the plenum. One supply comes in through the same line that provides the drive air to the CMAPS, and thus represents the compressor airflow. This flow passes through a choke plate and in between the mixer lobes. The other supply, simulating the CMAPS turbine exit flow, comes through the CMAPS bleed air lines directly into the mixer. After passing through the mixer chokes, this air combines with the "compressor" air. By independent control of the pressure of each supply, it should be possible to match both the nozzle flow pressure level and distribution profile of the actual CMAPS at a variety of conditions.

This plenum design should also match the actual CMAPS nozzle temperature distribution, since the actual CMAPS mixers are used. The current CMAPS design has demonstrated less than 6% nozzle temperature distortion, Figure 5-10. These data were measured at dry power operation during the simulator development program.

An analysis was conducted to assess the feasibility of also matching the actual temperature levels of the CMAPS compressor exit and turbine exit flows. To match the CMAPS compressor exit properties, air heated as high as 400°F must be supplied through the model. Under this condition, the temperature of the force balance would be near the 180°F limit of the balance. In addition, the thermal analysis indicated a large axial temperature gradient (≈50°F) would occur along the balance. Therefore, to provide a more uniform temperature environment for the balance and thereby reduce bias errors between test modes, it was decided to supply the jet-effects air at the same temperature levels as in the simulator mode, or about 200°F. Jet-effects operation at slightly lower nozzle temperatures than in the CMAPS mode should not greatly affect the data comparison between test modes, based on the Reference 13 test data. These data indicate only a 1 drag count difference due to nozzle jet temperature variations between 500 and 800°R, as shown in Figure 5-11.

C-2

$$T\,7\ Dist = \left(\frac{T\,7_{max} - T\,7_{min}}{T\,7_{avg}}\right) \times 100$$

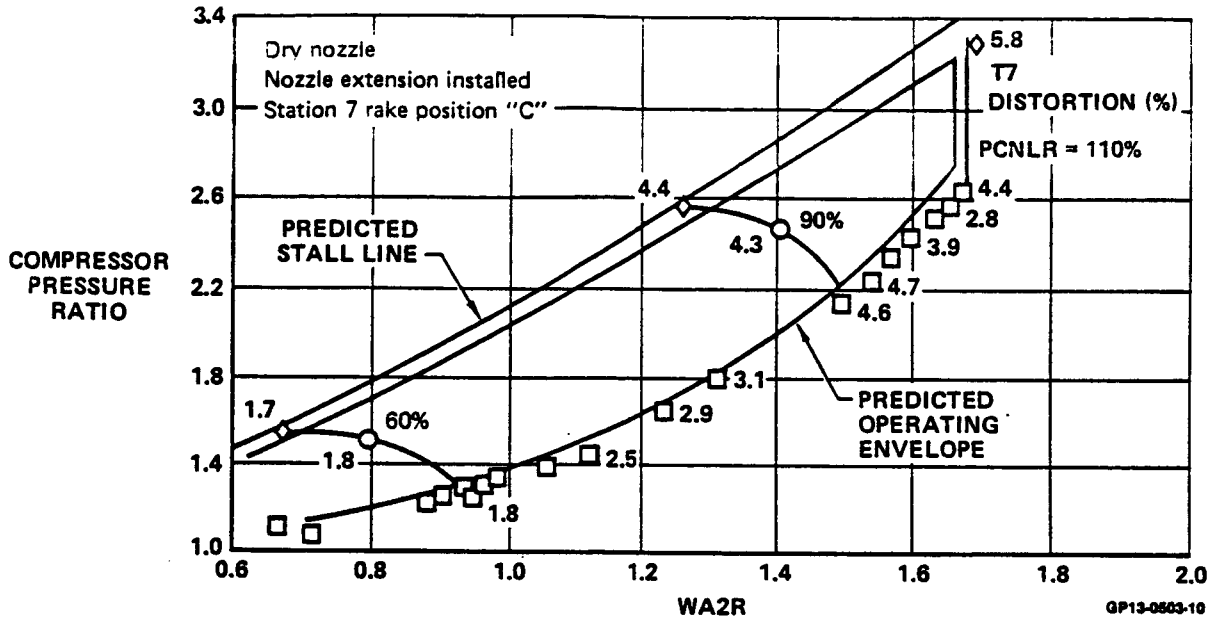

Ref: 1980 CMAPS testing at AEDC

FIGURE 5-10
CMAPS NOZZLE TEMPERATURE (T7) DISTORTION

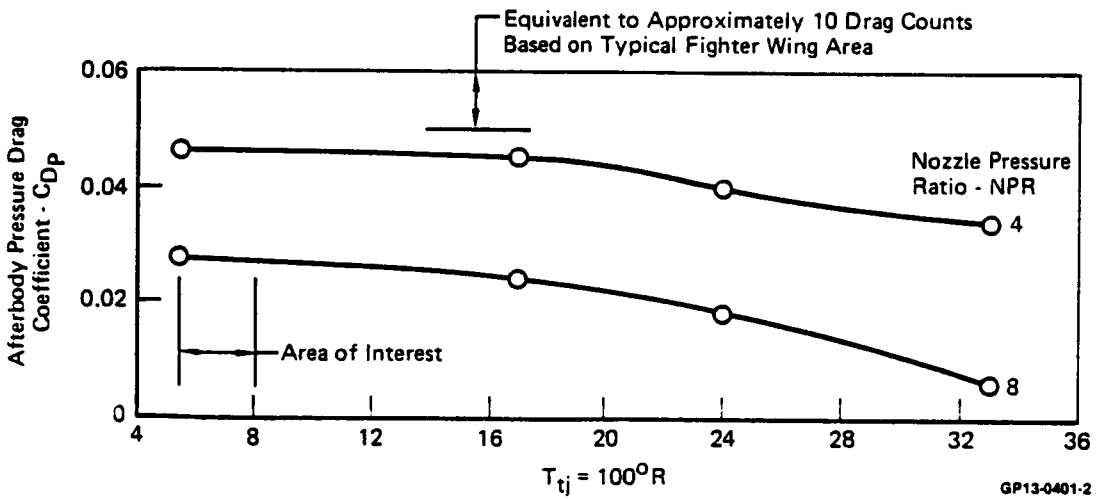

Notes:
1. Maximum CMAPS NPR = 6.7 @ M_o 0.9: P_{amb} = 5.5
2. Ref: AEDC-TR-76-109 & AEDC-TR-76-102

Figure 5-11. Effect of Jet Temperature on Afterbody Drag
$M_O = 0.9$ 15° Boattail Convergent Nozzle Geometry

6.0 INSTRUMENTATION

The model and CMAPS instrumentation for this program are extensive. Model force balance instrumentation is provided, as well as extensive internal flow measurements and external pressure instrumentation. CMAPS instrumentation is required to monitor/control operation and health. All instrumentation definition was thoroughly reviewed with NASA in Phase 1 to arrive at a preliminary set of requirements. In addition, the instrumentation routing in the model received considerable attention.

6.1 MODEL INSTRUMENTATION - The majority of the model instrumentation is common to all test modes. Some is test mode peculiar, relating to control/measurement of unique propulsion system simulation parameters, such as airflow and nozzle pressure ratio. A summary of the instrumentation and function is presented in Figure 6-1 for all test modes.

The model surface pressure instrumentation is used to diagnose the localized effects of flowfield coupling. Locations for these pressure orifices is defined in Figure 6-2. Since the nozzle boattail is non-metric in this installation, extensive boattail pressure measurement is provided for integration and assessment of boattail drag, as detailed in Figure 6-3.

6.2 CMAPS INSTRUMENTATION - The NASA furnished instrumentation for the CMAPS is used to monitor the units health and operation and to provide control variables. A list of this instrumentation is presented in Figure 6-4.

6.3 INSTRUMENTATION ROUTING - Routing of the large amount of the instrumentation in this model is critical, especially in the simulator mode. A full size layout of the overall model instrumentation routing is provided as Enclosure (2) to this report transmittal. The model static pressures will be routed to

SYMBOL	DEFINITION	QUANTITY	SIMULATOR	FLOW-THROUGH	JET EFFECTS	SIDE	PURPOSE
P_S	FUSELAGE/WING STATIC PRESSURE	81	X	X	X	SEE FIGURE 6-2	ASSESS EFFECTS OF FLOWFIELD COUPLING
P_{NB}	NOZZLE BOATTAIL STATIC PRESSURE	52	X	X	X	↓	NOZZLE DRAG INTEGRATION
P_{T2}	COMPRESSOR FACE TOTAL PRESSURE	30	X	X	X	10-L/20-R	STEAM THRUST; DISTORTION
P_{S2}	COMPRESSOR FACE STATIC PRESSURE	6	X	X	X	2-L/4-R	STEAM THRUST; DISTORTION
P_C	INTERNAL MODEL CAVITY PRESSURE	10	X	X	X	–	INTERNAL CAVITY PRESSURE TARE CORRECTION
P_{DS}	DUCT SEAL STATIC PRESSURE	5	X	X	X	L/R	INLET DUCT SEAL PRESSURE TARE CORRECTION
P_{AS}	AFT METRIC BREAK STATIC PRESSURE	8	X	X	X	L	AFT METRIC BREAK PRESSURE SEAL CORRECTION
T_{HOUS}	BALANCE HOUSING TEMPERATURE	8	X	X	X	–	BALANCE TEMPERATURE CONTROL
T_{BAL}	BALANCE TEMPERATURE	4	X	X	X	–	BALANCE TEMPERATURE MONITOR
B_L	BALANCE LEAD	1	X	X	X	–	BALANCE OUTPUT
BM_C	CANARD ROOT BENDING MOMENT	1	X	X	X	R	CANARD BENDING MOMENT DETERMINATION
δ_c	CANARD DEFLECTION ANGLE	1	X	X	X	L/R	CANARD POSITION
P_{T7}(1)	NOZZLE DUCT TOTAL PRESSURE	4	X		X	L/R	EPR; NPR DETERMINATION
T_{T7}	NOZZLE DUCT TOTAL TEMPERATURE	2	X		X	L/R	↓
P_{TNC}	NOZZLE CHOKE TOTAL PRESSURE	5		X		L/R	EXIT CHOKE AIRFLOW DETERMINATION
P_{NC}	NOZZLE CHOKE STATIC PRESSURE	4		X		L/R	↓
P_{TDM}	DRIVE AIR LINE STATIC PRESSURE	1	X			L/R	PRESSURE LOSS CALCULATION
P_{TBM}	BLEED AIR LINE TOTAL PRESSURE	1	X			L/R	↓
P_{TP}	AIR SUPPLY PLENUM TOTAL PRESSURE	1			X	L/R	JET-EFFECT DRIVE AIR CONTROL
P_{TM}	MIXER PLENUM TOTAL PRESSURE	1			X	L/R	↓
TOTAL			229	231	229		

Note: (1) One used for CMAPS controller for each simulator.

GP13-0503-11

FIGURE 6-1
MODEL INSTRUMENTATION SUMMARY

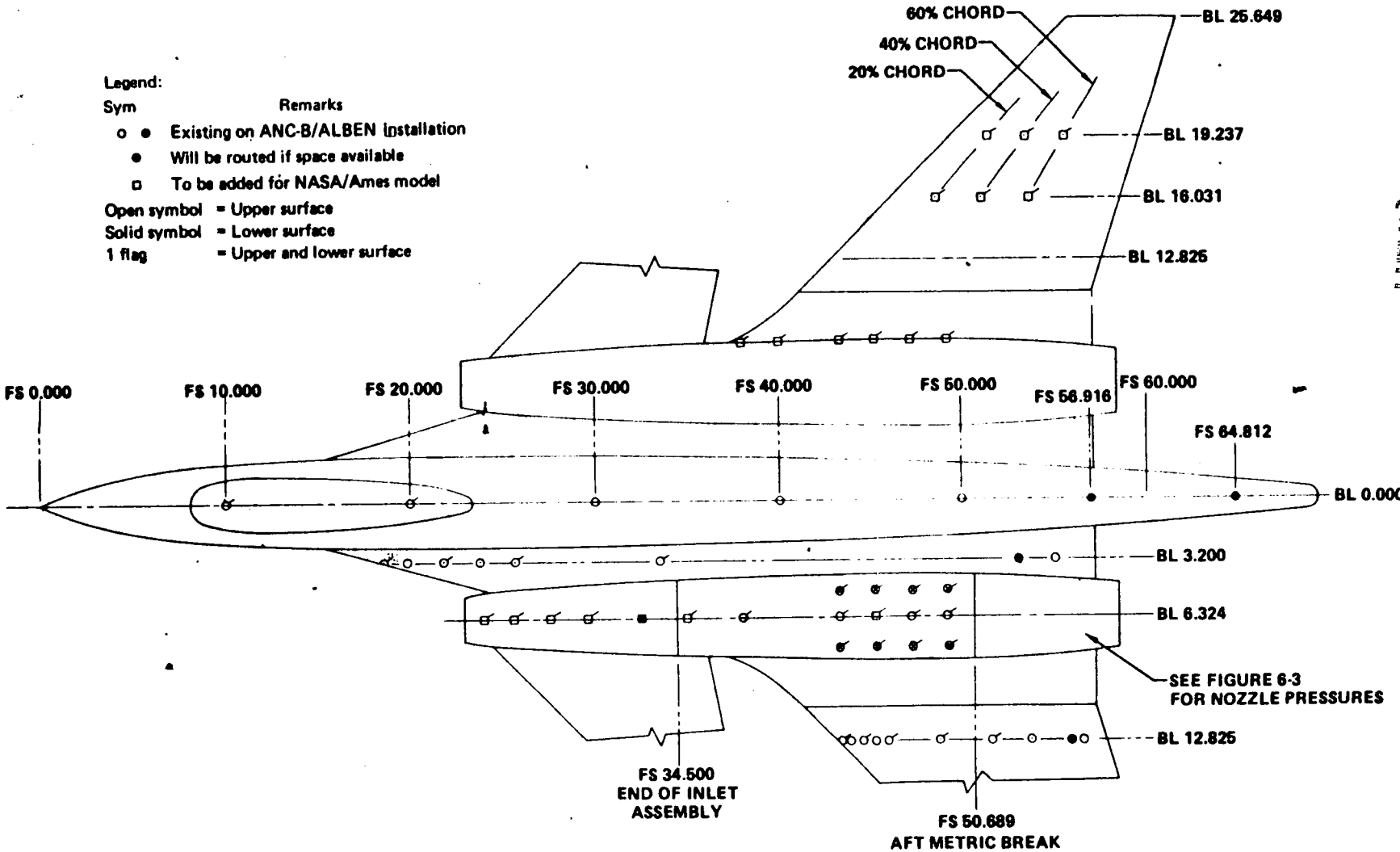

FIGURE 6-2
LOCATIONS FOR MODEL EXTERNAL PRESSURE INSTRUMENTATION
Plan View

GP13-0563-20

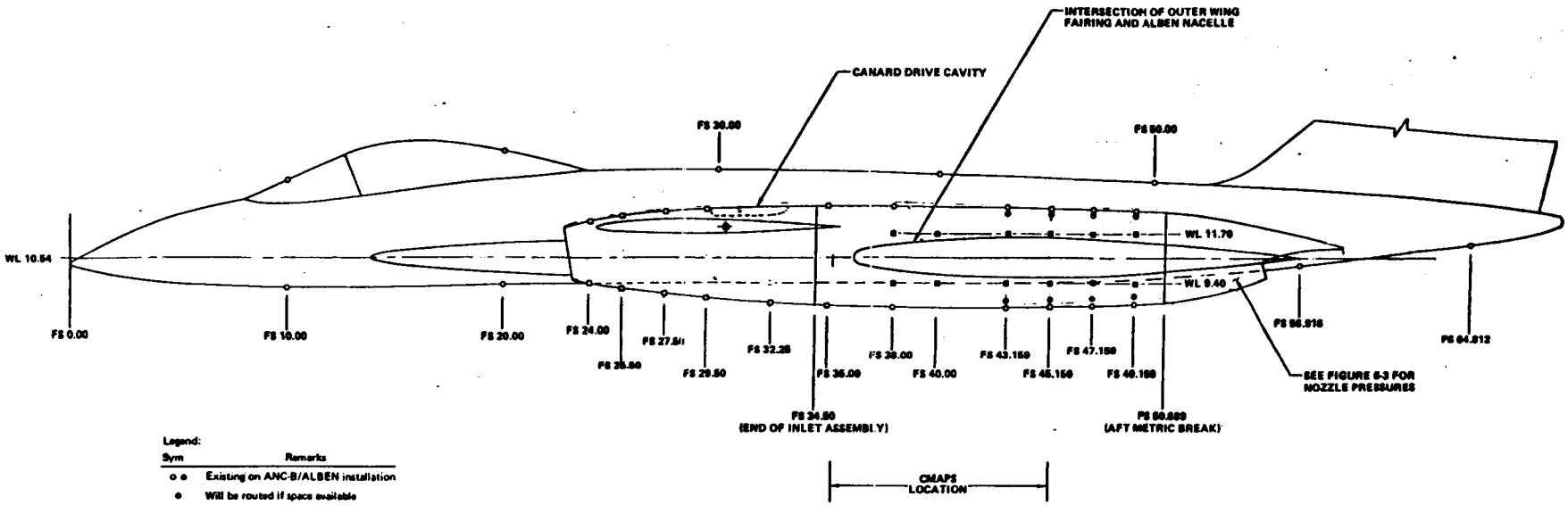

FIGURE 6-2 (Continued)
LOCATIONS FOR MODEL EXTERNAL PRESSURE INSTRUMENTATION
Sheer View

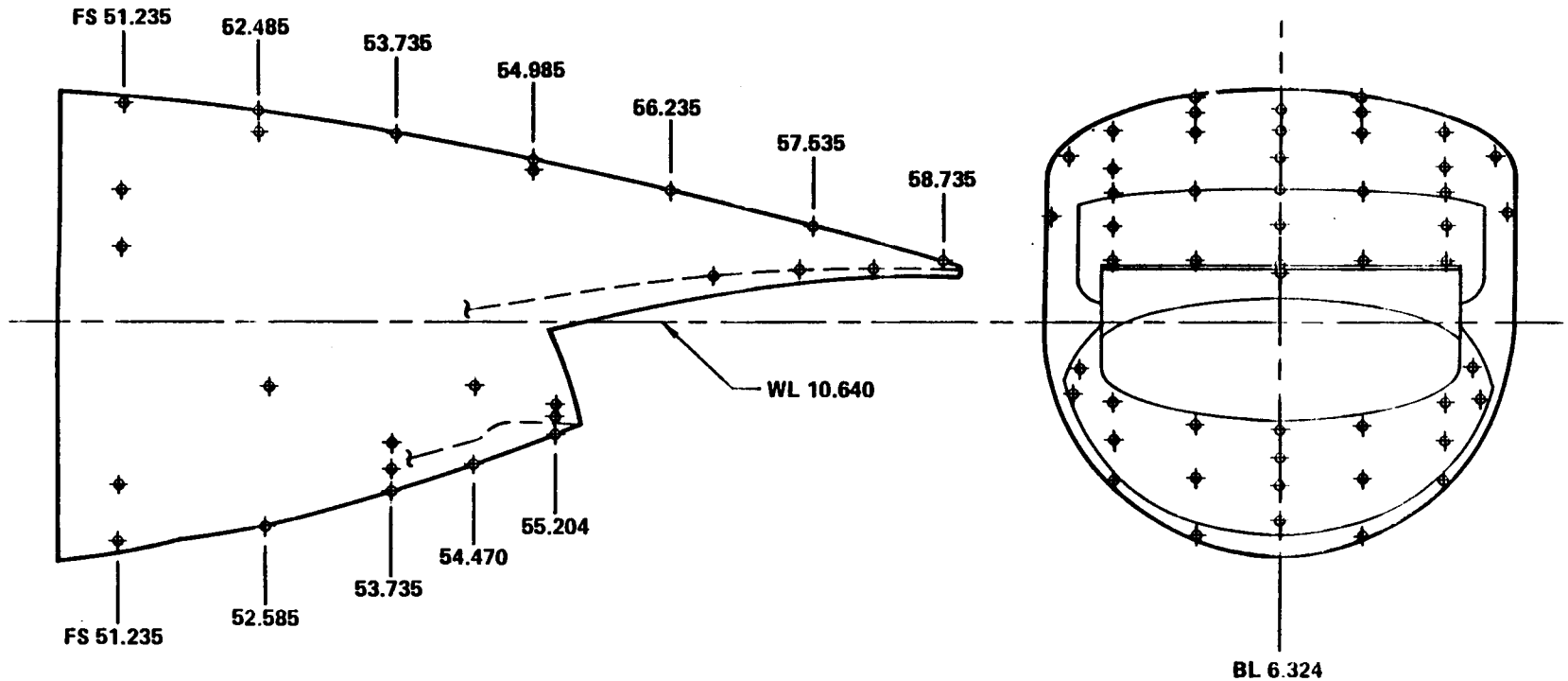

GP13-0503-13

FIGURE 6-3
LOCATIONS FOR ALBEN NOZZLE PRESSURE INSTRUMENTATION

SYM	DEFINITION	QTY	CONNECTS TO	FUNCTION
PT-2	COMPR FACE PRESS	1	CONTROLLER	EPR, STREAM THRUST
TBF-1	FWD BRNG TEMP	1	CONTROLLER	HEALTH/DIAGNOSTIC
TBF-2	FWD BRNG TEMP	1	BACKUP	HEALTH/DIAGNOSTIC
OVF	FWD OIL SCAVANGE	1	SCAVANGE SYSTEM	LUBE
OSF	FWD OIL SUPPLY	1	OIL SUPPLY SYSTEM	LUBE
N1	ROTOR SPEED	1	CONTROLLER	HEALTH/DIAGNOSTIC
N2	ROTOR SPEED	1	BACKUP	HEALTH/DIAGNOSTIC
TBA1, 2	AFT BRNG TEMP	2	CONTROLLER/BACKUP	HEALTH/DIAGNOSTIC
RT	ROTOR THRUST	1	CONTROLLER	HEALTH/DIAGNOSTIC
OVA-1	AFT OIL PRIME SCAVANGE	1	SCAVANGE SYSTEM	LUBE
OVA-2	AFT OIL SECONDARY SCAVANGE	1	SCAVANGE SYSTEM	LUBE
OSA	AFT OIL SUPPLY	1	OIL SUPPLY SYSTEM	LUBE
PS-57	MIXER PRESS	1	CONTROLLER	HEALTH/DIAGNOSTIC
PSK15	COMP DISCRG DYN PRESS	1	CONTROLLER	HEALTH/DIAGNOSTIC
TT-4	TURBINE INLET TEMP	1	CONTROLLER	HEALTH/DIAGNOSTIC
PS, PT-15	COMPR DISCH PRESS	2	CONTROLLER	W_2 (CORRECTED)
TT-15	COMPR DISCH TEMP	1	CONTROLLER	W_2 (CORRECTED)
PT-4	TURBINE INLET PRESS	1	CONTROLLER	HEALTH/DIAGNOSTIC
V1B	VIBRATION	1	CONTROLLER	HEALTH/DIAGNOSTIC
PT-7	NOZZLE TOTAL PRESS	1	CONTROLLER	NPR, EPR

GP13-0503-12

FIGURE 6-4
SIMULATOR INSTRUMENTATION SUMMARY
Per Simulator

Scanivalves inside the model. There are six 48-port, Type S Scanivalves in the model, two in the aft fuselage and four in the forward fuselage. The nozzle boattail instrumentation will be routed from the nozzle, through the inner wing, and to the aft Scanivalves, as shown in Figure 6-5. Due to space limitations, the pressures will be split between left and right hand nozzles. The remaining model static pressures will be routed to the forward Scanivalves. The total pressures for nozzle pressure ratio and CMAPS/jet effects high pressure air measurement will be routed to a NASA-supplied transducer pod located on the tunnel support system. The CMAPS instrumentation required for health monitoring and control will also be routed to this transducer pod.

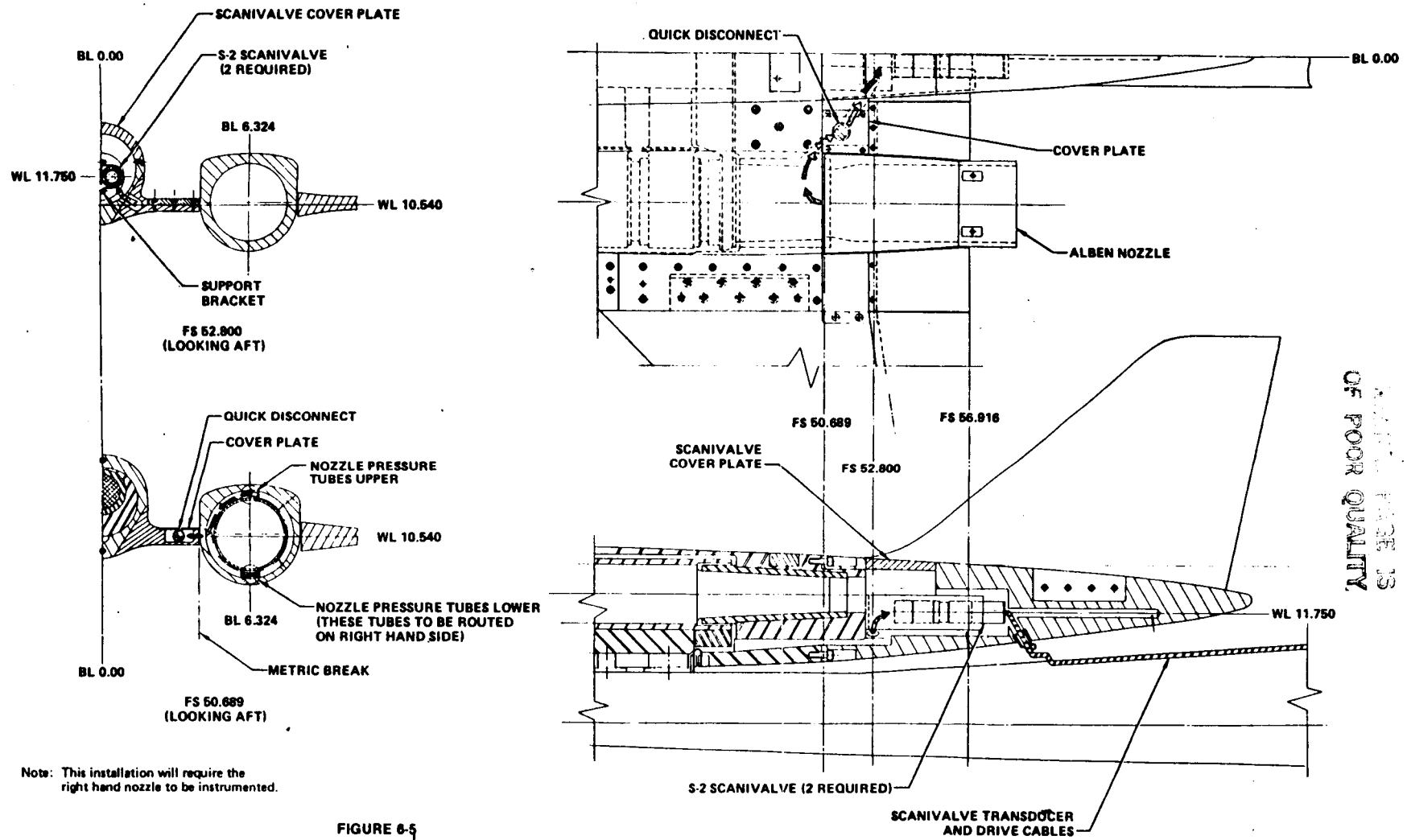

Note: This installation will require the right hand nozzle to be instrumented.

FIGURE 6-5
NOZZLE INSTRUMENTATION ROUTING

7.0 ERROR ANALYSIS

An error analysis was initiated in Phase 1 to assess the random error in key aerodynamic performance parameters (C_D, C_L, C_M) as measured by the model system. Purpose of this activity is to identify the major contributing error sources, and any necessary changes to the data acquisition/reduction procedures, instrumentation, calibration procedures, and possibly the model design. In Phase 1 activity, the error analysis methodology was established, the necessary data reduction equations were formulated, and errors were predicted for a sample case. This analysis will be finalized in Phase II after tests of the model under the ANC program are completed. This will permit actual model data (i.e. measurand values and calibration accuracies) to be used, thus ensuring maximum benefit from the analysis.

7.1 METHODOLOGY - The error analysis procedure being used is a comprehensive method developed under the Exhaust System Interaction Program, Reference 14. It has been implemented at MCAIR in a generalized error analysis computer program. This program was written according to the standard technique of propagation of errors as described in Reference 15. The procedure can be described briefly by letting x_1, x_2, x_3 ... represent random values whose true values are X_1, X_2, X_3 ... and letting u represent a derived quantity whose true value is given by,

$$U = f(X_1, X_2, X_3 \ldots)$$

and also letting e_1, e_2, e_3 ... represent the statistically independent errors (standard deviations) of x_1, x_2, x_3 ... respectively. Then the error induced in u, which will be denoted by δ, as a result of the errors e_1, e_2, e_3 ... has a variance equal to

Eq (a):

$$V(\delta) = \sigma^2(\delta)$$

$$= \left(\frac{\partial f}{\partial x_1}\right)^2 \sigma_{e_1} + \left(\frac{\partial f}{\partial x_2}\right)^2 \sigma_{e_2}{}^2 + \left(\frac{\partial f}{\partial x_3}\right)^2 \sigma_{e_3}{}^2 + \ldots$$

where $\partial f/\partial x_i$ is the sensitivity of u with respect to the variable x_i. These partial derivatives are computed by means of either a three point or a five point differentiation scheme at values equal to the measured values of X_1, X_2, X_3 ... From equation (a), the percent contributions to $\sigma^2(\delta)$ by x_1, x_2, x_3 ... can be computed by

$$\% \text{ Contribution} = \{ \sigma_{e_i}{}^2 \left(\frac{\partial f}{\partial x_i}\right)^2 / \sigma^2(\delta) \} 100.$$

The basic structure of the program is outlined in Figure 7-1. The aerodynamic coefficients of interest are calculated in several user provided function subroutines. These subroutines contain the data reduction equations which are included herein as Appendix C. User numerical input consists of the measurands and their associated one sigma (standard deviation, σ) uncertainties. A description of the measurands is also given in Appendix C.

7.2 SAMPLE CASE RESULTS - A sample test case has been run for the simulator test mode to demonstrate the content and format of the forthcoming error analysis. The sample case incorporates input data from tests in Phase 1 of the ANC program, and estimates for the CMAPS related quantities not measured in the ANC program. The ANC data, although not expected to accurately represent the current model, does provide a reasonably good data base from which the operation and usefulness of the procedure may be verified. The numerical results presented here should be interpreted accordingly.

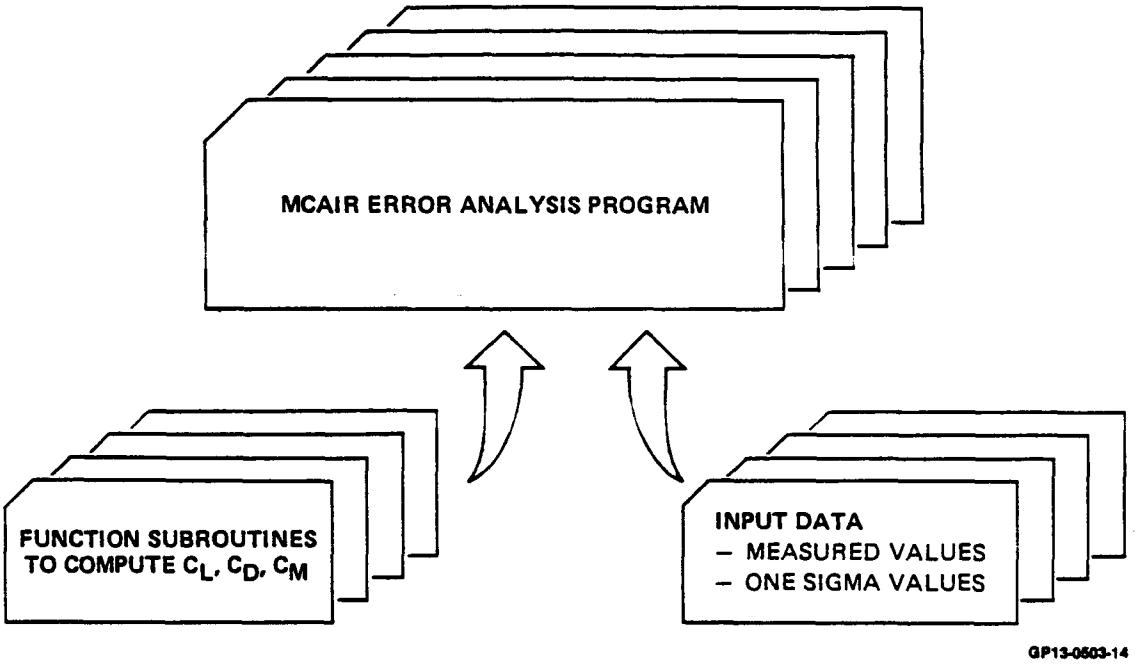

FIGURE 7-1
ERROR ANALYSIS COMPUTER PROGRAM STRUCTURE

The operating point selected for the sample case is at Mach 0.9, 4° angle of attack, and dry power. This corresponds to a typical subsonic cruise condition. The output of the MCAIR error analysis program for the sample test case is shown in Figure 7-2. Presented for each calculated quantity (i.e. C_L, C_D and C_M) are its value, variance and standard deviation (sigma). Also listed are the percent contributions to the total error of the major contributors. Only those measurands contributing more than .1% of the total variance are listed in the output. Taking the drag coefficient (CD) as an example, the standard deviation is 0.0011, or 11 counts, with the balance normal force contributing 68% of the total variance and axial force contributing 24%.

7.3 PLANNED ERROR ANALYSIS CASES - Plans are to complete the error analysis in Phase II, using data from the ANC model to be used in the NASA program. Each of the three test modes will be analyzed at three points. These points have been selected to be near important conditions on the DLI mission, as follows:

DLI MISSION SEGMENT	CONDITION
Supersonic Dash Out	Mach 1.4, α = 0°, A/B Power
Subsonic Cruise Back	Mach 0.9, α = 4°, Dry Power
Subsonic Maneuver	Mach 0.6, α = 20°, A/B Power

SAMPLE CASE OUTPUT

```
....CALCULATED QUANTITIES....JET EFFECTS TEST CASE                    PT  0 PAGE  10....

 NAME= CL          VALUE=      .30083    VAR=      .000163    SIGMA=      .012762
      MEAS. QUAN.   VALUE   SAMPLE ST.DEV.  CONTRIBUTION  PER-CENT OF VAR
      FNGA       712.100000   30.000000     1.623E-04        99.6
      CPCAV       -.005000     .008000      2.417E-07          .1

 NAME= CD          VALUE=      .02289    VAR=      .000001    SIGMA=      .001080
      MEAS. QUAN.   VALUE   SAMPLE ST.DEV.  CONTRIBUTION  PER-CENT OF VAR
      ALPHAM        .069800     .000300     8.145E-09          .7
      FNGA       712.100000   30.000000     7.931E-07        68.0
      FAGA        20.500000    1.250000     2.817E-07        24.1
      CPCAV       -.005000     .008000      5.396E-08         4.6
      M            .900000     .005000      1.555E-08         1.3
      TTR        540.000000    4.000000     4.312E-09          .4
      A2           7.069000    .047100      2.261E-09          .2
      PO           5.500000    .019600      3.461E-09          .3

 NAME= CM          VALUE=      .03091    VAR=      .000017    SIGMA=      .004089
      MEAS. QUAN.   VALUE   SAMPLE ST.DEV.  CONTRIBUTION  PER-CENT OF VAR
      MMGA      1169.900000  157.500000     1.668E-05        99.7
```

EXPLANATION OF TERMS

PARAMETER	DESCRIPTION
CL	LIFT COEFFICIENT, CALCULATED QUANTITY
CD	DRAG COEFFICIENT, CALCULATED QUANTITY
CM	PITCHING MOMENT COEFFICIENT, CALCULATED QUANTITY
VALUE	VALUE OF CALCULATED OR MEASURED QUANTITY
VAR	VARIANCE OF CALCULATED QUANTITY
SIGMA	STANDARD DEVIATION OF CALCULATED QUANTITY
SAMPLE ST DEV	STANDARD DEVIATION OF MEASURED QUANTITY
CONTRIBUTION	CONTRIBUTION OF MEASURED QUANTITY TO TOTAL VARIANCE
PERCENT OF VARIANCE	PERCENT CONTRIBUTION TO TOTAL VARIANCE
MEAS QUANTITIES	MEASURANDS
ALPHAM	MODEL ANGLE-OF-ATTACK
A2	COMPRESSOR FACE AREA
CPCAV	AVERAGE CAVITY PRESSURE
FAGA	BALANCE AXIAL FORCE READING
FNGA	BALANCE NORMAL FORCE READING
M	TUNNEL MACH NUMBER
MMGA	BALANCE PITCHING MOMENT READING
PO	TUNNEL STATIC PRESSURE
TTR	TUNNEL TOTAL TEMPERATURE

Note: Balance errors are taken to be 0.5% of the full scale reading

GP13-0503-15

FIGURE 7-2
ERROR ANALYSIS OUTPUT FOR SAMPLE CASE

8.0 REFERENCES

1. Air Force Contract F33615-77-C-2097, "Compact Multi-Mission Propulsion Simulator Development Program",

2. Air Force Contract F33615-77-C-3094, "Advanced Exhaust Nozzle System Concepts Demonstration (Part B)", September 1977.

3. MCAIR Letter M2Y-343-6710, "Phase I Preliminary Model Drawings and Stress Report Data Transmittal", Contract NAS 2-10791, dated 24 April 1981.

4. McDonnell Aircraft Company, "Propulsion and Airframe Aerodynamic Interactions of Supersonic V/STOL Configurations", (Technical Proposal), MDC A6219, dated 10 December 1979.

5. Hiley, P. E., Kitzmiller, D. E., and Willard, C. M., "Experimental Evaluation of Non-Axisymmetric Exhaust Nozzles", AFFDL-TR-78-185, December 1978, Air Force Contract No. F33615-76-C-3019.

6. McDonnell Aircraft Company, "Turbine Engine Multi-Mission Propulsion Simulator Wind Tunnel Demonstration", AFAPL-TR-76-73, dated November 1976.

7. McDonnell Aircraft Company, "Assessment of Installed Inlet Forces and Inlet/Airframe Interactions", AFFDL-TR-76-62, July 1976.

8. McDonnell Aircraft Company, "Investigation of Support System Interference on a Cylindrical Body", MDC A2188, 26 February 1973.

9. K. Lotter, and J. Malefakis, "Intake Design and Intake/ Airframe Integration For a Post-Stall Fighter Aircraft Concept", Paper No. 32, AGARD Symposium on High Angle of Attack Aerodynamics, Sandefjord, Norway, 4-6 October 1978.

10. Abbott, J. M., "Aerodynamic Performance of Scarf Inlets", NASA Technical Memorandum 79055, Lewis Research Center.

11. General Electric Company, "Final Pretest Report for Propulsion Simulator SN004/1 Aero/Mechanical Test and Evaluation", G.E. Technical Memorandum No. 80-210, dated 6 May, 1980.

12. McDonnell Aircraft Company, "Experimental Investigation of Several Fixed Geometry Inlets for Supersonic Aircraft at Mach Numbers from 0 to 2.0", MDC A3566, 17 October 1975.

13. AEDC, "Evaluation of Boattail Geometry and Exhaust Plume Temperature Effects on Nozzle Afterbody Drag at Transonic Mach Numbers", AEDC TR-76-102, October 1976.

14. Glaser, F. C. and Anderson, R. D., "Performance Projection of the Propulsion System Integrated with the Vehicle, Phase II Exhaust System Interaction Program", McDonnell Aircraft Company Report MDC A2817, 12 April 1974.

15. Mandel, J., "Statistical Analysis of Experimental Data", John Wiley & Sons, 1967.

APPENDIX A

TURBINE DRIVE AIR SYSTEM PRESSURE LOSS ANALYSIS

A detailed pressure loss analysis for the turbine drive system was conducted during Phase I of this program. The detailed results of this analysis are contained in this Appendix. The drive system was divided into the individual components shown in Figure A-1. A detailed geometric description of each component is contained in Figure A-2, along with the loss factors used and flow properties (total pressure, Mach number, and dynamic pressure) at each component.

ORIGINAL PAGE IS
OF POOR QUALITY

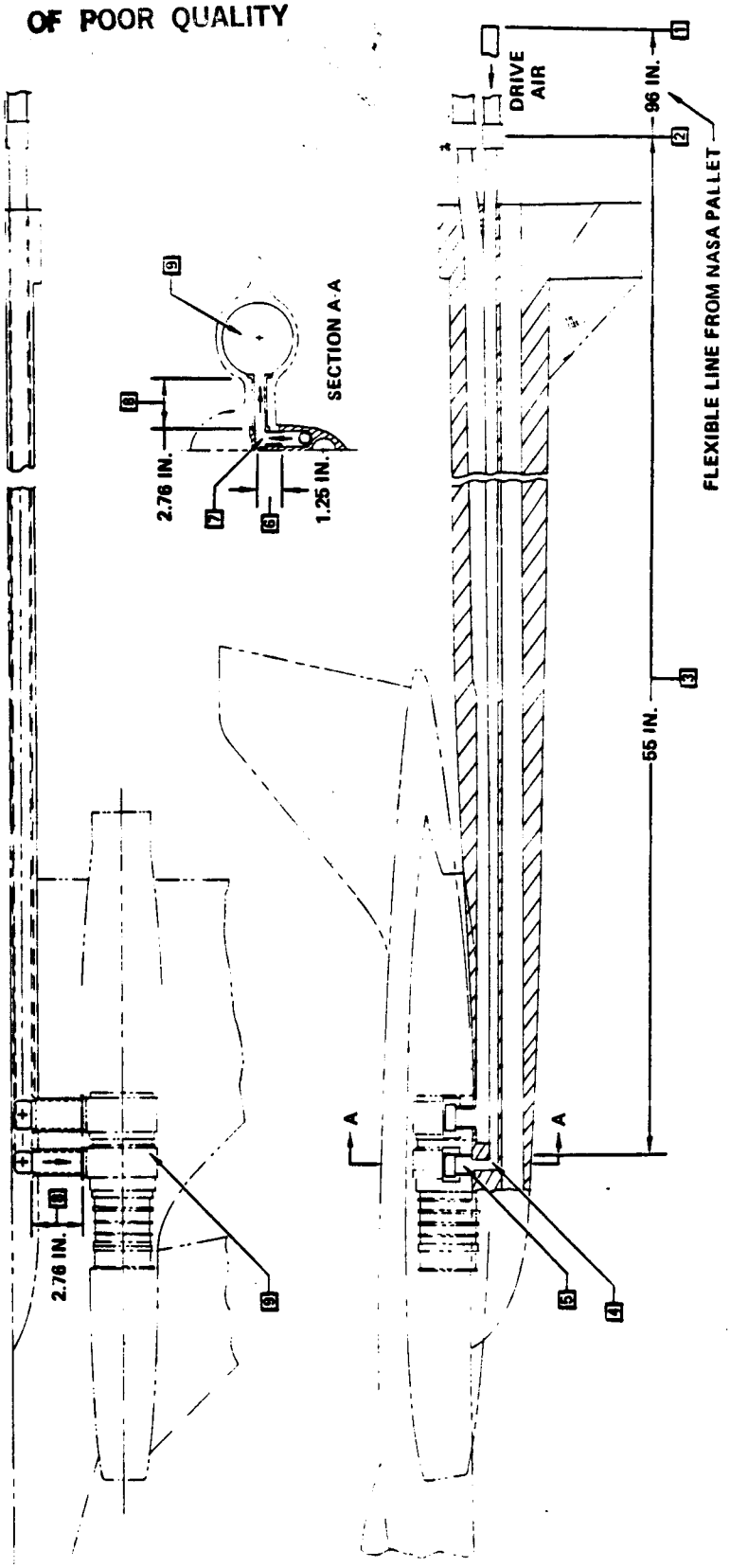

FIGURE A-1
TURBINE DRIVE AIR SYSTEM COMPONENTS

COMPONENT						FROM STATION		TO STATION				
NO.	DESCRIPTION	K_t	L (IN.)	DH (IN.)	4f	NO.	A (IN.^{2})	NO.	A (IN.^{2})	P_t	M	q
1	FLEXIBLE LINE FROM NASA FLOW CONTROL PALLET TO OFFSET ADAPTER (CONSTANT AREA SECTION PLUS GRADUAL TURNING)	3.84	96	1.0	0.030	1	0.785	2	0.785	1,947.5	0.101	13.8
2	TRANSITION INTO DRIVE LINE INSIDE MODEL STRUT (SUDDEN CONTRACTION)	0.24	–	–	–	2	0.785	3	0.366	1,931.4	0.224	66.3
3	CONSTANT AREA LINE INSIDE MODEL STRUT	2.022	55	0.68	0.025	3	0.366	4	0.366	1,797.3	0.242	71.8
4	TRANSITION FROM STRUT-TO-MODEL (90^0 CIRCULAR BEND, r/D = 1.0; $R_e = 1.1 \times 10^6$)	0.16	–	–	–	4	0.366	5	0.366	1,785.8	0.243	70.9
5	SUDDEN EXPANSION INSIDE MODEL	0.228	–	–	–	5	0.366	6	0.700	1,769.6	0.126	19.53
6	VERTICAL DRIVE LINE (CONSTANT AREA SECTION)	0.040	1.25	0.78	0.025	6	0.700	7	0.700	1,768.8	0.125	19.21
7	90^0 MITRE BEND	1.6	–	–	–	7	0.700	8	0.700	1,738.1	0.128	19.8
8	HORIZONTAL DRIVE LINE (CONSTANT AREA SECTION)	0.086	2.76	0.78	0.025	8	0.700	9	0.700	1,736.2	0.128	19.8
9	DRIVE MANIFOLD ENTRANCE-TO-TURBINE INLET (K_t PER FIGURE 7 OF SIXTH INTERIM REPORT "COMPACT MULTIMISSION PROPULSION SIMULATOR DEVELOPMENT", CONTRACT F33615-77-C-2097)	8.20	–	–	–	9	0.700	10	–	1,574.0	–	–

GP13-0503-62

Notes:

(1) K_t - Pressure loss coefficient $\frac{\Delta P_t}{q}$

(2) DH hydraulic diameter $\frac{4 \text{ area}}{\text{wetted perimeter}}$

(3) 4f - Friction factor

(4) K_t for typical components are

- Constant area section; $K_t = \frac{4fL}{DH}$
- Bends, contractions, and expansions; K_t per SAE manual and Crane Co. manual (Flow of Fluids)

FIGURE A-2
TURBINE DRIVE AIR SYSTEM PRESSURE LOSS ANALYSIS

APPENDIX B

TURBINE BLEED AIR SYSTEM PRESSURE LOSS ANALYSIS

A detailed pressure loss analysis for the turbine bleed system was conducted during Phase I of this program. The detailed results of this analysis are contained in this Appendix. The bleed system was divided into the individual components shown in Figure B-1. A detailed geometric description of each component is contained in Figure B-2, along with the loss factors used and flow properties (total pressure, Mach number, and dynamic pressure) at each component.

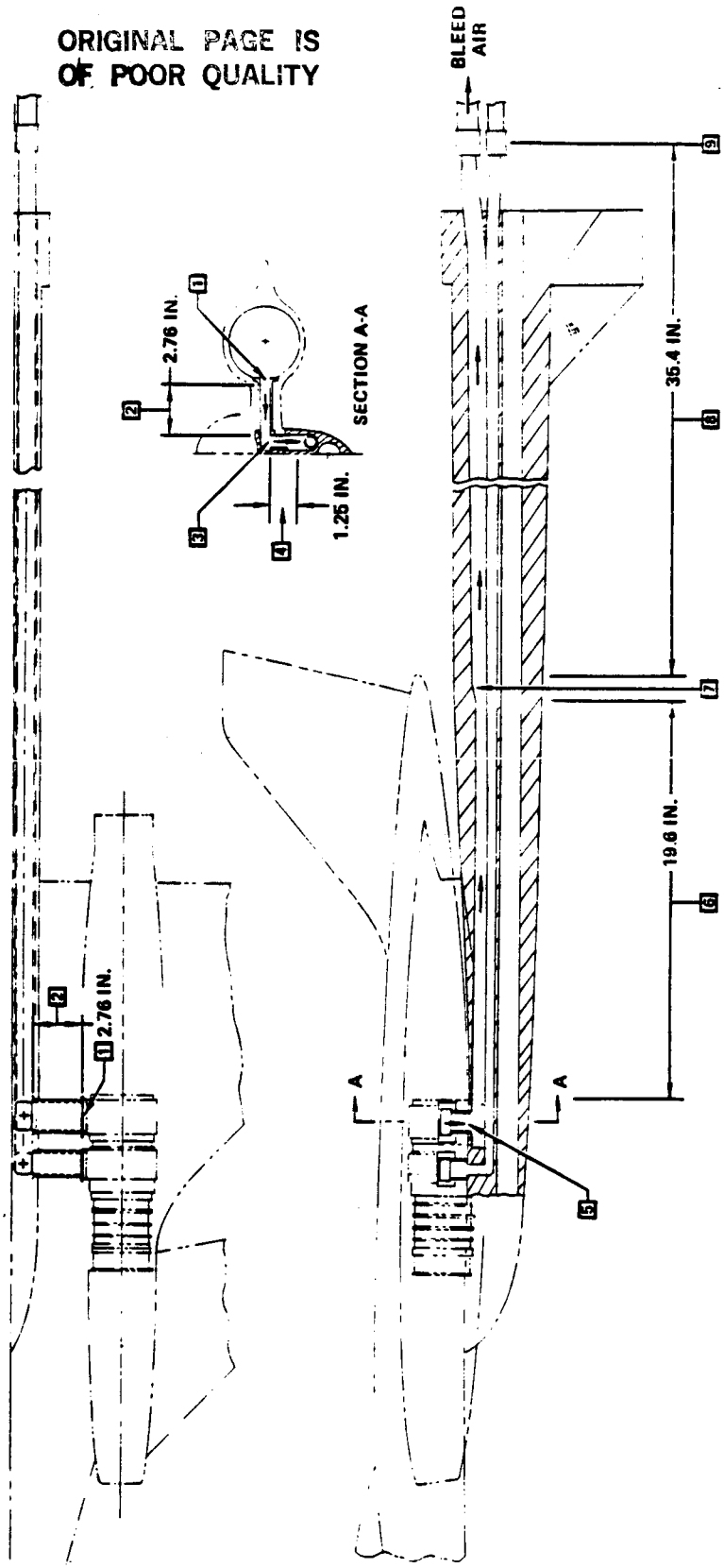

FIGURE B-1
TURBINE BLEED AIR SYSTEM COMPONENTS

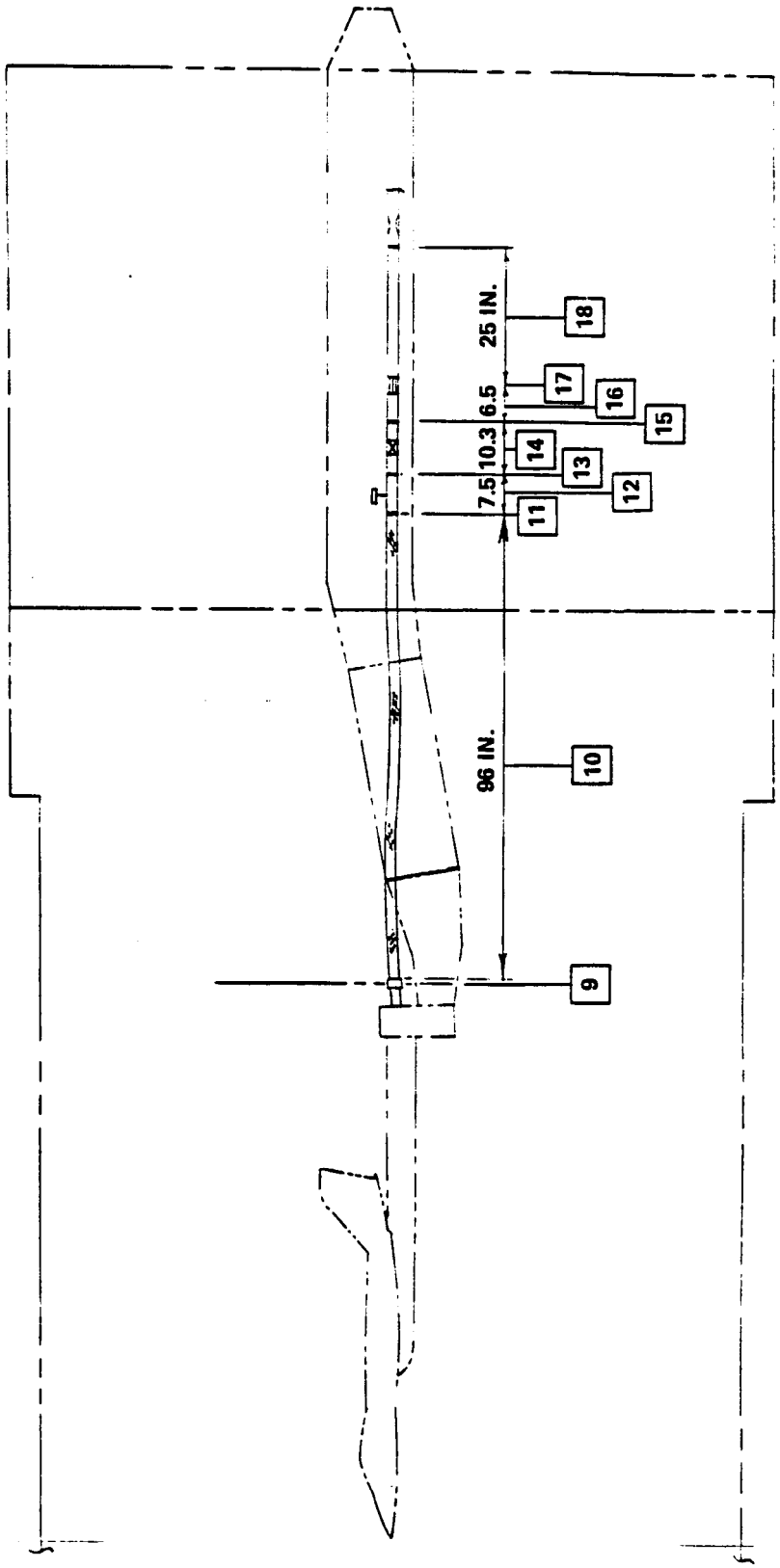

FIGURE B-1 (Continued)
TURBINE BLEED AIR SYSTEM COMPONENTS

COMPONENT						FROM STATION		TO STATION				
NO.	DESCRIPTION	K_t	L (IN.)	DH (IN.)	4f	NO.	A (IN.^{2})	NO.	A (IN.^{2})	P_t	M	q
1	BLEED MANIFOLD-TO-HORIZONTAL BLEED LINE (SUDDEN CONTRACTION)	0.13	–	–	–	1	1.606	2	1.05	114.24	0.328	7.83
2	HORIZONTAL BLEED LINE (CONSTANT AREA SECTION)	0.76	2.76	0.89	0.025	2	1.05	3	1.05	113.65	0.322	7.87
3	90° MITRE BEND	1.6	–	–	–	3	1.05	4	1.05	101.04	0.370	9.12
4	VERTICAL BLEED LINE (CONSTANT AREA SECTION)	0.035	1.25	0.89	0.025	4	1.05	5	1.05	100.72	0.371	9.13
5	TRANSITION FROM MODEL-TO-STRUT (90° MITRE BEND + EXPANSION)	1.7	–	–	–	5	1.05	6	1.23	85.25	0.375	7.89
6	FORWARD SECTION OF MODEL STRUT (CONSTANT AREA SECTION)	0.485	19.6	1.01	0.025	6	1.23	7	1.23	81.42	0.396	8.34
7	TRANSITION TO INCREASED AREA IN STRUT (SUDDEN EXPANSION)	0.060	–	–	–	7	1.23	8	1.62	80.92	0.290	4.59
8	AFT SECTION OF MODEL STRUT (CONSTANT AREA SECTION)	0.632	35.4	1.4	0.025	8	1.62	9	1.62	78.02	0.302	4.78
9	TRANSITION FROM OFFSET ADAPTERS-TO-FLEXIBLE LINE (SUDDEN EXPANSION)	0.234	–	–	–	9	1.62	10	3.14	76.90	0.152	1.23
10	FLEXIBLE LINE (CONSTANT AREA SECTION PLUS GRADUAL TURNING)	1.35	96.0	2.0	0.025	10	3.14	11	3.14	75.24	0.155	1.25
11	TRANSITION FROM FLEXIBLE LINE TO NASA FLOW CONTROL PALLET (SUDDEN CONTRACTION)	0.035	–	–	–	11	3.14	12	2.44	75.18	0.186	1.79
12	RUPTURE DISK ASSEMBLY (RUPTURE DISK PLUS 7.5 IN. CONSTANT AREA SECTION)	0.202	7.25	1.783	0.025	12	2.44	13	2.44	74.82	0.198	2.02
13	TRANSITION INTO FLOW CONTROL VALVE (SUDDEN CONTRACTION)	0.190	–	–	–	13	2.44	14	1.353	73.36	0.401	7.69

GP13 0503-83

FIGURE B-2
TURBINE BLEED AIR SYSTEM PRESSURE LOSS ANALYSIS

COMPONENT						FROM STATION		TO STATION				
NO.	DESCRIPTION	K_t	L (IN.)	DH (IN.)	4f	NO.	A ($IN.^2$)	NO.	A ($IN.^2$)	P_t	M	q
14	FLOW CONTROL VALVE (FULL OPEN VALVE, K_t = 0.1, PLUS 10.25 IN. CONSTANT AREA SECTION, K_t = 0.195)	0.295	10.25	1.313	0.025	14	1.353	15	1.353	71.89	0.416	7.98
15	TRANSITION TO CONSTANT AREA LINE (SUDDEN EXPANSION)	0.238	–	–	–	15	1.353	16	2.64	69.19	0.203	1.96
16	CONSTANT AREA LINE FROM CONTROL VALVE TO FLOW STRAIGHTENER	0.090	6.5	1.834	0.025	16	2.64	17	2.64	69.01	0.204	1.91
17	FLOW STRAIGHTER (BLOCKAGE EQUAL TO 16% OF FLOW AREA)	0.617	–	–	–	17	2.64	18	2.64	67.92	0.207	2.00
18	CONSTANT AREA LINE FROM FLOW STRAIGHTENER TO VENTURI	0.341	25.0	1.834	0.025	18	2.64	19	2.64	67.24	0.209	2.02

GP13-0503-84

Notes:

(1) K_t - Pressure loss coefficient $\frac{\Delta P_t}{q}$

(2) DH hydraulic diameter $\frac{4 \text{ area}}{\text{wetted perimeter}}$

(3) 4f - Friction factor

(4) K_t for typical components are

- Constant area section; $K_t = \frac{4fL}{DH}$
- Bends, contractions, and expansions; K_t per SAE manual and Crane Co. manual (Flow of Fluids)
- Flow straightener; K_t per AF technical report no. 6289

FIGURE B-2 (Continued)
TURBINE BLEED AIR SYSTEM PRESSURE LOSS ANALYSIS

APPENDIX C

ERROR ANALYSIS DATA REDUCTION EQUATIONS

Presented in this appendix are the preliminary data reduction equations used to calculate C_L, C_D and C_M in the error analysis program for the simulator mode. The equations however are identical for all three test modes except for the duct related parameters. These differences are noted. Also presented is a description of the measurands used in the data reduction equations.

The final data reduction equations will be derived as part of Phase II activity.

Measurand	Description
AAFSLT	Aircraft balance axial force installation correction, LB.
ACAVN	Projected normal cavity area
AFASC	Aircraft balance axial force strut cavity pressure correction, LB.
AFASP	Aircraft balance axial force seal pressure correction, LB.
AFB	Total pressure-area integrated boattail axial force, LB.
AFBU	Upper surface pressure-area integrated nozzle boattail axial force, LB.
AFBL	Lower surface pressure-area integrated nozzle boattail axial force, LB.
AFSW	Total pressure-area integrated sidewall axial force, LB.
AFSWIB	Inboard pressure-area integrated sidewall axial force, LB.
AFSWOB	Outboard pressure-area integrated sidewall axial force, LB.
ALA(I)	Nozzle area assigned to pressure tap I in the axial direction.
ALN(I)	Nozzle area assigned to pressure tap I in the normal direction.
ALPHAM	Model angle of attack.
ALPHAN	Nozzle angle of attack, DEG.
ANFSLT	Aircraft balance normal force installation correction, IN-LB.
APMSLT	Aircraft balance pitching moment installation correction, IN-LB.
ACAVA	Projected axial cavity area.
AWET1	Nacelle wetted area, IN^2.
AWET2	Nacelle plus nozzle wetted area, IN^2

Measurand	Description
A2	Compressor face duct area, IN^2.
CAB	Total pressure-area integrated boattail axial force coefficient.
CABU	Upper surface pressure-area integrated nozzle boattail axial force coefficient.
CABL	Lower surface pressure-area integrated nozzle boattail axial force coefficient.
CAFA	Aircraft balance corrected axial force coefficient.
CASW	Pressure-area integrated sidewall axial force coefficient.
CASWIB	Inboard pressure-area integrated sidewall axial force coefficient.
CASWOB	Outboard pressure-area integrated sidewall axial force coefficient.
CBAR	Mean aerodynamic chord.
CDA	Aircraft balance corrected drag coefficient.
CDARON	Total nozzle pressure-area integrated drag coefficient.
CDARONF	Total nozzle pressure-area integrated drag coefficient plus nozzle skin friction coefficient.
CDAROT	Total model drag coefficient using pressure-area integrated nozzle drag.
CDAROTF	Total model drag coefficient using pressure-area integrated nozzle drag plus nozzle skin friction.
CDB	Total pressure-area integrated boattail drag coefficient.
CDBL	Lower surface pressure-area integrated boattail drag coefficient.
CDBU	Upper surface pressure-area integrated boattail drag coefficient.
CDNSF	Nozzle skin friction coefficient.

Measurand	Description
CDSW	Total pressure-area integrated sidewall drag coefficient.
CDSWIB	Inboard pressure-area integrated sidewall drag coefficient.
CDSWOB	Outboard pressure-area integrated sidewall drag coefficient.
CFN(1)	Nacelle skin friction coefficient.
CFN(2)	Nacelle plus nozzle skin friction coefficient.
CLA	Aircraft balance corrected lift coefficient.
CLA2	$(CLA)^2$
CLARON	Total nozzle pressure-area integrated lift coefficient.
CLAROT	Total model lift coefficient using pressure-area integrated nozzle lift.
CLB	Total pressure-area integrated boattail lift coefficient.
CLBU	Upper surface pressure-area integrated boattail lift coefficient.
CLBL	Lower surface pressure-area integrated boattail lift coefficient.
CLSW	Total pressure-area integrated sidewall lift coefficient.
CLSWIB	Inboard pressure-area integrated sidewall lift coefficient.
CLSWOB	Outboard pressure-area integrated sidewall lift coefficient.
CMARON	Total nozzle pressure-area integrated pitching moment.
CMAROT	Total model pitching moment coefficient using pressure-area integrated nozzle pitching moment.
CMLA	Aircraft balance rolling moment coefficient transferred to Model Reference.

Measurand	Description
CMMA	Aircraft balance pitching moment coefficient transferred to Model Reference.
CMNA	Aircraft balance yawing moment coefficient transferred to Model Reference.
CMMAS	Same as CMMA
CNB	Total pressure-area integrated boattail normal force coefficient.
CNBU	Upper surface pressure-area integrated nozzle boattail normal force coefficient.
CNBL	Lower surface pressure-area integrated nozzle boattail normal force coefficient.
CNFA	Aircraft balance corrected normal force coefficient.
CNSW	Pressure-area integrated sidewall normal force coefficient.
CNSWIB	Inboard pressure-area integrated sidewall normal force coefficient.
CNSWOB	Outboard pressure-area integrated sidewall normal force coefficient.
CP(I)	Pressure coefficient at tap I.
CPCAV	Average cavity pressure coefficient.
CPMB	Boattail pitching moment coefficient.
CYFA	Aircraft balance corrected side force coefficient.
DDELC	Left hand minus right hand canard deflection angle, DEG.
DELALP	Nozzle deflection due to applied loads, DEG.
DELCL	Left hand canard deflection angle.
DELCR	Right hand canard deflection angle.
DELNOZ	Nozzle geometric deflection angle, DEG.
FAA	Aircraft balance corrected axial force, LB.

Measurand	Description
FAA2P	Aircraft balance axial force corrected for weight tare, LB.
FNA	Aircraft balance corrected normal force, LB.
FNA2P	Aircraft balance normal force corrected for weight tare, LB.
FRAM	Ram drag, LB.
FSEALA	Inlet duct seal axial force tare.
FSEALN	Inlet duct seal normal force tare.
FYA	Same as FYGA, LB.
FYA2P	Same as FYGA, LB.
F2SEAL	Compressor face stream thrust.
KAA1,2,3	Loads induced model deflection constants.
KST28-35	Installation effects matrix.
M	Tunnel Mach Number.
M2	Compressore face Mach Number.
MLA2P	Aircraft balance rolling moment corrected for weight tare, IB-LB.
MLAPP	Aircraft balance rolling moment transferred to Model Reference.
MLAP	Same as MLA2P, IN-LB.
MMAP	Aircraft balance corrected pitching moment, IN-LB.
MMA2P	Aircraft balance pitching moment corrected for weight tare, IN-LB.
MMAPP	Aircraft balance pitching moment transferred to Model Reference.
MNA2P	Aircraft balance yawing moment correct for weight tare, IN-LB.
MNAP	Same as MNA2P, IN-LB.

Measurand	Description
MNAPP	Aircraft balance yawing moment transferred to Model Reference.
MSEAL	Inlet duct seal pitching moment tare.
NAFSC	Aircraft balance normal force strut cavity pressure correction, LB.
NFB	Total pressure-area integrated boattail normal force, LB.
NFBU	Upper surface pressure-area integrated nozzle boattail normal force, LB.
NFBL	Lower surface pressure-area integrated nozzle boattail normal force, LB.
NFSW	Total pressure-area integrated sidewall normal force, LB.
NFSWIB	Inboard pressure-area integrated sidewall normal force, LB.
NFSWOB	Outboard pressure-area integrated sidewall normal force, LB.
NSF	Nozzle skin friction, LB.
P	Static pressure, PSFA
PMASC	Aircraft balance normal force contribution to pitching moment, strut cavity pressure correction, IN-LB.
PMASCA	Aircraft balance axial force contribution to pitching moment, strut cavity pressure correction, IN-LB.
PMASP	Aircraft balance axial force contribution to pitching moment, seal pressure correction, IN-LB.
PMB	Nozzle boattail pitching moment, IN-LB.
PMSW	Sidewall pitching moment, IN-LB.
PO	Static pressure, PSIA.
PT	Total pressure, PSFA.
PTO	Total pressure, PSIA.

Measurand	Description
PTJLF	Average nozzle total pressure, PSIA.
PTJLFI(I)	Nozzle total pressure at probe I.
PT2I(I)	Compressor face total pressure at probe I.
P2C	Compressor face static pressure, PSIA.
Q	Tunnel dynamic pressure, PSF.
QO	Dynamic pressure, PSI.
RE	Tunnel Reynolds Number.
RPA	Water line of model reference.
RPMA(I)	Water line of pressure tap I.
RPMN(I)	Fuselage station of pressure tap I.
RPM	Fuselage station of model reference.
SPAN	Wing span.
SW	Wing reference area.
TARE7	Internal duct drag correction, LB.
TARE8	Body axis ram drag, LB.
TT	Tunnel total temperature, °F.
TTR	Tunnel total temperature, °R.
VO	Freestream velocity, FT/SEC.
WAF	Nozzle mass flow, LB/SEC.
X(I)	Nacelle length, IN.
X(2)	Nacelle plus nozzle length, IN.
XCAV	Moment arm for normal cavity force.
XMTA	Axial distance from balance center to model reference.
XNTA	Lateral distance from balance center to model reference.
ZCAV	Moment arm for axial cavity force.
ZTA	Vertical distance from balance center to model reference.

DATA REDUCTION EQUATIONS

		Term	Source	Units
1.0	Tunnel operating conditions			
1.1 a)	Total Pressure	PT	Facility	PSFA
b)	Static Pressure	P	Facility	PSFA
c)	Dynamic Pressure	Q	Facility	PSF
d)	Total Temperature	TT	Facility	°F
e)	Total Temperature	TTR	Facility	°R
f)	Reynolds Number/Foot	Re/ℓ	Facility	Ft^{-1}
g)	Mach Number	M		
1.2	Pressures in pounds per square inch			
a)	PTO = PT/144	PT	1.1a	PSAF
		PTO	1.2a	PSIA
b)	PO = P/144	P	1.1b	PSFA
		PO	1.2b	PSIA
c)	QO = Q/144	Q	1.1c	PSF
		QO	1.2c	PSI

	Term	Source	Units
1.3 Model, nozzle and canard angle of attack			
a) Wing angle of attack			
ALPHAM - facility support corrected for sting deflection	ALPHAM		DEG
b) Canard deflection angles			
DELCL	DELCL		DEG
DELCR	DELCR		DEG
1.4 Calculated model angles			
a) DDELC = DELCL - DELCR (Canrard deflection is measured with potentiometers on each side Eq. 1.4 (a) is a check of asymetric canard deflection)	DELCL	1.3b	DEG
	DELCR	1.3b	DEG
	DDELC	1.4a	DEG
	DELALP	15.0d	DEG
	DELNOZ	CONST	DEG
	ALPHAM	1.3a	DEG
b) ALPHAN = ALPHAM - DELALP + DELNOZ	ALPHAN	1.4b	DEG
1.5 Model pressures listed in Figure 6-1	P(I)	1.5	PSIA

	Term	Source	Units
2.0 Pressure coefficients	P(I)	1.5	PSIA
$CP(I) \frac{P(I) - PO}{QO}$	PO	1.2b	PSIA
	QO	1.2C	
	CP(I)	2.0	

2.1 Nozzle boattail pressure area integration

a) $NFBU = QO \Sigma CP(I) ALN(I)$	QO	1.2c	PSIA
	CP(I)	2.0	
b) $NFBL = QO \Sigma CP(I) ALN(I)$	ALN(I)	CONST.	IN^2
	ALA(I)	CONST.	IN^2
c) $AFBU = QO \Sigma CP(I) ALA(I)$	RPA	CONST.	IN
	RPMA(I)	CONST.	IN
d) $AFBL = QO \Sigma CP(I) ALA(I)$	RPN	CONST.	IN
	RPMN(I)	CONST	IN
e) $RPMA1(I) = RPMA(I) - RPA$	RPMA1(I)	2.1e	IN
	RPMN1(I)	2.1f	IN
f) $RPMN1(I) = - (RPMN(I) - RPN)$	NFBU	2.1a	LB.
	NFBL	2.1b	LB.
g) $PMB = QO \Sigma CP(I) [ALN(I)] [RPMN1(I)]$	AFBU	2.1b	LB.
$+ QO \Sigma CP(I) [ALA(I)] [RPMA1(I)]$	AFBL	2.1d	LB.
	PMB	2.1g	LB.
h) $NFB = NFBU + NFBL$	NFB	2.1h	LB.
i) $AFB = AFBU + AFBL$	AFB	2.1i	LB.

3.0 Nozzle sidewall pressure area integration forces

a) $NFSWIB = Q0 \Sigma CP(I) ALN(I)$

b) $NFSWOB = Q0 \Sigma CP(I) ALN(I)$

c) $AFSWIB = - Q0 \Sigma CP(I) ALA(I)$

d) $AFSWOB = - Q0 \Sigma CP(I) ALA(I)$

e) $PMSW = Q0 \Sigma CP(I) [ALN(I)] [RPMN1(I)] + Q0 \Sigma CP(I) [ALA(I)] [RPMA1(I)]$

f) $NFSW = NFSWIB + NFSWOB$

g) $AFSW = AFSWIB + AFSWOB$

Term	Source	Units
Q0	1.2c	PSI
CP(I)	2.0	
ALN(I)	CONST.	IN
NFSWIB	3.0a	LB
NFSWOB	3.0b	LB
ALA(I)	CONST.	IN
AFSWIB	3.0c	LB
AFSWOB	3.0d	LB
RPMN1(I)	2.1f	IN
RPMA1(I)	2.1e	IN
PMSW	3.0e	IN-LB
NFSW	3.0f	LB
AFSW	3.0g	LB

4.0 Nozzle boattail body axis pressure area

a) $CNBU = 2(NFBU)/[(Q)(SW)]$

b) $CNBL = 2(NFBL)/[(Q)(SW)]$

c) $CABU = 2(AFBU)/[(Q)(SW)]$

d) $CABL = 2(AFBL)/[(Q)(SW)]$

e) $CPMB = 2(PMB)/[(Q)(SW)(CBAR)]$

f) $CNB = CNBU + CNBL$

g) $CAB = CABU + CABL$

NFBU	2.1a	LB
Q	1.1c	PSF
SW	CONST.	FT^2
CNBU	4.0a	
NFBL	2.1b	LB
CNBL	4.0b	
AFBU	2.1c	LB
CABU	4.0c	
AFBL	2.1d	LB
CABL	4.0d	
PMB	2.1g	IN-LB
CBAR	CONST	IN
CPMB	4.0e	
CNB	4.0f	
CAB	4.0g	

	Term	Source	Units
5.0 Nozzle sidewall body axis pressure area integration coefficients			
a) CNSWIB = 2(NFSWIB)/[(Q)(SW)]	NFSWIB	3.0a	LB
	Q	1.1c	PSF
	SW	CONST.	FT^2
	CNSWIB	5.0a	
b) CNSWOB = 2(NFSWOB)/[(Q)(SW)]	NFSWOB	3.0b	LB
	CNSWOB	5.0b	
c) CASWIB = 2(AFSWIB)/[(Q)(SW)]	AFSWIB	3.0c	LB
	CASWIB	5.0c	
d) CASWOB = 2(AFSWOB)/[(Q)(SW)]	AFSWOB	3.0d	LB
	CASWOB	5.0d	
e) CPMSW = 2(PMSW)/[(Q)(SW)(CBAR)]	PMSW	3.0e	IN-LB
	CBAR	CONST.	IN
	CPMSW	5.0e	
f) CNSW = CNSWIB + CNSWOB	CNSW	5.0f	
g) CASW = CASWIB + CASWOB	CASW	5.0g	
6.0 Nozzle boattail stability axis pressure area integration coefficients	CNBU	4.0a	
	ALPHAN	1.4b	DEG
	CABU	4.0c	
a) CLBU = (CNBU) cos (ALPHAN) - (CABU) sin (ALPHAN)	CLBU	6.0a	
	CNBL	4.0b	
b) CLBL = (CNBL) cos (ALPHAN) - (CABL) sin (ALPHAN)	CABL	4.0d	
	CLBL	6.0b	
c) CDBU = (CNBU) sin (ALPHAN) + (CABU) cos (ALPHAN)	CDBU	6.0c	
	CDBL	6.0d	
d) CDBL = (CNBL) sin (ALPHAN) + (CABL) cos (ALPHAN)	CLB	6.0e	
	CDB	6.0f	
e) CLB = CLBU + CLBL			
f) CDB = CDBU + CDBL			

	Term	Source	Units
7.0 Nozzle sidewall stability axis pressure area integration coefficients	CNSWIB	5.0a	
	ALPHAN	1.4b	DEG
	CASWIB	5.0c	
a) CLSWIB = (CNSWIB) cos (ALPHAN) - (CASWIB) sin (ALPHAN)	CLSWIB	7.0a	
	CNSWOB	5.0b	
b) CLSWOB = (CNSWOB) cos (ALPHAN) - (CASWOB) sin (ALPHAN)	CASWOB	5.0d	
	CLSWOB	7.0b	
c) CDSWIB = (CNSWIB) sin (ALPHAN) + (CASWIB) cos (ALPHAN)	CDSWIB	7.0c	
	CDSWOB	7.0d	
d) CDSWOB = (CNSWOB) sin (ALPHAN) + (CNSWOB) cos (ALPHAN)	CLSW	7.0e	
	CDSW	7.0f	
e) CLSW = CLSWIB + CLSWOB			
f) CDSW = CDSWIB + CDSWOB			

8.0 Total nozzle stability axis pressure area integration coefficients	CLB	6.0e	
	CLSW	7.0e	
	CDB	6.0f	
a) CLARON = CLB + CLSW	CDSW	7.0f	
	CPMB	4.0e	
b) CDARON = CDB + CDSW	CPMSW	5.0e	
	CDNSF	14.0c	
c) CMARON = CPMB + CPMSW	CLARON	8.0a	
	CDARON	8.0b	
d) CDARONF = CDARON + CDNSF	CMARON	8.0c	
	CDARONF	8.0d	

		Term	Source	Units
9.0	Aircraft balance net loads corrected for model weight tares			
	a) FNA2P (Ames Std Equations)	FNA2P	9.0a	LB
	b) FAA2P (Ames Std Equations)	FAA2P	9.0b	LB
	c) FYA2P (Ames Std Equations)	FYA2P	9.0c	LB
	d) MMA2P (Ames Std Equations)	MMA2P	9.0d	IN-LB
	e) MNA2P (Ames Std Equations)	MNA2P	9.0e	IN-LB
	f) MLA2P (Ames Std Equations)	MLA2P	9.0f	IN-LB

10.0 Flow parameters

a) $V0 = M\left[(2403.076)\frac{TTR}{1 + 0.2M^2}\right]^{1/2}$

b) $PTJLF = \frac{1}{5}\sum_{1}^{5} PTJLFI(I)$

c) $PT2 = \frac{1}{10}\sum_{1}^{10} PT2I(I)$

d) $M2 = F(WAF, PT2, TTR, A2)$

e) WAF:

SIMULATOR MODE

WAF = provided by simulator

Flow Through Mode

WAF = look up on calibration curve

= F(TTR, PTJLF, P0)

f) $P2C = PT2/(1 + .2*M2^{3.5})$

Term	Source	Units
M	1.1g	
TTR	1.1e	°R
V0	10.0a	FT/SEC
PTJLFI(I)		PSIA
PT2I(I)		PSIA
PTJLF	10.0b	PSIA
PT2	10.c	PSIA
M2	10.0d	
WAF	10.0e	LB/SEC
PT2	10.0c	PSIA
TTR	1.1e	°R
A2	CONST.	IN^2
WAF	10.0e	LB/SEC
TTR	1.1e	°R
PTJLF	10.0b	PSIA
P0	1.2b	PSIA
PT2	10.0c	PSIA
M2	10.d	
P2C	10.0f	PSIA

	Term	Source	Units
10.1 Inlet Duct Seal Correction			
a) FSEALN = to be defined	FSEALN	10.1a	LB
b) FSEALA = to be defined	FSEALA	10.1b	LB
c) MSEAL = to be defined	MSEAL	10.1c	LB
d) F2SEAL = to be defined	F2SEAL	10.1d	LB

11.0 Flow tare corrections	WAF	10.0e	LB/SEC
	V0	10.0a	FT/SEC
a) $FRAM = 2 \frac{WAF}{32.174} V0$	FRAM	11.0a	LB
	A2	CONST.	IN^2
	P2C	10.0f	PSIA
b) $F2 = A2[P2C(1 + 1.4M^2) - P0] + F2SEAL$	M	1.0g	PSIA
	P0	1.2b	PSIA
c) TARE7 = F2 - FRAM*[COS(ALPHAM)]	F2SEAL	10.1d	LB
	F2	11.0b	LB
d) TARE8 = -FRAM*[SIN(ALPHAM)]	ALPHAM	1.3a	DEG
	TARE7	11.0c	LB
	TARE8	11.0d	LB

	Term	Source	Units
12.0 Model cavity tare corrections	CPCAV	2.0	
	Q0	1.2c	PSI
a) NAFSC = -(CPCAV)(Q0)(ACAVN)	ACAVN	CONST.	IN^2
	NAFSC	12.0a	LB
b) PMASC = (NFASC)(XCAV)	XCAV	CONST.	IN
	PMASC	12.0b	IN-LB
c) AFASC = (CPCAV)(Q0)(ACAVA)	ACAVA	CONST.	IN^2
	AFASC	12.0c	
d) PMASCA = (-AFASC)(ZCAV)	PMASCA	12.0d	IN-LB
	ZCAV	CONST.	IN
NOTE: To be determined during cavity pressurization calibration.			
13.0 Aft seal pressure area integration aircraft tare correction			
a) AFASP = Q0 Σ ([Cp(I)][ALA(I)])	CP(I)	2.0a	
	ALA(I)	CONST.	IN^2
b) PMASP = - Q0 Σ ([CP(I)][ALA(I)][RPMA1(I)]),		AFASP	13.0a LB
	RPMA1(I)	2.1e	IN
	PMASP	13.0b	IN-LB
14.0 Nozzle skin friction calculation			
a) $CFN(I) = \left[\frac{.455}{\text{LOG}_{10}[(Re)X(I)]^{2.58}}\right] * [1 + .2M^2]^{-.467}, I = 1,2$	Re	1.0f	1/FT
	X(I)	CONST.	FT
	M	1.0g	
	CFN(I)	14.0a	
		AWET(I)	CONST. FT^2
	Q	1.0c	PSF
b) NSF = [CFN(2) AWET(2) - CFN(1) AWET(1)]Q	NSF	14.0b	LB
	SW	CONST	FT^2
c) $CDNSF = \frac{NSF}{(Q)(SW)}$			

15.0 Installation effects on aircraft balance loads

a) ANFSLT = (KST28)(FNA2P) + (KST29)(MMA2P) + (KST30)(FAA2P)

b) AAFSLT = (KST31)(FNA2P) + (KST32)(MMA2P) + (KST35)(FAA2P)

c) APMSLT = (KST34)(FNA2P) + (KST35)(MMA2P) + (KST36)(FAA2P)

d) DELALP = (KAA1)(FNA2P) + KAA2(MMA2P) + KAA3

Term	Source	Units
KST28	CONST.	
KST29	CONST.	
KST30	CONST.	
KST31	CONST.	
KST32	CONST.	
KST33	CONST.	
KST34	CONST.	
KST35	CONST.	
KST36	CONST.	
FNA2P	9.0a	LB
MMA2P	9.0d	IN-LB
FAA2P	9.0b	LB
ANFSLT	15.0a	LB
AAFSLT	15.0b	LB
APMSLT	15.0c	IN-LB
KAA1	CONST.	DEG/LB
KAA2	CONST.	DEG/LB
KAA3	CONST.	DEG/LB
DELALP	15.0d	DEG

16.0 Aircraft loads tare correction.

a) FNA = FNA2P + NAFSC + ANFSLT + TARE8 + FSEALN

b) FYA = FYA2P

c) FAA = FAA2P + AFASC + AFASP + AAFSLT + TARE7 + FSEALA

d) MMAP = MMA2P + PMASC + PMASCA + PMASP + APMSLT + MSEAL

e) MNAP = MNA2P

f) MLAP = MLA2P

Term	Source	Units
FNA2P	9.0a	LB
ANFSLT	15.0a	LB
FNA	16.0a	LB
FAA2P	9.0b	LB
AAFSLT	15.0b	LB
FAA	16.0c	LB
MMA2P	9.0d	IN-LB
APMSLT	15.0c	IN-LB
MMAP	16.0d	IN-LB
NAFSC	12.0a	LB
TARE8	11.0d	LB
FSEALN	11.0a	LB
FYA	16.0a	LB
FYA2P	9.0c	LB
AFASC	12.0c	LB
AFASP	13.0a	LB
PMASC	12.0b	IN-LB
PMASCA	12.0d	IN-LB
MNAP	16.0e	IN-LB
PMASP	13.0b	IN-LB
TARE7	11.0c	LB
FSEALA	10.1b	LB
MSEAL	10.1c	IN-LB
MLAP	16.0f	IN-LB
MNA2P	9.0e	IN-LB
MLA2P	9.0f	IN-LB

17.0 Aircraft balance moment transfer to Model Reference

a) MMAPP = MMAP - (XMTA)[FNA + (ZTA)(FAA)]

b) MNAPP = MNAP - (XNTA) (FYA)

c) MLAPP = MLAP + (ZTA) (FYA)

Term	Source	Units
MMAP	16.0d	IN-LB
XMTA	CONST.	IN
FNA	16.0a	LB
ZTA	CONST.	IN
FAA	16.0c	LB
MMAPP	17.0a	IN-LB
MNAP	16.0e	IN-LB
XNTA	CONST.	IN
FYA	16.0b	LB
MNAPP	17.0b	IN-LB
MLAP	16.0f	IN-LB
MLAPP	17.0c	IN-LB

18.0 Aircraft balance body axis coefficients at Model Reference

a) CNFA = FNA/[(Q)(SW)]

b) CYFA = FYA/[(Q)(SW)]

c) CAFA = FAA/[(Q)(SW)]

d) CMMA = MMAPP/[(Q)(SW)(CBAR)]

e) CMNA = MNAPP/[(Q)(SW)(SPAN)]

f) CMLA = MLAPP/[(Q)(SW)(SPAN)]

FNA	16.0a	LB
Q	1.1c	PSF
SW	CONST.	FT^2
CNFA	18.0a	
FYA	16.0b	LB
CYFA	18.0b	
FAA	16.0c	LB
CAFA	18.0c	
MMAPP	17.0a	IN-LB
CBAR	CONST.	IN
CMMA	18.0d	
MNAPP	17.0b	IN-LB
SPAN		IN
CMNA	18.0e	IN-LB
MLAPP	17.0c	IN-LB
CMLA	18.0f	

	Term	Source	Units
19.0 Aircraft balance stability axis coefficients	CNFA	18.0a	
	ALPHAM	1.3a	DEG
a) CLA=(CNFA) cos (ALPHAM) - (CAFA) sin (ALPHAM)	CAFA	18.0c	
	CLA	19.0a	
	CDA	19.0b	
b) CDA=(CAFA) cos (ALPHAM) + (CNFA) sin (ALPHAM)	CMMA	18.0d	
	CMMAS	19.0c	
	CLA2	19.0d	
c) CMMAS = CMMA			
d) CLA2 + (CLA)(|CLA|)			
20.0 Total model stability axis coefficients with the nozzle forces calculated by pressure area integration	CLA	19.0a	
	CLARON	8.0a	
	CLAROT	20.0a	
	CDA	19.0b	
	CDARON	8.0b	
	CDAROT	20.0b	
	CDARONF	8.0d	
	CDAROTF	20.0c	
	CMMAS	19.0c	
	CMARON	8.0c	
	CMAROT	20.0d	
	CLAROT2	20.0e	
a) CLAROT = CLA + CLARON			
b) CDAROT = CDA + CDARON			
c) CDAROTF = CDA + CDARONF			
d) CMAROT = CMMAS = CMARON			
e) CLAROT2 = (CLAROT) (|CLAROT|)			

1. Report No.	2. Government Accession No.	3. Recipient's Catalog No.
NASA CR-177369		

4. Title and Subtitle	5. Report Date
PROPULSION AND AIRFRAME AERODYNAMIC INTERACTIONS OF SUPERSONIC V/STOL CONFIGURATIONS PHASE I - FINAL REPORT	Sept 85
	6. Performing Organization Code

7. Author(s)	8. Performing Organization Report No.
M. R. Mraz and P. E. Hiley	

9. Performing Organization Name and Address	10. Work Unit No.
McDonnell Aircraft Company P.O. Box 516 St. Louis, Missouri 63166	T-3288Y
	11. Contract or Grant No. NAS2-10791
	13. Type of Report and Period Covered
12. Sponsoring Agency Name and Address	Contractor Report
National Aeronautics and Space Administration Washington, D.C. 20546	14. Sponsoring Agency Code 505-43-01

15. Supplementary Notes

Point of Contact: Technical Monitor, Rodney O. Bailey
(415) 694-6265 Ames Research Center, Moffett Field, CA 94035

16. Abstract

A wind tunnel model of a supersonic V/STOL fighter configuration has been tested to measure the aerodynamic interaction effects which can result from geometrically close-coupled propulsion system/airframe components. The approach was to configure the model to represent two different test techniques. One was a conventional test technique composed of two test modes. In the Flow-Through mode, absolute configuration aerodynamics are measured, including inlet/airframe interactions. In the Jet-Effects mode, incremental nozzle/airframe interactions are measured. The other test technique is a propulsion simulator approach, where a sub-scale, externally powered engine is mounted in the model. This allows proper measurement of inlet/airframe and nozzle/airframe interactions simultaneously.

17. Key Words (Suggested by Author(s))	18. Distribution Statement
Flowfield Interactions Propulsion Simulators Supersonic V/STOL	[redacted] Until August 1987 Star Category 02

19. Security Classif. (of this report)	20. Security Classif. (of this page)	21. No. of Pages	22. Price*
Unclassified	Unclassified	132	

*For sale by the National Technical Information Service, Springfield, Virginia 22161